INVESTIGATION OF MAGNETIC PROPERTIES IN THE CASE OF THREE FAMILIES OF 1-DIMENSIONAL MAGNETS: M(II)A(4,4'-BIPYRIDINE); M=Fe, Co, Ni, Cu A= Cl_2, $(N_3)_2$, (ox)

A Dissertation

Submitted to

The Temple University Graduate Board

in Partial Fulfillment

of the Requirements for the Degree

DOCTOR OF PHILOSOPHY

By

Dušan S. Danilović

May, 2010

Examining Committee Members:

Tan Yuen, Advisory Chair, Physics

Chyan-Long Lin, Physics

Peter R. Riseborough, Physics

Theodore Burkhardt, Physics

Jing Li, Chemistry, Rutgers University

Frank Spano, External Member, Chemistry

To my beloved wife Jelena for all of these years of love and understanding, for making me a better man.

Волим Те Срећко мој.

ABSTRACT

Dušan Stevan Danilović
Doctor of Philosophy
Temple University, 2010
Advisor: Dr. Tan Yuen

Magnetic properties of three families of metal-organic coordinated networks which have the general form of M(II)A(4,4'-bipyridine), where M=Fe, Ni, Co, and Cu and A=Cl_2, (ox) and $(N_3)_2$, are studied in this dissertation. Novel Ni$(N_3)_2$(4,4'-bipyridine), Co$(N_3)_2$(4,4'-bipyridine) and Cu$(N_3)_2$(4,4'-bipyridine) have been synthesized. We applied different synthesis procedures and produced Ni, Co, and Cu azide compounds for the first time, thus leaving the hydrothermal route procedure. Powder x-ray diffraction at room temperature was done in order to establish the crystal structure of the members of these three families. It was found that all of them crystallize in orthorhombic structure, where transitional metals have an octahedral coordination. Since all three families have identical crystal structure we got opportunity to examine how ligands facilitate magnetic interaction between metallic centers and also to test existing magnetic theoretical models. Since 4,4'-bipyridine is much longer than other ligands, our systems can be considered as 1-D magnetic systems. Their interchain magnetic interactions are very weak, and they order magnetically at very low temperatures of the order of few K. Measurements of M(H) at temperatures T=1.9K and T=2K and χ(T) in different external magnetic fields in zero field and field cooled modes have been made. In the case of MCl_2(4,4'-bipyridine) family of compounds, we observed ferromagnetic interactions between metal ions within

the chains and antiferromagnetic interactions between adjacent chains. M(ox)(4,4'-bipyridine) family of metal-organic compounds has antiferromagnetic interactions between the transitional metal ions within the chain, while weak ferromagnetic interaction exists between the chains. All members in the $M(N_3)_2$(4,4'-bipyridine) family except in the case of the copper compound were found to have ferromagnetic interactions between metal ions within the chains and then antiferromagnetic interactions between adjacent chains. The copper compound does not show magnetic ordering in the temperature range we considered. All the metal ions in these compounds were detected in high spin states. The magnetic susceptibility data was fit to appropriate 1-D models, which in the case of MCl_2(4,4'-bipyridine) and $M(N_3)_2$(4,4'-bipyridine) were the Classical Spin Fisher model, and the Bonner Fisher model in the case M(ox)(4,4'-bipyridine). The experimental results and fitting to the appropriate model with the accuracy of 0.995 suggests that shorter Cl-M-Cl distances facilitate ferromagnetic interactions, which are more sensitive to the total spin value then to the sole distance between metal ions. The magnetic behavior of $M(N_3)_2$(4,4'-bipyridine) family of coordinated metal-organic compounds is very interesting because family members exhibit both ferromagnetic and antiferromagnetic behavior. The ferromagnetic characteristics decrease with decreasing spin. Fitting the results for all compounds of the M(ox)(4,4'-bipyridine) family have shown that strong anisotropy exists in all of them, being highest in Ni(ox)(4,'4-bipyridine) and lowest in Co(ox)(4,4'-bipyridine). Specific heat measurements were performed in the case of cobalt and copper azide compounds and then compared with previously obtained results for the iron coordinated network of the same family. Although none of these compounds show the characteristic λ shaped

transition indicating magnetic ordering, all of them have unusually large values of the constant γ, which indicates significant magnetic contribution to the observed specific heat, since the free electron contribution in these observed families is negligible. We have concluded that total spin of the transitional metal plays a more important role than the distance between ions within the chain in determining magnitude of interaction, and that $(N_3)_2$ is a better facilitator of ferromagnetic interaction between ions than Cl_2.

ACKNOWLEDGMENTS

Although it would be impossible to thank everyone who contributed to the completion of this thesis, I would like to thank those people who in my eyes most directly contributed to my education and scientific development that culminated in this dissertation.

I would like to thank Professor Tan Yuen for the enormous help she was willing to give me in every stage of my graduate academic career. Her friendship as well her understanding of physics and experimental techniques was indispensable. She made transition from the astrophysics into the condensed state physics possible and fully joyful. Professor Yuen devoted more of her time and energy to my research than anyone would imagine and hope for and I am eternally grateful to her. I could never ask for better adviser, and I am so honored she accepted me as her graduate student on one rainy day in March little bit more than five years ago.

Professor Chyan Long Lin provided me with advice and guidance in the completion of the experiments performed for this study. The patience Prof. Lin shown in reading final draft of the dissertation humbled me. His vast knowledge of all things experimental is legendary, and I am deeply privileged that I had chance to collaborate with him. When I think of Professor Lin I always see his smiling face.

Professor Jing Li from Chemistry and Chemical Biology Department, Rutgers University generously helped me with compound synthesis and understanding how

chemistry works. She unlocked one whole new filed for me which was mystery for many years.

I would like to thank Professor Peter Riseborough for introducing me to the field of condensed state physics thus opening whole new professional world to me. Professor Riseborough's willingness to give his time to freely discuss any of the physics involved in this thesis will always be cherished.

Without Professor Theodore Burkhardt this dissertation would not exist in today's shape, and I am not first graduate student to say that. His command of physics and written English in finishing phases put it simply are highly treasured.

Professor Frank Spano as an external reviewer was the knight in white armor who took gargantuan task of reading my dissertation on such short notice making possible for me to finish it in required time frame. That will be always remembered

Mr. Youcef Hamida and I forged deep friendship while we grew in understanding of the scientific field and respective cultures we are immersed in. I can only hope that I will be as helpful to him in his dissertation work as he was to me.

Dr. Xiaoying Huang and Dr. Joen Yong Lee introduced me to the chemistry lab. They had patience and eagerness to spend time introducing me to all these small tricks one desperately needs when producing such very delicate compounds, despite the fact they had their own thesis to finish. Mr. Matthew Eibling known as to friends as Will used his amazing imagination which helped me produce one compound that I was desperately pursuing for almost a year.

Another graduate student wrote that Mr. Ed Kaczanowicz's knowledge about the experiments performed at Temple University was possibly one of the most undervalued

commodities in this department. I must say I could not agree more. Big Ed was simply Big Ed and I thank him for that.

I would like to thank Professor. Zbigniew Dziembowski, and Professor Diter Forester, for their support of my goals and belief in my talent and ability. Throughout my time at Temple, they provided me with advice and encouragement when I needed it most.

The help and the guidance and the smiles provided by the administrative staff of the physics department, namely Ms. Janis Zambrano and Ms. Evelyn Washington was greatly appreciated.

Special thanks go to Dr. Vladimir Lukić currently at University of Pennsylvania for his willingness to share vast knowledge of theoretical condensed physics and to be involved in my professional evolution since we started our undergraduate studies of astrophysics at Belgrade University. His friendship along with that of Florentin Butaru and were able to bring me back from the edge of academic despair and allow me to focus on what I was working for.

Finally, I would like to thank my family. My wife Jelena was from the beginning of this long journey when I entered halls of Department of Astronomy at Belgrade University. She gave me love that I did not even dream existed. Having her by my side makes me the luckiest man in the world, and that is huge understatement. My father's and sister's undying support and love guided me towards realizing my goals and for that and enormous kindness in the deepest moments of doubt I can never fully repay them.

If I have left anyone out, I assure you it was not intentional. I thank you all from the bottom of my heart for everything you have given me. I only hope that I can do as good job of supporting those who need my help.

TABLE OF CONTENTS

Page

LIST OF FIGURES

LIST OF TABELS

CHAPTER 1

INTRODUCTION

1.1 The Essence of Magnetism and Magnetic Materials

Magnetic materials play a critical role in our daily life, their use for the compass being historically the first, and new magnetic materials used in electronics the most common one. Magnetism was first discovered by the ancient Greeks, according to Aristotle by Thales of Miletus (625-545 BC) [ref. 66]. Thales recognized that certain ore attracts objects made of iron. This mineral was mined in the province of Magnesia in southeast Thessaly, hence its name magnetite and the entire discipline magnetism. In the 11th century magnets had been already used by the Chinese to create a "south pointing" compass [ref. 68], which was first used for terrestrial navigation. Only by the end of the 12th century did the Chinese used magnets for naval navigation. In the Western world, the use of compass is recorded first in 1187 by the Englishman A. Neckam (1157-1217), a scholar and teacher, in his works *De Utensilibus* and *De Natuuris Rerum* [ref. 71]. Since the invention of the compass, the number of devices that use magnetic components has skyrocketed, especially at the end of the 20th and the beginning of 21st centuries. The relative ease of production and very favorable cost benefit analysis of production are principal reasons for wide usage

of magnetic materials today. Common applications of magnetic materials in everyday life include frictionless bearings, medical devices, magnetic separators, loudspeakers, microphones, switches, sensors, data storage devices, motors and generators [ref. 18, 28, 43, 82]. Their extensive commercial availability and application propel research of different types of magnetic materials.

Scientific studies of magnetism started in 1600 when William Gilbert of Colchester (1544-1603), English physician and natural philosopher, published *De Magnete* [ref. 67]. Colchester gathered all previously known facts about magnetism, trying to explain them systematically according to the knowledge of his epoch. By the 18th century the magnets were used and discussed in medicine. The German physician Mesmer (1734-1815) used magnets to treat patients suffering from shallow breathing [ref. 68]. Mesmer was so influential that his name entered the English language via the word mesmerizing, meaning hypnotic. Early modern physicists Colchester, Descartes, Oersted, Ampere, and Faraday [ref. 67, 68, 71] experimentally established the connection between electric and magnetic phenomena central to the unified theory of electromagnetism. The experimental achievements by these giants of early magnetism enabled James Clerk Maxwell (1831-1879) to accomplish his *Treatise on Electricity and Magnetism* [ref. 68]. Published in 1873, the *Treatise* is still considered the most comprehensive scholarly work in classical theoretical physics. Contrary to the prevalent contemporary belief, Maxwell's *Treatise* was the beginning, rather than the end, of experimental and theoretical investigations in magnetism.

The major developments of physics in the 20th century are related mainly to the development of quantum mechanics [ref. 67, 68, 71]. Therefore, progress in the

modern understanding of magnetism depends, to a great extent, on the scientific progress in quantum physics. Conversely, the greatest contributions in the theory of magnetism for the understanding of physical world are in the field of statistical mechanics and thermodynamics [ref. 71]. Whereas in the 19th century the understanding in these important branches of physics was limited to the theory of gases, the study of magnetism as a cooperative phenomenon led to the most significant advances in the theory of thermodynamic phase transitions, which were obtained a century later [ref. 67, 68, 71]. In turn, the theory of thermodynamic phase transitions transformed statistical mechanics into one of the sharpest and the most significant tools for the study of solid state matter.

Without any pretension to give a complete overview of the development of magnetism in the 20th century, the contributions of P. Weiss, P. Currie, W. Heisenberg, P.A.M Dirac, J. Van Vleck, J. C. Slater, E. Ising [ref. 68] should be mentioned as important advances in theoretical and experimental magnetism. The introduction of now widely-used microcomputers and new experimental tools, such as neutron scattering, both elastic and inelastic, and NMR, gave the research additional impetus [ref. 85]. The real explosion in the production of novel magnetic materials using different experimental techniques in the last several decades and new questions posed by magnetic behavior of these novel materials are other very important reasons for the growth of the field. The fact that some questions in the understanding of magnetism have not yet been completely explored motivates theoretical and experimental physicists to work relentlessly in the field [ref. 7, 13, 57].

The phenomenon that involves magnetism comes from magnetic moments of atoms in certain materials. Magnetic materials in real-life applications and thus crucial for experimental work, which study is undertaken in this dissertation, are characterized, via the so-called cooperative magnetism, where individual magnetic moments interact with their environment. Moreover, the question of dimensionality is crucial for connecting real-life experiments to theoretical models that correspond to experimental results. Although magnetic interactions occur in three dimensions, the type and strength of these interactions can vary with direction. The dimensionality of magnetic materials comes from ratio of the strengths of exchange interaction between magnetic moments in different dimensions. These interactions are characterized by the exchange constants (*J*). [ref. 20]. Therefore, magnetic materials are usually defined as one- (1D), two- (2D), and three- (3D) dimensional magnetic materials depending on the strengths of the exchange constants.

1.2. The Relevance of the Research of 1D Magnets Presented in this Dissertation

The current research on magnetism touches important branches of condensed matter physics: High-T_c and other nonconventional superconductivity, magnetic semiconductors, spintronics, and other interesting phenomena such as the Haldane gap [ref. 1, 7, 52, 57, 66]. Our investigations focused on 1D magnetic chains. By observing how our metal-organic compounds' interactions are changing with the change in temperature, we may provide some better understanding of current challenges in condensed physics today.

High-T_c superconductors exhibit five main superconducting properties below T_c which compete with magnetism: zero resistance, the Meissner Effect, flux quantization, the Josephson Effect, and gaps in excitation energy spectra. These superconducting properties are explained by 2D conduction, short coherence length ξ_0 ($\approx$10 A), high T_c ($\approx$100 K), type two magnetic behavior with two energy gaps, and *d* wave Cooper pairing wave function, the last phenomenon being crucial motivational factor for magnetic research.

The bosons responsible for the interaction between the Cooper pairs are magnetic excitations, also called spin waves. A spin wave can be considered as a local perturbation of the antiferromagnetic state, which can then propagate in space. To describe magnetic mechanism correctly, the superconductivity, therefore, must be of the *d* type symmetry. In current research the magnitude of electron-electron coupling in the strong coupling limit cannot be accurately estimated because elementary excitations are not sufficiently known. A better understanding of excited states, which

depend on temperature changes studied in magnetism, would contribute to a better understanding of high T_c superconductivity.

The one-dimensionality of magnetic chains implies the possibility of complex excitations, which are still far from being completely understood. It is not the ordering in these chains that is crucial, but their excitations, because unless the interchain interactions are strong enough, these chains do not show order. A neutron scattering experiment involves a change of spin of one, which implies a creation or annihilation of single magnon in a three-dimensional systems. Neutron scattering experiments have confirmed that these excitations do exist in some 1D antiferromagnetic chains [ref. 7, 29, 57], which puts studies of 1D magnetic compounds on the forefront of current studies in magnetism and condensed state physics.

As early as in 1964 theoretical studies suggested that 1D system and, especially those with organic molecules, might provide a route to room temperature superconductivity [ref. 82, 92]. The low effective dimensionality of 1D organic molecules reduces the screening of the Coulomb interaction. The reduced Coulomb interaction's screening has the two opposite effects: 1) the increasing of the strength of electron-lattice interaction, which should favor superconductivity, and 2) the increasing of the mutual repulsion of the electrons, which should inhibit the formation of Cooper pairs and thus oppose superconductivity. The response of the 1D systems to this combination of a stronger indirect force of attraction (which may results from the effects other than electron-phonon interaction) and a stronger direct repulsion could be a contributory factor in encouraging the electrons (or holes) to form Cooper

pairs with *d*-wave symmetry rather than the isotropic *s*-wave symmetry of elemental superconductors. The spins would again be antiparellel, but then the wavefunction would vanish as the particle separation tends to zero, reducing the energy cost of short-range repulsion. The experimental results of excited states observed in 1D metal-organic compounds described in this dissertation, can contribute to a better understanding of excited states in high-T_c superconductors.

The ability to manipulate and amplify currents of different spin types is the basis of the emerging field of spintronics [ref. 7, 13, 71]. Using the physical principles of spintronics and various combinations of semiconductors, metallic ferromagnets, and non-magnetic materials, which may be organic in their nature, scientists attempt to fabricate different electronic devices. Conventional electronics is based only on the charge of the electron and ignores electronic spin. However, spintronics considers different mobility of spin-up and spin-down electrons in ferromagnets. A crucial quantity in this phenomenon is the degree of spin polarization in a given ferromagnet. The experimental results of interactions of electrons of different spin orientations in metal-organic compounds report in this dissertation can also contribute to a better understanding of principles of spintronics.

The excitons in the case of half-integer spin chains are spinons, which are gapless excitons. Haldane conjectured that something different would happen for integer spin chains, namely that there would be a gap in exciton spectrum [ref. 1, 7, 52]. A 1D chain is now known as a Haldane chain, and the gap in the exciton spectrum is known as a Haldane gap. This fundamental difference between half-integer and integer spin chains is related to the difference between fermions and

bosons under exchange. This different exchange symmetry has a topological origin and has a significant effect on the gap-nature of excitons. The metal-organic compounds with full spin considered in this dissertation are potential candidates for further studies of Haldane gap.

Low-dimensional magnets are interesting for other reasons as well. First, in theoretical considerations low-dimensional magnets can be treated much easier than their higher dimensional relatives. In some magnetic crystals, a 1D magnetic pathway occurs naturally between metallic ions as a consequence of chemical structure. Alternatively, 1D magnetic pathways result from the interaction between ionic components of magnetic organic complexes. Second, the novel inorganic-organic hybrid networks assemblies represent one of the most active areas of materials science and connect theoretical and experimental research in physics and chemistry [ref.16, 28, 46, 55, 60, 61]. Chemists are interested in new properties that these hybrid networks offer, and thus their possible practical usage. The incorporation of transitional metal ions into organic systems often significantly improves the bulk properties of these materials, such as magnetism, thermal stability, and dielectricity. The bonds formed in these coordination networks are usually stronger, more resistant to free-radical cleavage reactions, and exhibit higher thermal stability. A significant amount of research has been dedicated to molecular-based magnets, the structures of which are built upon inorganic motifs containing magnetic ions bridged by organic compounds [ref. 16, 46].

Many important physical properties of metal-organic compounds depend on their structures and topography. Therefore, rational design and the construction of

new materials with specific networks has become a timely subject. This interdisciplinary situation coordinates the work of chemists and solid state physicists on multiple levels. Since the physics theory of superexchange is well understood, chemists tend to investigate empirically the variation of exchange constant with the bond length and bond angles. They are using different families of 1D magnetic compounds, and are relaying on the complete and accurate statistical mechanical knowledge, otherwise not available for the compounds of higher magnetic dimensionality. The rational control of the formation of desired one-dimensional, two-dimensional and the three-dimensional (3D) polymers, is particularly important in the investigation of the molecular magnets and their networks because the rational control enables close monitoring during the polymers' production. Moreover, the relative ease of procedures, which are used in production of these frameworks, as well as the relatively low cost of the whole process are a strong motivational factors in the field.

The selection of the organic building blocks is crucial in the construction of the frameworks with certain desired characteristics [ref. 28, 55, 60, 61]. One illustrative example is $CoCl_2 \cdot 2H_2O$, to be a known as 'poor' 1D magnet [ref. 10]. If large organic pyridines, however, replace the H_2O molecules, in order to produce $CoCl_2 \cdot 2NC_5H_5$ instead of $CoCl_2 \cdot 2H_2O$, the Co^{2+} ion chains are pushed much further apart, thus enhancing significantly the 1D character of the compound [ref. 10].

It is a known scientific fact that the exchange energy is very sensitive to the spacing of the metallic ions as well as a number of other factors, the nature of superexchange path being the most prominent. In this dissertation the particular focus

is, therefore, placed on the property of various materials to act as rigid, organic building blocks in metal-organic compounds. In particular, we aimed to attain and investigate 1D compounds that can be used to test different magnetic and, more broadly, condensed matter theoretical models. Because of the low temperature of magnetic ordering, these materials are reliable building blocks for magnetic devices at extremely low working temperatures. The organometalic materials we studied offer expanded options for the choice of material for magnetic devices. By employing 4,4'-bipyridine as one of the organic building block in the compounds, and then combining with another organic ligand, we get three families of coordinated networks studied in this dissertation: M(ox)(4,4'-bipyridine), MCl_2(4,4'-bipyridine), and $M(N_3)_2$(4,4'-bipyridine).

The property of bi-functional 4,4'-bipyridine (bpy) to act as rigid, rod like organic building block in the self-assembly of coordination frameworks is well-known and documented (Fig 1.1) [ref. 28, 55, 60, 61]. Much of the research has been done on the metal oxalate ($C_2O_4^{2-}$) compounds (Fig 1.2) [ref. 61] in the context of studies of organometallic magnets and open framework structures.

Metal-organic coordination networks which combine (bpy) with other multifunctional ligands such as (Cl_2) and (N_3)$_2$ (Fig 1.3) have also been studied preliminary [ref. 28, 55].

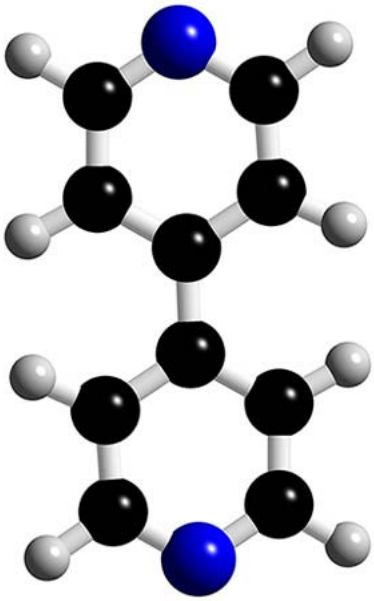

Fig. 1.1 4,’4-bipyridine, computer model

[Source of image: Gerloch, M., Constable, E.C., *Transition Metal Chemistry*, John Wiley & Sons-VCH, New York, **1994**, Fig. 4.5]

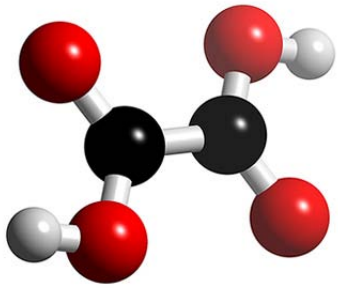

Fig. 1.2. $H_2C_2O_4$, computer model

[Source of image: Gerloch, M., Constable, E.C., *Transition Metal Chemistry*, John Wiley & Sons-VCH, New York, **1994**, Fig. 4.12]

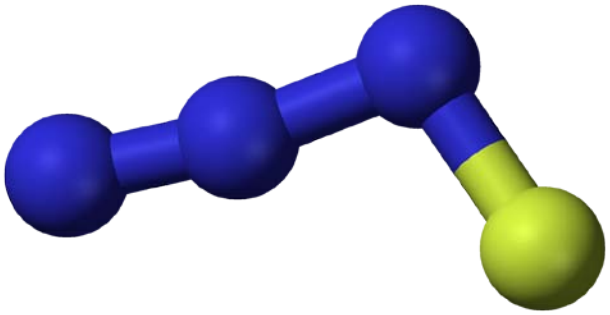

Fig. 1.3. HN_3, computer model

[Source of image: Gerloch, M., Constable, E.C., *Transition Metal Chemistry*, John Wiley & Sons-VCH, New York, **1994**, Fig. 4.22]

In these coordinated networks metal centers are bonded by ligands to form 1D magnetic chains. A second, lengthier and more rigid bridging ligand such as 4,4'-bipyridine (bpy) is then used to complete the metal coordination and to interconnect the parallel chains. The process results in 2D network structures. The intrachain metal-metal magnetic interactions constitute the primary cause for the magnetic ordering in these compounds, whereas interchain magnetic interactions are usually of secondary importance. Evidently, the magnetic properties of these coordinated networks are directly affected by the nature of the bridging ligand.

With the right combination of bridging ligands and metal ions, we aimed to create compounds with a magnetic structure that can be used as a practical tool for theoretical model testing of different magnets and condensed matter. In addition, relatively low ordering temperatures which are of the order of few K in case of these materials eliminate other interactions, such as phonons, and leave only the magnetic part considered in statistical physics. Potential real-life applications of these materials should not be underestimated. Low temperature of magnetic ordering of these materials is suitable for magnetic devices at extremely low working temperatures. We have used previously known data to investigate further magnetic properties of known compounds, with the possibility of producing additional entirely new coordinating networks of these families of compounds, with metal centers which were omitted in previous investigations. The primary aim was to study magnetic interactions of these ligands and their applicability in further research. The magnetic exchange interaction between ions in transitional metal complexes is of primary interest throughout the

dissertation. However, for a given cation-ligand-cation configuration the calculation of the magnitude of superexchange interaction to a reasonable accuracy remains a difficult task and is addressed in this study.

Previously published data established that exchange interactions are remarkably sensitive to the separation between the metal ion centers [ref. 16]. The metal ion centers involved into this research are M^{2+} where M=Fe, Co, Ni, and Cu. Because all of them are transitional metals with 3*d* orbital not completely filled and because their $\vec{L}$ quenched by the ligands' field, these metals represent very good test cases for spin only magnetism [ref. 13]. We describe the magnetic behavior of these compounds as a 1D chain, where metallic ions can interact ferromagnetically or antiferromagnetically. Theoretically, regardless if the nature, of interaction is ferro- or antiferromagnetic between constituent elements of these chains, of an ideal 1D chain does not order, as shown first by Ising [ref. 41]. However, in real solid material, the chains are never perfectly isolated from each other. Consequently, there are interchain interactions in addition to the dominant intrachain interactions, resulting in 3D spontaneous magnetic ordering at very low temperature. So from observed magnetic susceptibility, magnetization and specific heat data and using appropriate theoretical models we tried to explain magnetic behavior of studied metal-organic coordinated networks. These facts are addressed in more detail in chapter 4, which discuss the results of our experimental measurements.

1.3. A Note on Units, References, and Some Obstacles

The choice of units in magnetism presents a continual inconvenience in the field. Published materials in literature primarily use CGS (Gaussian) units, instead of SI of units. The CGS system has two crucial advantages: 1) the permeability of free space is one, and 2) the unit of magnetic field, the Oersted, has a very convenient size for the practical applications. For compatibility and convenience sake CGS system was used in this dissertation.

Moreover, theoretical and experimental physicists in the field of magnetism use not only different languages but also unrelated terminology. The seminal paper written by de Jongh, L.J. and Miedema A.R [ref. 20] is crucial in addressing this semantic problem. The very condensed but very useful review of theoretical accomplishments in theory of 1D magnetism, supplemented with extensive reference list written by Bonner, J.C. [ref. 10] provided important guidance in this dissertation, as well as a more recent but less comprehensive paper written by Blundell, S.J. [ref. 6].

Attempts to grow single crystals of the studied materials were made, however no sizable products could be obtained.

CHAPTER 2

THEORETICAL OVERVIEW

The goal of a theoretical physicist in the field of magnetism is to better understand the behavior of magnetic systems. Most of the progress in theoretical investigations results from the introduction of various lattice models, followed by the introduction, of different theoretical models of magnetic behavior. In this way, physicists have been able to obtain exact or approximate solutions for the behavior of thermodynamic quantities near phase transitions. Otherwise, these calculations would not be possible to work out due to the insurmountable mathematical problems associated with cooperative phenomena. These theoretical investigations led to the conclusion that the dimensionality of the lattice has a greater influence on the thermodynamic functions than does the particular lattice structure within given dimensionality. In this chapter only major theoretical contributions and their relevance to the magnetic properties of the studied families of metal-organic compounds are discussed.

2.1. Magnetic Effects in Atoms: Diamagnetism and Paramagnetism

On the atomic level, there are two responses to the application of external magnetic field: diamagnetism and paramagnetism.

Diamagnetic behavior is characterized by repulsion of the substance by an applied magnetic field. This behavior arises from the interaction of the applied magnetic field with the atomic and molecular orbitals containing paired electrons. With the exception of the hydrogen radical, all atomic and molecular materials show some diamagnetic behavior. Diamagnetic behavior is temperature independent, and the strength of the diamagnetic interaction in the material is roughly proportional to the molecular weight of the material in question described with the Pascal relationship:

$$\chi_m = \sum \left(n_i \chi_i + \lambda_i \right) \quad (2.1)$$

where χ_i are susceptibilities per gram of atom and λ_i are bonds in molecule.

Paramagnetism is characterized by the attraction of the substance by an applied magnetic field. This behavior arises as a result of an interaction between the applied magnetic field and unpaired electrons in atomic and molecular orbitals. Typically, paramagnetic materials contain one or more unpaired electrons, and the strength of paramagnetic interactions are temperature dependent. However, some substances exhibit temperature independent paramagnetism (TIP) (ref. 16) results from a coupling between the magnetic ground state and the non-thermally populated excited states, and it is usually associated with electrically conducting materials. In a paramagnetic

material each individual electron spin behavior is unaffected by its neighbors' spin conduct (Fig. 2.1). The spins of a paramagnetic material can easily be aligned by an applied magnetic field. However, this type of alignment is weak, and upon removal of the external magnetic field the system relaxes back to a random distribution of magnetic moments.

It should be emphasized that true paramagnetic materials are extremely rare.

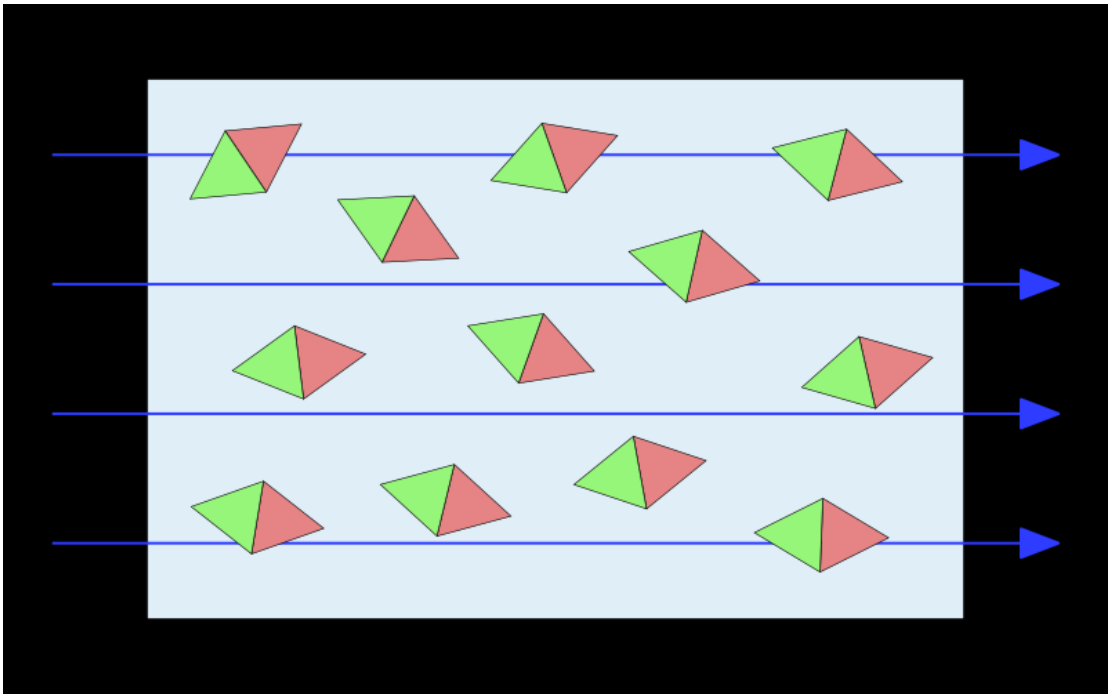

Fig. 2.1 Schematic representation of paramagnetic material

[Source of image: Miller, S.A., *Magnetic Interactions in Molecular Materials*, PhD Dissertation, California Institute of Technology, Pasadena, **1998**, Fig. 4]

2.2 The Types of Magnetism: Cooperative or Bulk Magnetism

Common usage the term magnetism refers to the so-called cooperative or bulk magnetism characterized by substances that at the atomic level exhibit temperature dependent paramagnetic behavior. At the atomic level the non-zero spin angular moment associated with an unpaired electron gives rise to a magnetic moment. In general, bulk magnetic properties arise as a result of long-range interactions between spins of these unpaired electrons.

Over fourteen different possible interactions of cooperative magnetism have been described in literature [ref. 67], but the four types of magnetic interactions for describing and understanding the cooperative magnetic behavior of the materials considered in this dissertation are: paramagnetism, ferromagnetism, antiferromagnetism, and ferrimagnetism [ref. 16, 46]. These classes of magnetic interactions describe how adjacent magnetic moments interact with each other at absolute zero in presence or in absence of an external magnetic field (Fig 2.2).

2.2.1. The Types of Magnetic Interactions: Ferromagnetism

Ferromagnetism is characterized by parallel alignment of adjacent magnetic spins that results in a very large net magnetic moment (Fig 2.2, section B). Ferromagnetic alignment of adjacent magnetic spins occurs rarely in nature, since it can only be achieved if there is zero quantum mechanical overlap between the spin-

containing orbitals. In this case alignment of the spins, which correlates electron motions and thus minimizes electron-electron repulsion, is the most stable state. At macroscopic level unlike paramagnets, ferromagnets exhibit a net magnetic moment in the absence of an applied external magnetic field below ordering temperature.

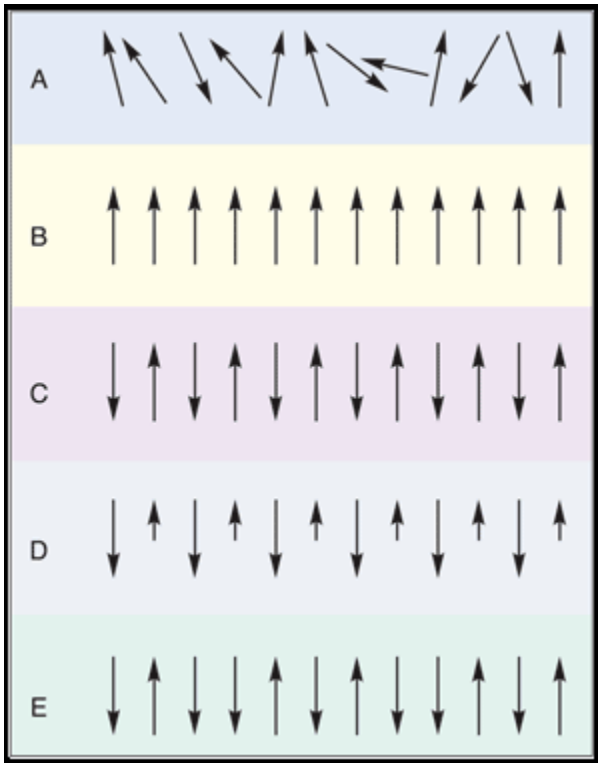

Fig. 2.2. Schematic representations of different types of corporative behavior [Source of image: Skomski, R., *Simple Models of Magnetism*, Oxford University Press, Oxford, **2008**, Fig. 3.4]

2.2.2. The Types of Magnetic Interactions: Antiferromagnetism

In the case of an antiferromagnetic compound, adjacent magnetic spins are aligned antiparellel, which results in a material with no net magnetic moment. We can think of an antiferromagnetic material as comprised of two sublattices in which the magnetic ions order ferromagnetically, but these two sublattices have opposite orientation of their respective spins (Fig 2.3, section C). At temperature absolute zero, the antiferromagnets exhibit a diamagnetic response to an applied external magnetic field. The alignment of spins antiferromagnetically is analogous to the bonding spin-containing orbitals and is thus energetically favorable. Antiferromagnetism is the most commonly observed bulk magnetic behavior. Long-range antiferromagnetism is even exhibited by materials that locally order ferromagnetically.

2.2.3. The Types of Magnetic Interactions: Ferrimagnetism

Ferrimagnetism can be considered as a special case of antiferromagnetism, where the magnetic material consists of a lattice of rigidly alternating spins of different magnitudes (Fig 2.2, section D). As in the case of regular antiferromagnetism, the adjacent magnetic spins align antiparellel. However, since the adjacent spins are of different magnitudes, the material exhibits a net magnetic moment in the absence of an applied magnetic field. This kind of magnetic ordering is very common when two or more different types of magnetic ions are involved in the magnetic compound.

2.3. Inorganic and Organic Magnets

The most common magnetic materials are two- and three-dimensional arrays of inorganic atoms composed of transition metal or lanthanide metal containing spin units. These materials are typically produced at very high temperatures using the metallurgical methodologies. In contrast to these traditional magnetic materials, molecular magnets are organic or inorganic/organic hybrid materials, composed of either metal containing spin units or organic radical containing spin units. Magnetic compounds that consist only of organic radicals have very limited use, and their transition temperatures are rather very low. An alternative strategy to enhance the magnetic characteristics and interactions of compounds in question is to use transition metal or rare earth ions to provide the magnetic center. Organic groups, otherwise called ligands, provide the bridges between these centers and mediate the magnetic interactions between metallic ions. These magnetic metal-organic compounds can be constructed by linking transition metal ions in chains using bridging ligands with a large intrachain exchange constant *J*, which is the measure of the interaction between metallic centers. It is important that the ligands in interchain direction be either bulky or do not transmit exchange interactions very efficiently.

The extensive theoretical investigations have helped understand why metal-organic compounds allow low temperature synthesis of magnetic materials [ref. 28, 45, 55, 60, 61]. Extensive production of these coordinated networks is one of the most active areas of today's material science and chemistry. The intense interest in the

organometalic coordinated materials is driven to a large extent by their physical and chemical properties with great potential in various applications, such as magnetic devices [ref. 28, 45, 55, 60, 61], electrical conductivity [ref. 16, 28, 45, 46, 55, 60, 61], photomechanism [ref. 28, 45, 55, 60], host-guest chemistry, ion exchange, shape specificity [ref. 28, 45, 55, 60], catalysis agents [ref. 28, 45, 55, 60], high-temperature, and flame-resistant fibers. Even if the observed magnetic compound, does not order magnetically, it may exhibit bistability and hence be surprisingly useful in applications such as memory materials. A spectacular example of this bistability is the spin crossover effect, sometimes known as a spin transition. Because their properties can be anticipated and engineered using new experimental approaches, organometallic materials with very low ordering temperatures are also used as efficient and relatively inexpensive testing tools for various fundamental theories of the condensed state.

2.4. The Molecular Field Theory (MFT)

Pierre Weiss proposed an important early theoretical model in magnetism. In 1907, Weiss introduced the concept of a molecular field or *mean* field, analogous to van der Waals' theory of nonideal gases. In 1930, Weiss wrote [ref.68]:

'In 1895, in his famous memoire "On the Magnetic Properties of the Bodies at Various Temperatures", Pierre Curie gave the first experimental study of the magnetization of a ferromagnet, iron, as a function of field and temperature. He concluded from the curves that he obtained, that "by analogy with the hypothesis about fluids, the rapid increase of magnetization occurs when the magnetic intensity of the particles is sufficiently strong to permit them to interact." But he also cautions against attaching too much importance to this similarity. There seems to be no reason to doubt the truth of Pierre Curie's idea, nor that are many aspects of paramagnetism to ferromagnetism what perfect gases are to dense fluids. The theory of the molecular field is an outgrowth of this idea…theory is modeled on van der Waals concept of internal pressure, yet different…'

The main idea of the theory is that the interactions, of known or unknown origins, all add to provide a single molecular field H_m, such that the total field acting on each spin is the sum of the molecular field H_m plus any external, field H applied to the sample. The equation for determining H_m is constitutive equation of mean field theory (MFT).

Weiss' guess, without detailed microscopic justification, is that H_m is proportional to the magnetization:

$$H_m = \lambda M \quad (2.2)$$

where λ is called the Weiss field constant and M is magnetization of the material.

In this dissertation we restrict ourselves to the temperatures above T_c (Curie temperature), so that the total magnetic field H_T acting on the sample is the sum of H_m and the external field H_{ext}.

$$H_T = H_{ext} + H_m \quad (2.3)$$

The magnetic susceptibility is, then:

$$\frac{M}{H_T} = \frac{M}{(H_{ext} + \lambda M)} = \frac{C}{T}$$

$$\chi = \frac{M}{H_{ext}} = \frac{C}{(T - \lambda C)} \quad (2.4 \text{ and } 2.5)$$

When H_{ext}=0, M is not zero at T_c, because of existence of H_m, under these conditions T_c=λC and then susceptibility is in that case:

$$\chi = \frac{C}{(T - T_c)} \quad (2.6)$$

which is the Curie-Weiss law. This formula applies only for T>T_c and usually has form:

$$\chi = \frac{C}{(T - \theta)} \quad (2.7)$$

Magnetization of the paramagnet can be described by:

$$M = Ng\mu_B JB_J(\eta)$$

$$\eta = g\mu_B H_T / k_B T \quad (2.8, 2.9, \text{ and } 2.10)$$

$$B_J(\eta) = (\frac{J+1}{3})\eta$$

J here is total angular momentum and $B_J(\eta)$ the Brillouin function.

The discontinuity of C and the divergence of χ at T_c are the principal results of the MFT [ref.68]. This is an example of a second-order phase transition, in which the system changes continuously, from an ordered magnetic phase below T_c to a disordered phase above T_c.

The discovery of antiferromagnetic materials tested the very foundations of MFT, for it introduced a geometrical, internal structure and the breaking of homogenous, isotropic symmetries of the Weiss field. Following the discovery of these materials other magnetic materials were found. Spiral, canted, triangular magnetic structures were found by neutron scattering and other experiments. Van Vleck observed that:

'There is one class of materials known as "antiferromagnetic" in which it is quite clear that suppression of paramagnetism is to be indentified with the exchange coupling. These substances have susceptibility which passes a maximum as the temperature is raised. This is explained theoretically in the following way. Suppose we have crystal whose constituent atoms can be resolved into two sublattices A and B such that the nearest neighbors of the atoms A are B and vice versa. The simple-cubic and body-centered cubic lattices are both of this type. With a negative exchange integral (connecting nearest-neighbors) the exchange energy of two atoms is a minimum if their spins are antiparellel. Hence the configuration of the deepest energy of the crystal as whole is that in which the spins of sublattice A all point northward, and those of B all southward and vice versa' [ref. 71].

This molecular field originates in the microscopic forces, which are quantum-mechanical in nature, but come in various guises depending on the specific mechanisms of electron transport in the solid. Generally, the interactions are quite short-ranged. Therefore, taking into account nearest and next nearest neighbor forces is enough for theoretical considerations.

However, there are other two types of long-ranged interactions. The first interaction is the dipole-dipole electromagnetic force-weak, long ranged, and

anisotropic. The second long-ranged interaction is the Rudeman-Kittel-Kasuya-Yoshida (RKKY), also in literature known as indirect-exchange mechanism [ref. 67]. The RKKY is operative only in metals and it is generally oscillatory. Long-ranged consequences of the interactions are: 1) the shape of the sample contributes to the overall energy, and 2) the ordering creates magnetic domains in ferromagnetism. The long-ranged ordering has no effect in: 1) causing a phase transition, and 2) bearing on the other magnetic structures: antiferromagnetic, spiral, spin-glass.

Qualitatively, this is what is happening. At high temperatures, the paramagnetic spins are uncorrelated, which means that their relative spin orientations are completely random. Seen from that perspective, the paramagnet is the magnetic analogue of an ideal gas. Just as intermolecular interactions become more important in a gas as the temperature is lowered towards the boiling point or the pressure is increased, a magnetic interaction becomes more important as k_BT decreases and becomes comparable to the exchange constant J. These short-range correlations among the magnetic moments start to appear even above $T_{c,}$ and this is called short-range order. However, most of these considerations are not applicable in the low-temperature range used for the examination of selected compounds in this dissertation. Therefore, we considered the MFT only for temperature ranges above 80K.

Clearly, the deficiencies of the Molecular Field Theory are even more evidently exposed in systems of the low dimensionality. The experimental results for 1D and 2D systems prompt new explanatory models. Moreover, the shortcoming of MFT results from the introduction of the effective field, which replaces interactions of the magnetic moment with its neighbours by an average interaction taken over the

whole magnetic system. Therefore, by studying the correlations of the given reference spin and its neighbours we can get more accurate information about magnetic structure of the compound that we observe [ref. 20].

2.5. Magnetic Models

Theoretical results for models such as the Heisenberg, Ising and XY models, offer better understanding of the ordering at low temperatures, in the compounds we studied. Our preliminary experimental results corresponded to Heisenberg model and its variants as well as to the Ising model and its variants. However, the XY model failed to fit the experimental data with any statistical significance. That is why the XY model is not considered in this thesis in more detail.

2.5.1. Heisenberg Model of a Magnet

The effective spin Hamiltonian in the Heisenberg model is of the form

$$H = -2J\sum_{i=1}^{N}(aS_i^z S_{i+1}^z + bS_i^x S_{i+1}^x + cS_i^y S_{i+1}^y) \quad (2.11)$$

We assume bilinear spin couplings, between nearest-neighbor spins only. The effective exchange constant is J multiplied for spin couplings in different directions by factors *a*, *b*, and *c*. The Ising model is obtained by putting *b*=*c*=0, or by having any two of these factors equal to zero. The XY model is obtained by setting *a*=0 or in general by letting any one of factors equal to zero. If *a*=*b*=*c*, there is complete

rotational symmetry in spin space, and the Heisenberg model may be written in vector form:

$$H = -2J\sum_{i=1}^{N}\overrightarrow{S_i}\cdot\overrightarrow{S_{i+1}} \quad (2.12)$$

If J>0, the spins lower their energy by aligning parallel, resulting in a Heisenberg ferromagnet. If J<0, the antiparellel spin alignment is favored, resulting in an antiferromagnet. If *a*, *b*, and *c* are not equal, spin anisotropy prevails. In the case of *a*>*b*=*c*, there is a uniaxial (easy axis) anisotropy. Then again, if *a*<*b*=*c*, planar (easy plane) anisotropy results. The magnitude and type of anisotropy in the effective spin Hamiltonian results from crystal field effects introduced by ligands which are part of the compound in question. The effects of an applied magnetic field can be represented by the addition of Zeeman term of the form $-g\mu_B H\cdot\sum_i\overrightarrow{S_i}$ to the Hamiltonian given above. Crystal field effects corresponding term $\Delta\sum_i(S_i^z)^2$. Finally, the spin value may range over $1/2\leq S\leq\infty$.

The static properties commonly measured by experimentalists are the susceptibility χ, the specific heat at constant field c_H, and magnetization isotherms as a function of the applied field, M_T vs. H. These experimental data can be compared with theoretical information function for the major magnetic models: Ising, Heisenberg, and XY.

The effects of magnetic dimensionality are now reasonably well understood, quantitatively and qualitatively. These three major factors – dimensionality, spin, and

model variation – are essential in identifying the magnetic model. These factors also underline experimental results on, preferably, more than one of static properties.

1D magnets are, by definition, low-dimensional and have broad maxima in magnetic specific heat and in susceptibility. These maxima do not correspond to cooperative long-range-order (LRO) transitions. For the short-range interactions, nearest-neighbor forces at $T_c=0$ cause ordering for ideal one-dimensional systems. At relatively small T_c (<5K), these forces cause ordering for 'good' 1D systems. The broad maxima consequently correspond to short-range-order (SRO).

It is commonly understood that 3D magnetic systems show $T_c>0$ phase transitions whereas 1D systems show no phase transition [refs.7, 67]. However, even in 1D theoretical models, if magnetic interactions become sufficiently long-ranged, $T_c>0$, the system can order. In the case of 'real' one-dimensional magnetic systems, weak interchain interactions ultimately result in a three-dimensional cooperative ordering anomaly. This anomaly occurs at a lower temperature than the characteristic 1D rounded maximum in a 'good' 1D example. This phenomenon was exactly demonstrated by Onsager in the 2D net Ising with unequal 'horizontal' and 'vertical' exchange constants [ref. 73].

2.5.2. The Ising Model and Its Variants

The purely classical Ising model of magnetism, in contrast to a quantum mechanical spin model has significant limitations in explaining static and dynamic magnetic phenomena, especially in three dimensions [ref. 68, 73]. The entropy

argument is crucial since an ideal Ising chain, which does not order even at T=0K, would necessarily acquire all its entropy of ordering above T_c. A typical Hamiltonian includes the interactions of all pairs of spins assumed to be at points of a regular lattice. Nevertheless, the Ising model is applicable in low-dimensional systems, when it is exactly solvable. Moreover, because of the established relevance of Ising model to MFT, it was possible to use specific configurations of the model for examining 1D metal-organic compounds in this dissertation. Last, but not least, exact or very accurate numerical results obtained in one dimension, are always good testing grounds for approximate techniques used in 3D and many-body cooperative phenomena.

In Ising model, a spin S_i=+1 or S_i=− 1 is assigned to each of N sites on the fixed lattice. The spins which are situated on the vertices of the lattice interact with one another by the means of bonds with energy of J_{ij}. In addition, the spins can interact with external fields H_i of arbitrary strengths. The total energy is given by:

$$E = -\sum J_{ij} S_i S_j - \sum H_i S_j \quad (2.13)$$

In the most familiar version of the Ising model, the interactions are limited to nearest-neighbors on the lattice, and the magnetic filed is homogenous, H_i=const.

The Ising model was proposed by Lenz in 1920 [ref. 58, 66, 74, 85]. Lenz's student Ising gave the calculation for one-dimensional chain only of this microscopic theory as part of his PhD dissertation [ref. 10]. The results were not encouraging, because they did not reveal ordering above the absolute zero of temperature. The ground state corresponds to all spins parallel, yet the long-range order disappears at

any finite temperature. Thus, despite the nearest-neighbor bonds, this model displays only paramagnetic behavior at finite T. Ising addressed the problem:

> *'At that time Stern and Gerlach were working in the same institute on their famous experiment, on the space quantization. I discussed the results of my paper widely with Prof. Lenz and Dr. Wolfgang Pauli, who at that time was teaching in Hamburg. There was some disappointment that the linear model did not show the expected ferromagnetic properties.'* [ref. 68]

The phase diagram of the lattice gas has been obtained by Lee and Yang in two papers [ref. 71, 99, 100], based on the large amount of information from 2D Ising model. The equation of state they obtained gave the mixed phase region correctly. Lee and Yang drew attention to the importance of extending the model parameters, such as the external field, into the complex plane. Their study of the zeroes of the partition function in complex fields created a new tool for the study of phase transitions. However, Lee and Yang were not the first to treat the Ising model of magnetism within a unified formalism.

Peierls recognized that ferromagnetism, order-disorder transformations in alloys, and the very existence of phase transitions in the microscopic theory could all be reduced to the examinations of Ising model in 2D or 3D, but not in one [ref. 71, 74]. Peierls contributed an important theorem that in 2D or higher, there is long range order at sufficiently low temperature. Conversely, long range order is known to disappear above some critical temperature, when there is a sufficient thermal disorder. Therefore, Peierls established the relevance of the Ising model to the Curie problem.

By the early 1960s a variety of one-dimensional magnetic insulator models developed. Fisher demonstrated a very simple analytical solution for the classical spin ($S=\infty$) linear chain in $H=0$ [ref. 26]. The solution yielded both thermal properties and

correlation functions [ref. 26] and remains popular theoretical model among experimentalists. The one-dimensional XY model with the spin S=1/2 was solved analytically with the emphasis on correlation functions by Lieb, Shultz, and Mattis independently [ref. 58]. Katsura solved the model with the emphasis on the thermal and magnetic properties [ref. 47]. Katsura's solution included exact results for one dimensional Ising model. An analytical solution for S=1/2 Heisenberg linear chain is still not available, though important progress has been made [ref. 6].

Bonner and Fisher developed a technique of numerical extrapolation of exact results for sequence of finite Heisenberg chains of increasing N to the N=∞ limit [ref. 9]. This approach remains one of the most used models by the experimentalists in the field of magnetism. Other important results for the S=1/2 Heisenberg chains are analytical calculations by des Cloizeaux and Pearson [ref. 22] and an analytic result for the zero-point susceptibilities by Griffiths [ref. 34]. The relevance of these theoretical solutions to real experimental systems was demonstrated for the first time by Griffiths in conjunction with the Kamerlingh Onnes Laboratorium in Leiden, the Netherlands [ref. 10]. With this interpolation of theoretical and experimental work, great interest in one-dimensional magnets continues until today.

It is known that metallic centers Co^{2+} are anisotropic in octahedral symmetric surrounding and, furthermore, Fe^{2+} and Ni^{2+} are also mentioned as Ising-like materials [ref. 20]. However, in these materials the crystalline field anisotropy and magnetic interaction are often of the same order of magnitude. As a consequence at high temperatures Fe^{2+} and Ni^{2+} compounds behave like Heisenberg compounds with S=2 and S=1, respectively. At low temperatures, Fe^{2+} and Ni^{2+} compounds become

strongly anisotropic. Considering this behavior of the mentioned transitional metal ions, the comparison with the theoretical models is more difficult [ref.20]. Therefore, the effective spin quantum number is considered as temperature dependent. That is why many of the compounds having these two metal ions may be described by Ising model as far as their low temperature part ($T<T_c$) behavior is concerned. The critical behavior may be also described within the boundaries of the Ising model.

Coupled with the results from the PXRD, we conclude that there is strong anisotropy in crystal structure which allows the usage of the Ising model with necessary modifications. Preliminary measurements performed on some of the compounds such as MCl_2(4,4'bipyridine) showed that they exhibit metamagnetic behavior. This metamagnetic change is closely connected with rather pronounced anisotropy in the material in question. The measurements again point to the applicability of a modified Ising model for describing magnetic structure. The metamagnet must have significant ferromagnetic interactions, even though the overall magnetic structure is antiferromagnetic [ref. 16].

To the best of our knowledge, the first attempt to deal with Ising chain statistics under the existing H_{ext} was published by K. Takeda and M. Wada in 1980 [ref. 90]. In this dissertation we followed similar approach. We use Ising Chain statistics to explain magnetic behavior of M(ox)(4,'4bipyridine). We use Heisenberg linear chains to characterize MCl_2(4,4'bipyridine) and $M(N_3)_2$(4,'4bipyridine) families of compounds. The adopted magnetic models respond to real systems with large amounts of short-range order that eventually undergo long-range-order at low temperature. No matter how small the deviation from ideal system may be, eventually

it becomes important enough to cause 3D transitions. Any interaction between chains no matter how weak will cause such a transition. In other words, any anisotropy in real metal-organic compounds will cause long-range order. Nevertheless, the very nature of the ordered state when it is derived from a set of formerly independent linear chains generally differs from the usual 3D examples.

2.6. Theoretical Magnetic Models Used to Explain Magnetic Behavior of the Studied Compounds

2.6.1. The Choice of the Model

The PXRD measurements and initial fittings at high temperature range above T=80 K for all three families of coordinated networks that we studied suggest a predominant interaction between metallic ions along one direction. In the case of MCl_2(4,4'-bipyridine) that direction is along *c*-direction, for M(ox)(4,4'-bipyridine) predominant direction is along the *a*-axis, and finally for $M(N_3)_2$(4,4'-bipyridine) again along the *c*-direction. The fact that distances along the next closest directions are almost 2.5-4 times longer than *c*, *a*, and *c* directions, respectively, initiated a choice of a theoretical model of quasi-1D chains. These quasi-1D chains interact among themselves only very weakly at very long temperatures and eventually lead to the ordering of these metal-organic magnetic compounds.

The experimentally measured susceptibility of linear chains with anisotropic coupling as those we studied is conventionally explained with the Bonner-Fisher

theoretical model for linear chains [ref. 9]. The Bonner-Fischer model is quite often used as a theoretical model by experimentalists. Martin J.D. at al. [ref. 64] have already used this theoretical approach to approximate their compounds with weakly interacting magnetic linear chains. Additionally, ligand bridges in the compounds, which Martin J.D. at al. studied, are Cl. In MCl_2(4,4'-bipyridine), which we studied, Cl is also a bridging ligand, which makes this choice of theoretical model reasonable. Furthermore, the best documented examples of chain compounds with an Ising behavior are certain Co(II) derivates [ref. 10, 16, 46]. Therefore, we used the Bonner-Fisher theoretical model [ref. 46] for our studied families of compounds.

In the Bonner-Fisher theoretical model the magnetic ions are arranged in chains with strong interactions within chain but rather weak between chains. Except at the lowest temperatures ranging from few mK to 30 K, depending on the material studied, the chains should be almost independent. Theoretical predictions based on the one-dimensional model may be directly compared with experimental measurements. The Bonner-Fisher one-dimensional model is similarly valid for magnetically active polymeric molecular chains. First, it was derived for the finite chains and rings. Second, the infinite length approximation is used. The Hamiltonian that describes this system with the spin S=1/2 of weakly interacting chains has the form:

$$H = -2J\sum_{i=1}^{N}\{S_i^z S_{i+1}^z + \gamma(S_i^x S_{i+1}^x + S_i^y S_{i+1}^y)\} - g\mu_B\sum_{i}^{N}\vec{H}\vec{S}_i \quad (2.14)$$

In the Hamiltonian γ assumes values between 0 and 1. In the case of total anisotropy, γ=0, while the case of total isotropy γ=1. The magnetic parallel

susceptibility in respect to the external magnetic field for linear antiferromagnetic chains derived from this Hamiltonian is of the form:

$$\chi_{II}(\gamma=0)=\frac{g^2\mu_B^2 N}{4k_B T}e^{-|J|/(k_B T)}\left(\frac{1-(-\tanh K)^N}{1+(-\tanh K)^N}\right) \quad (2.15)$$

K is defined as:

$$K=\frac{|J|}{2k_B T} \quad (2.16)$$

This is the case when N is close or equal to Avogadro's number N_A. The parallel magnetic susceptibility has a somewhat simpler form

$$\chi_{II}(\gamma=0)=\frac{g^2\mu_B^2 N}{4k_B T}e^{-|J|/(k_B T)} \quad (2.17)$$

The perpendicular magnetic susceptibility is given by:

$$\chi_{\perp}=\frac{g^2{\mu_B}^2 N}{4|J|}\left(\tanh K+K\sec h^2 K\right) \quad (2.18)$$

In the case γ=0, *K* is already defined with the equation (Eq. 2.16). Quite generally this parallel magnetic susceptibility can be written as:

$$\chi_N(T)=\frac{g^2\mu_B^2 N}{4k_B T}\xi_N(T) \quad (2.19)$$

Where we have:

$$\xi_N(T)=\frac{4}{N}<(\sum_{i=1}^{N}S_i^2)^2> \quad (2.20)$$

The angular brackets indicate thermal average. In the limit case $N\to+\infty$, $\xi_N(T)$ diverges for all values γ as $T\to 0$. For Ising chains the divergence is exponentially fast, as:

$$\xi(T) = e^{\frac{J}{k_B T}} \quad (2.21)$$

Then again, in the limit $N \to +\infty$ perpendicular magnetic susceptibility $\chi_\perp$ is $\chi_\perp = \chi_0$. Since our compounds are in the form of polycrystalline powder standard procedure is to find total magnetic susceptibility of the sample in the following form [ref.2]:

$$\chi = 0.33\chi_{II} + 0.67\chi_\perp \quad (2.22)$$

In the experiments the exact ratio of these two different susceptibilities was determined on the case by case basis for each compound that is examined. In our research, typically parallel susceptibility has greater percentage than theory predicts. This question is addressed within the discussion of the studied compounds fitted in the theoretical Bonner-Fisher model.

In our experimental work, furthermore, the symbols parallel and perpendicular in the susceptibilities refer to the external (measuring) magnetic field direction with the respect to the direction of spin-quantization or alignment within chains, rather than to the chemical or structural arrangement of the chains. For the most of the examples of the compounds studied, the spins assume an arrangement perpendicular to the chain direction [ref. 16, 17, 31, 46]. The widely accepted explanation for such behavior is dipole-dipole interaction.

In the case of total isotropy described by Heisenberg quantum model, the antiferromagnetic susceptibility is

$$\chi = \frac{N_A g^2 \mu_B^2}{k_B T} \frac{2.0 + 0.0194x + 0.777x^2}{3.0 + 4.346x + 3.2322x^2 + 5.834x^3} \quad (2.23)$$

$$x = \frac{|J|}{k_B T} \quad (2.24)$$

Ferromagnetic susceptibility in the case of total isotropy for the ion with total spin *S*=1/2 is

$$\chi = \frac{N_A g^2 \mu_B^2}{k_B T}\left(\frac{1.0 + 5.79799x + 16.902653x^2 + 29.376885x^3 + 29.832959x^4 + 14.036918x^5}{1.0 + 2.7979916x + 7.0086780x^2 + 8.6538644x^3 + 4.5743114x^4}\right)^{2/3} \quad (2.25)$$

$$x = \frac{|J|}{k_B T} \quad (2.26) \text{ (ref.1)}$$

This formula is only applicable for $Cu(N_3)_2$(4,'4-bipyridine) of all our compounds in the family $M(N_3)_2$(4,4'-bipyridine). For other compounds that we have studied we applied classical spin calculation approach which was developed by Fisher [ref. 26], because all chlorides and the rest of azides exhibited ferromagnetic behavior in our measurements. Moreover, chlorides and azides have larger spin numbers (*S*=1, 1.5, 2). Therefore ferromagnetic susceptibility only in the case of total isotropy for the ion with total spin *S*=1/2 is unacceptable. This new formalism was scaled to the total spin *S*=5/2 (ref. 22). The magnetic susceptibility is given by:

$$\chi = \frac{N_A g^2 \mu_B^2 S(S+1)}{3k_B T}\frac{1+u}{1-u} \quad (2.27)$$

where *u* is:

$$u = \coth\left(\frac{JS(S+1)}{k_B T}\right) - \left(\frac{k_B T}{JS(S+1)}\right) \quad (2.28)$$

Though this approach is valid for high spins which are close to the classical, we applied it to $Cu(N_3)_2$(4,'4-bipyridine) in order to compare it with the quantum

mechanical approach for this compound. By using the statistical analysis we have concluded that Fisher Classical Spin model is applicable in the case of $Cu(N_3)_2$(4,'4-bipyridine). Indeed, in 'real' 1D systems weak inter-chain interactions will ultimately result in three-dimensional cooperative ordering anomalies, which are situated at lower temperature than the characteristic one-dimensional maximum. This is the case with the materials of all three families that we have examined – MCl_2(4,4'-bipyridine), M(ox)(4,4'-bipyridine), and $M(N_3)_2$(4,4'-bipyridine).

2.6.2. The Jahn-Teller Effect

One of our main goals was to determine the type of symmetry of the local environment of each one of metallic ions in the studied compounds in order to deduce magnetic properties of each network. Sometimes, however, the magnetic properties of the observed material can influence the symmetry of the local environment. It can be energetically favorable for a complex molecule with octahedral symmetry to spontaneously distort because the energy cost of increased elastic is balanced by the electronic energy saving due to the distortion. Such an effect is known in literature as the Jahn-Teller effect [ref. 7].

Theoretically, in complex metal-organic molecules the distortion of the system can be quantified by a parameter Q, which denotes the distance of distortion along an appropriate normal mode coordinate. The distortion gives rise to an energy cost which is quadratic in Q and thus can be written in the form

$$E(Q) = \frac{1}{2} M\omega^2 Q^2 \quad (2.29)$$

where M and ω are, respectively, the mass of the anion and the angular frequency corresponding to the particular normal mode. Clearly, the minimum distortion energy is zero, and it is obtained when Q=0 (case of no distortion).

The distortion also raises the energy of certain orbitals while lowering the energy of others. If all the orbitals are either completely full or completely empty, the Jahn-Teller effect is not significant for our investigations. However, in the cases of partially filled orbitals, Jahn-Teller effect can have high, significance because the observed system can have a net reduction in total energy.

The electronic energy dependence on Q can be rather complicated, but it can be calculated as Taylor series in Q. In the case when the distortion is small, it is mathematically legitimate to keep only the term of the expansion which is linear in Q. The energy of the given orbital has a term either AQ or $-AQ$ corresponding to the rising or lowering of the electronic energy, where A is a suitable constant, supposed to be positive. Then, the total energy $E(Q)$ is the sum of the electronic energy and the elastic energy:

$$E(Q) = \pm AQ + \frac{1}{2} M\omega^2 Q^2 \quad (2.30)$$

here the two possible choices of the sign of the AQ term give rise to two separate energy curves. If we consider only energy curve we can find minimum energy for the orbital in question using:

$$\frac{\partial E}{\partial Q} = 0 \quad (2.31)$$

which yields a value of *Q* given by:

$$Q_0 = \frac{A}{M\omega^2} \quad (2.32)$$

so that:

$$E_{\min} = -\frac{A^2}{2M\omega^2} \quad (2.33).$$

If only that one orbital is occupied, then the system saves energy by spontaneously distorting.

This is known in theory as a static Jahn-Teller effect [ref. 7]. In a static Jahn-Teller model the distortion which can occur spontaneously is fixed on a particular axis of an octahedron. In reality, the distortion can switch from one axis to another at higher temperatures, giving rise to a dynamic Jahn-Teller effect [ref. 7], which we also considered in out investigations. Yet another effect is the cooperative Jahn-Teller transition [ref. 7]. It happens below a certain critical temperature, which depends on the compound, and corresponds to as Jahn-Teller distortion a throughout the crystal. The cooperative Jahn-Teller transition usually is seen in lanthanide complexes, and thus, is not relevant to our study.

The Jahn-Teller effect most often occurs in compounds with Cu(II) as a metallic ion. This ion has one unpaired electron in any kind of geometry, hence in the octahedral case too [ref. 2]. However, this ion rarely occupies a site of high symmetry. In the case of octahedral complexes, two trans-ligands are frequently found substantially further from metal than the remaining four ligands. Similarly, the dynamic Jahn-Teller effect has been frequently reported in magnetic investigations of Cu compounds at low temperatures [ref. 16]. Although less frequently, other

transitional metals also show noticeable Jahn-Teller behavior [refs. 16, 46]. Therefore, we also tried to examine the Jahn-Teller effect and its implications on the magnetic structure of our studied complexes, as discussed in the chapter 4 of this dissertation.

CHAPTER 3

EXPERIMENTAL TECHNIQUES

3.1. Sample Préparations

A promising hydrothermal route has been applied to the synthesis of metal coordination networks. [ref. 28, 55, 60, 61] Although the method is well-known to promote crystal growth and has been widely adopted in the preparation of many solid-state inorganic materials, it is relatively unexplored in the synthesis of coordination compounds. It has been shown that hydrothermal reactions often produce metastable compounds that may otherwise not be accessible by other synthesis methods. [ref. 61] This synthesis method was applied in making of chloride and oxalate compounds. It is also learned in the previous investigations of our metal organic coordinated networks that compounds generated under supercritical conditions are often very difficult to obtain by conventional solution synthesis. [ref. 28, 55, 60, 61] Production of azides used this conventional approach in solution synthesis where it has shown results only after numerous trials, thus proving that it is less efficient and reliable method in synthesis of coordination networks.

3.1.1 Compound Synthesis: MCl_2(4,4'-bipyridine)

Synthesis of $FeCl_2$(4,4'-bipiridine): Brownish crystals of $FeCl_2$(4,4'-bipiridine) were obtained from reactions of $FeCl_3$ (0.1622 g), $H_2C_2O_4 \cdot 2H_2O$ (0.1261 g), bpy (0.1562 g) and H_2O (5 mL) in the mole ratio 1:1:1:278. The reactions were carried out in 23 mL acid digestion bomb at temperature of 170 ^oC for 7 days (Fig. 3.1). The product was then washed with water and acetone and then dried in air.

Fig. 3.1. Bombs that are used in hydrothermal route for production of compounds [Source of image: Danilović, D.]

Synthesis of $CoCl_2$(4,4'-bipiridine): Pale pink-purplish crystals of $CoCl_2$(4,4'-bipiridine) were produced using a stoichiometric mixture of $CoCl_2$ (0.1298 g) and bpy

(0.1562 g) in H_2O (5 mL) in the mole ratio 1:1:444. The production procedure is then identical like in the case of $FeCl_2$(4,4'-bipiridine).

Synthesis of $NiCl_2$(4,4'-bipiridine): Pale green-yellowish crystals of were obtained from reactions of $NiCl_2$ (0.1296 g), and bpy (0.1562 g) and H_2O (4 mL) in same mole ratio like $CoCl_2$(4,4'-bipiridine), using the same production procedure for all chlorides.

3.1.2. Compound Synthesis: M(ox)(4,4'-bipyridine)

Synthesis of Fe(ox)(4,4'-bipiridine): Red crystals of Fe(ox) (4,4'-bipiridine) were isolated from reactions $FeBr_2 \cdot 6\ H_2O$ (0.1618 g), bpy (0.0781 g), oxalic acid (0.0630 g) and H_2O (4 mL) in mole ratio 1:1:444. The reactions were carried out in 23 mL acid digestion bomb at temperature of 170 ^oC for 7 days. The product was then washed with water and acetone and then dried in air.

Synthesis of Co(ox)(4,4'-bipiridine): Orange crystals of Co(ox)(4,4'-bipiridine) were produced in reaction of $CoBr_2 \cdot 6\ H_2O$ (0.1638 g), bpy (0.0781 g), oxalic acid (0.0630 g) and H_2O (4 mL) in the same mole ratio and using same production procedure like in the case of Fe(ox) (4,4'-bipiridine).

Synthesis of Ni(ox)(4,4'-bipiridine): Light blue crystals of Ni(ox)(4,4'-bipiridine) were grown from a hydrothermal reaction containing $NiBr_2 \cdot 3\ H_2O$ (0.2665 g), bpy (0.1562 g), oxalic acid (0.1260 g) and H_2O (8 mL) in the same mole ratio and using same production procedure like in the case of Fe(ox) (4,4'-bipiridine).

Synthesis of Zn(ox)(4,4'-bipiridine): Colorless transparent crystals of Zn(ox)(4,4'-bipiridine) were obtained from reactions of $ZnCl_2$(0.1363 g), bpy(0.1562 g), sodium oxalate (0.1340 g) and H_2O (8 mL) in the same mole ratio and using same production procedure like in the case of Fe(ox) (4,4'-bipiridine).

3.1.3. Compound Synthesis: $M(N_3)_2$(4,4'-bipyridine)

Synthesis of $Fe(N_3)_2$(4,4'-bipiridine): Brown polycrystals were obtained combining bpy (0.1562 g) in methanol (10 mL) with aquenous solution (20 mL) of $FeCl_2 \cdot 4\ H_2O$ (0.1988 g). This mixture was stirred for 5s before aquenous solution (20 mL) of NaN_3 (0.1300 g) was added. After additional 5s of stirring mixture was filtered and treated with anhydrous ether.

Synthesis of $Co(N_3)_2$(4,4'-bipiridine): Pale pinkish polycrystals were produced by adding aquenous solution (20 mL) of $CoCl_2 \cdot 6\ H_2O$ (0.2379 g) to solution of bpy(0.1562g) in methanol (10 mL). Then, the mixture was stirred for 5s before aquenous solution (20 mL) of NaN_3 (0.1300 g) was added. After additional 5s of stirring mixture was then covered protective waxed foil and left at room temperature for 20 hours. Following that, sample was centrifuged for 20 minutes and washed by water and then treated with anhydrous ether. Sample was then left in the oven at $T=70^oC$ for 45 minutes to dry.

Synthesis of $Ni(N_3)_2$(4,4'-bipiridine): Pale green polycrystals were obtained by adding aquenous solution (20 mL) of $NiCl_2 \cdot 6\ H_2O$ (0.2377 g) to solution of

bpy(0.1562g) in methanol (10 mL). The rest of the production procedure is identical like in the case of $Co(N_3)_2$(4,4'-bipiridine).

Synthesis of $Cu(N_3)_2$(4,4'-bipiridine): Green polycrystals were obtained by adding aquenous solution (20 mL) of $CuCl_2 \cdot 6\ H_2O$ (0.1705 g) to solution of bpy(0.1562g) in methanol (10 mL). The rest of the production procedure is identical like in the case of $Co(N_3)_2$(4,4'-bipiridine) and $Ni(N_3)_2$(4,4'-bipiridine)

3.2. Structure Analysis Powder X-ray Diffraction (PXRD)

All the samples that were synthesized underwent room temperature X-Ray diffraction measurements to ensure that they were single phase, to determine the lattice parameters in the case of compounds that were produced for the first time. These measurements were performed at the Chemistry Department, Rutgers University on the Rigaku Ultima, Dmax-2200T powder X-Ray diffractometer, with a computer controlled data acquisition system [ref. 18, 83] (Fig 3.2).

All of the X-Ray samples were grinded, the samples were attached to a glass slide with silicone grease, and then the slide was mounted in the X-Ray diffractometer. Note that silicone grease does not have any effect on the powdered sample and shows no lines in the diffraction pattern that is observed. The resulting diffraction pattern was then analyzed to determine the lattice parameters for novel materials and to confirm structure of those compounds that were produced before, using Bragg's law: $2d \sin\theta = n\lambda$, where "*d*" is spacing between the two nearest planes f the crystal relating to the Miller's indices (*h, k, l*), "λ" is the wavelength of the incoming X-rays to the

sample, "θ" is the angle between the incoming X-rays and the (h, k, l) plane and "n" is the order of the diffraction peak. The weighted average of λ=0.15418nm for the $k_{\alpha 1}$ and $k_{\alpha 2}$ wavelengths of the Cu target was used to analyze the diffraction pattern for low angles in this study. The analysis of the patterns was done by using the XRD data analysis JADE 6.5+ program.

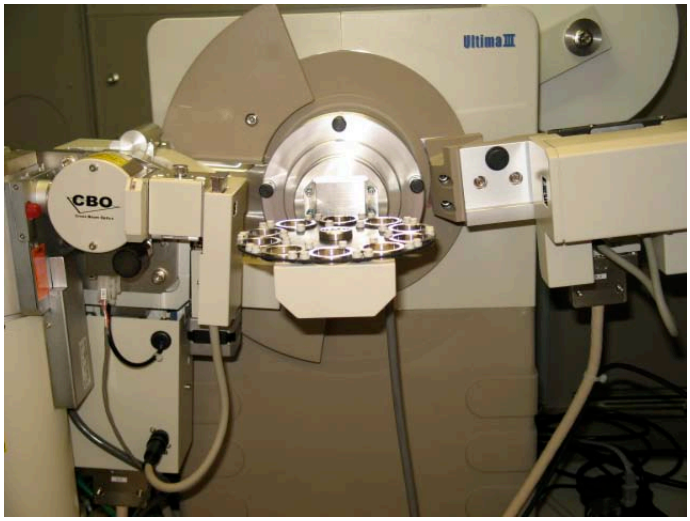

Fig. 3.2. Rigaku Ultima, Dmax-2200T powder X-Ray diffractometer

[Source of image: Danilović, D.]

3.3. Magnetization

The magnetic susceptibility temperature dependence $\chi(T)$, and magnetization as a function of the field $M(H)$, were measured with a commercial Superconducting Quantum Interference Device (SQUID) magnetometer in the temperature range from 1.8 K to 315 K and in magnetic fields up to 5.5 T (Fig 3.3).

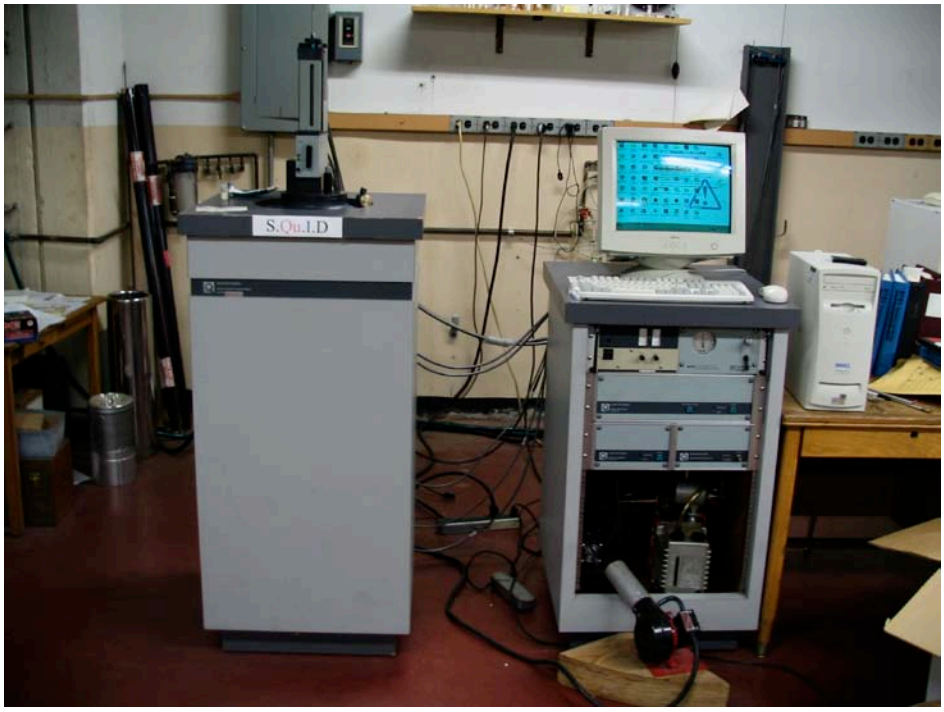

Fig. 3.3. SQUID used in measurements of studied metal organic compounds [Source of image: Danilović, D.]

Samples with a mass of approximately 15-20 mg were inserted into the plastic straw, which is nonmagnetic and does not to affect the magnetization measurements. The straw is then attached to the end of a 2.0 mm diameter brass rod. This rod is permanently attached to the end of a 1.5 m long stainless steel rod, which is also 2.0 mm in diameter and runs from the top of the SQUID down to the measurement area in the interior of the SQUID. After the sample was loaded into the SQUID and before the measurement itself was performed, the sample position was centered by applying a small ≈50 G field to the sample and allowing the SQUID to take single measurement. The SQUID was then set to take data, using MPMS MultiVu Windows-based Software Interface program to vary the temperature and/or magnetic field. This sequence of measurements was generated based on the type of measurement needed for the particular sample. Samples that were produced in this investigation were in powdered form in a small container which was then inserted into the straw. The container was made from weighing paper of very small mass (≈10mg), of the square shape, with a small diamagnetic susceptibility in comparison to that of to the coordinated networks. In order to obtain the total magnetic susceptibility of the observed material, the diamagnetic susceptibilities of the weighing paper and the organic ligands which constitute building blocks of coordinated metal organic networks were subtracted, form measured values. Since the measured magnetic susceptibilities for examined compounds are much larger than these diamagnetic susceptibilities, these corrections are negligible. The only exception is for the Cu azide compound where these corrections were taken into account this work.

The major detection components of DC SQUID magnetometer consists of a second derivative detection coil and two Josephson junctions linked in the superconducting loop shown in figure. The second derivative coil is located in the sample chamber and consists of a single wire wound into four loops, as shown in Fig 3.4. The detection coil is inductively linked to the superconducting loop.

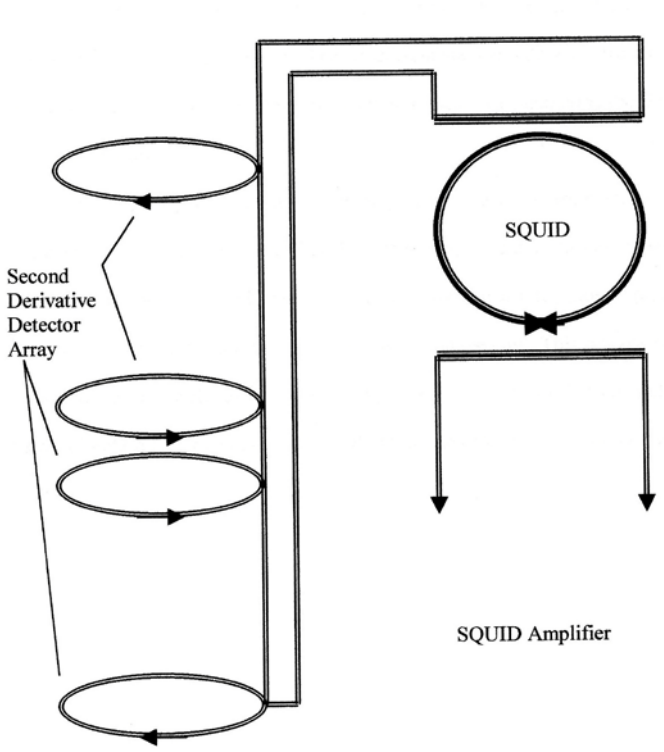

Fig. 3.4. Schematic representation of SQUID detection and measurement [Source of image: Zan, J.A., *Anomalous Magnetic Ground States of $CeGe_X$ System*, PhD Dissertation, Temple University, Philadelphia, **2004**, Fig 3.5]

The phase change of a current flowing around the superconducting loop should be an integer multiple of 2π. To generate current around the loop, a time-varying flux is passed through the loop. This is accomplished by moving the sample to different

positions in the detection coil and measuring the dc current generated in the loop at each position. The total phase change around the loop is

$$\arcsin(\frac{I_s}{I_c}) - \frac{2e}{\hbar}\phi_{tot} = 2\pi n \quad (3.3)$$

where I_s is the superconducting current, and I_c is the critical current of the Josephson junction. The superconducting current through the loop is given by:

$$I_s = I_c \sin(2\pi \frac{\phi_{tot}}{\phi_0}). \quad (3.4)$$

The superconducting current is made time-dependent by the application of an additional flux from the sample. This loop is, in turn, inductively connected to an RLC circuit driven by an RF generator. The RF current and the induced current related to the superconducting loop are both measured as a means of calculating the flux through the loop.

The SQUID measures the voltage required to create current, through known resistor, to counteract the flux through the superconducting loop at each position in the detection coil. These voltages are then plotted as a function of the position in the detection coil. This process is repeated multiple times for each measurement until improved resolutions of measurements defined by the instrument specifications were not acquired. Computer then uses the calibration factors unique to the SQUID in order to calculate the magnetic moment of the given sample.

3.4. Specific Heat

The heat capacity was measured in the temperature range from 1.2 K to 35 K using a semi-adiabatic heat pulse method. For temperatures from 1.2 K to 35 K a liquid He^4 cryostat was used. [ref. 101, 102] During the measurement, the current is applied to the sample heater for a short period of time. The temperature of the sample is monitored and the changed in temperature (ΔT) is recorded. The amount of heat added to the sample can be calculated using

$$Q = I^2 R\Delta t \quad (3.1),$$

where R is the resistance of the heater, and Δt is the duration of current pulse. In terms of the mass (m) and molecular weight (M) of the sample, the specific heat is given by:

$$C = \frac{MI^2 R\Delta t}{m\Delta T} \quad (3.2).$$

In the temperature range T=1.2 K to 35 K a sample with mass of approximately 0.3g was used. Measurements were performed for $Co(N_3)_2$(4,4'-bipyridine) and $Ni(N_3)_2$(4,4'-bipyridine) since these compounds were produced in sufficient quantities to make these measurements possible.

CHAPTER 4

RESULTS AND DISCUSSION

4.1. STRUCTURE

Powder X-ray diffraction (PXRD) measurements were performed to determine crystal structure and lattice parameters of all samples of the compounds studied. The confirmation was required that compounds obtained in the study are isostructural to the ones previously produced [ref. 28, 55, 60, 61]. The crystal structure and lattice parameters of the compounds Ni, Co, Cu with $(N_3)_2$ and (4, 4'-bipyridine), needed to be determined since they were produced for the first time during this research.

While the distances along the one direction are longer in comparison with other two directions because usage of 4, 4'-bipyridine as ligand in the first direction, and stacking of layer onto layer in the second direction, relatively strong magnetic exchange interactions along the third direction may be anticipated for all studied compounds, thus making them effectively 1D magnetic chains.

4.1.1. Structure: MCl_2(4,4'-bipyridine)

All of these compounds are isostructural and belong to the orthorhombic crystal system, space group *Cmmm* (No. 65). (Fig. 4.1)

As shown in Fig. 4.1, the crystal structure of this family of compounds consists of 2D MCl_2(4, 4'-bipyridine) networks built upon MCl_4(4, 4'-bipyridine)$_2$ building blocks. The divalent metal centers have a distorted octahedral coordination with four μ_2-Cl and by two bridging 4, 4'-bipyridine at trans positions [ref. 55]. The two-dimensional layers are formed in the *ac* plane by connecting metal centers via bridging chlorine and 4, 4'-bipyridine ligands. These ligands are stacked on the top of each other along the *b*-axis at distance of ½ *b* to complete the three-dimensional structure (Fig 4.2).

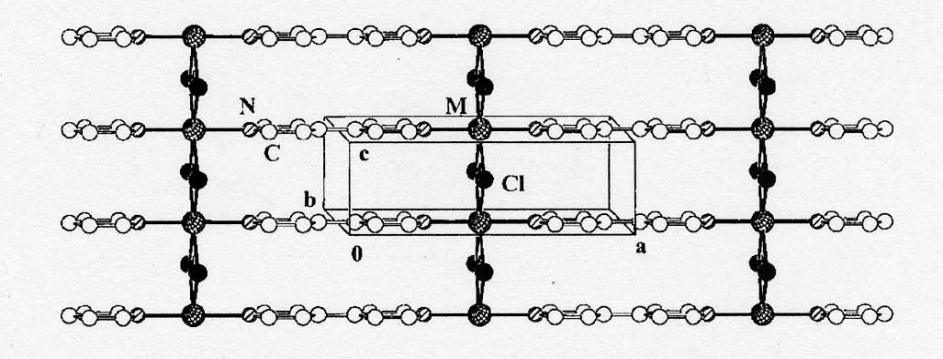

Fig. 4.1. Crystal structure of MCl_2(4,4'-bipyridine) family of compounds
[Source of image: Lawandy, M. A.; Huang, X.; Wang R.; Li, J.; Lu, J.Y.; Yuen T.; Lin, C.L.; Two-Dimensional Coordination Polymers with 1D Magnetic Chains: Hydrothermal Synthesis, Crystal Structure, and Magnetic and Thermal Properties of $^2{}_\infty$[MCl_2(4,4'-bipyridine)] (M=Fe, Co, Ni, Co/Ni), *Inorg. Chem.* **1999**, *38*, Fig. 1]

Values that we have obtained for our compounds from x-ray diffraction for unit cells are:

Compound name	*a*(A)	*b*(A)	*c*(A)
$FeCl_2$(4,4'-bipyridine)	11.929(2)	11.447(2)	3.638(1)
$CoCl_2$(4,4'-bipyridine)	11.964(2)	11.420(1)	3.625(1)
$NiCl_2$(4,4'-bipyridine)	11.993(2)	11.374(2)	3.611(1)

Table 4.1. Newly measured parameters MCl_2(4,4'-4, 4'-bipyridine)

The crystal structure of produced MCl_2(4,4'-bipyridine) compounds are consistent with the previously obtained. All N-M-Cl and N-M-N angles are precisely 90^o and 180^o respectively.

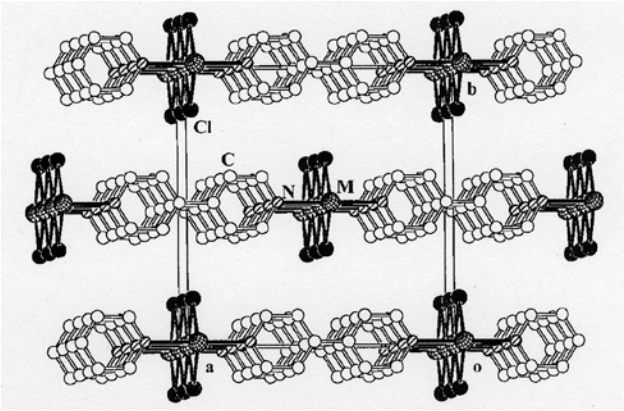

Fig. 4.2. View along the *c*-axis showing stacks of layers of MCl_2(4,4'-bipyridine) [Source of image: Lawandy, M. A.; Huang, X.; Wang R.; Li, J.; Lu, J.Y.; Yuen T.; Lin, C.L.; Two-Dimensional Coordination Polymers with 1D Magnetic Chains: Hydrothermal Synthesis, Crystal Structure, and Magnetic and Thermal Properties of $^2{}_\infty[MCl_2$(4,4'-bipyridine)] (M=Fe, Co, Ni, Co/Ni), *Inorg. Chem.* **1999**, *38*, Fig. 2]

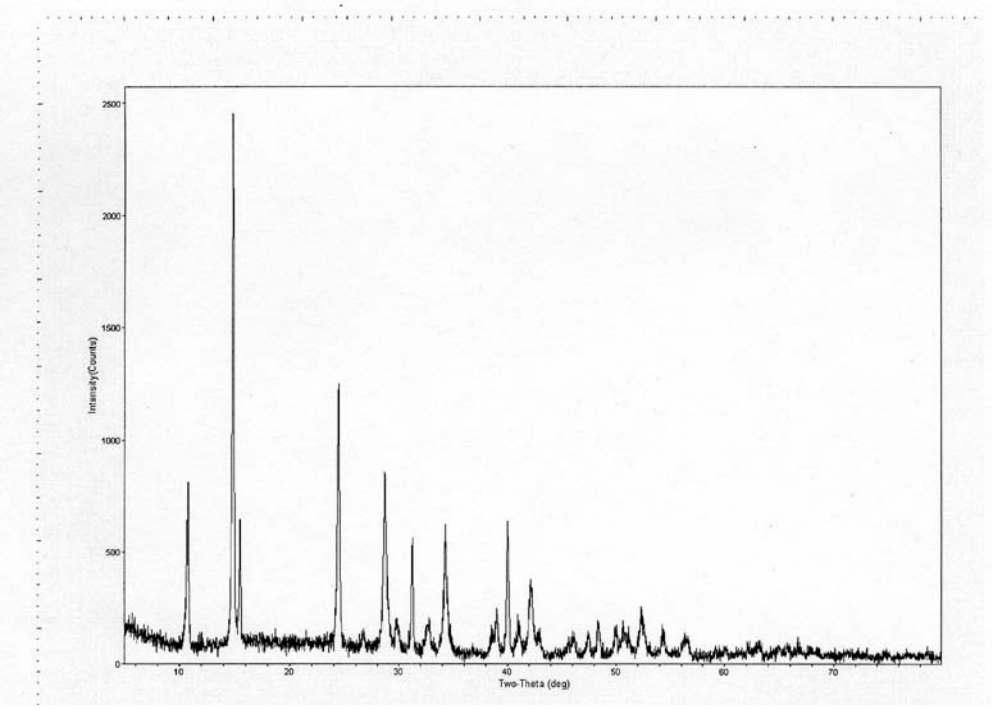

Fig. 4.3. PXRD pattern for $FeCl_2$(4,4'-bipyridine)

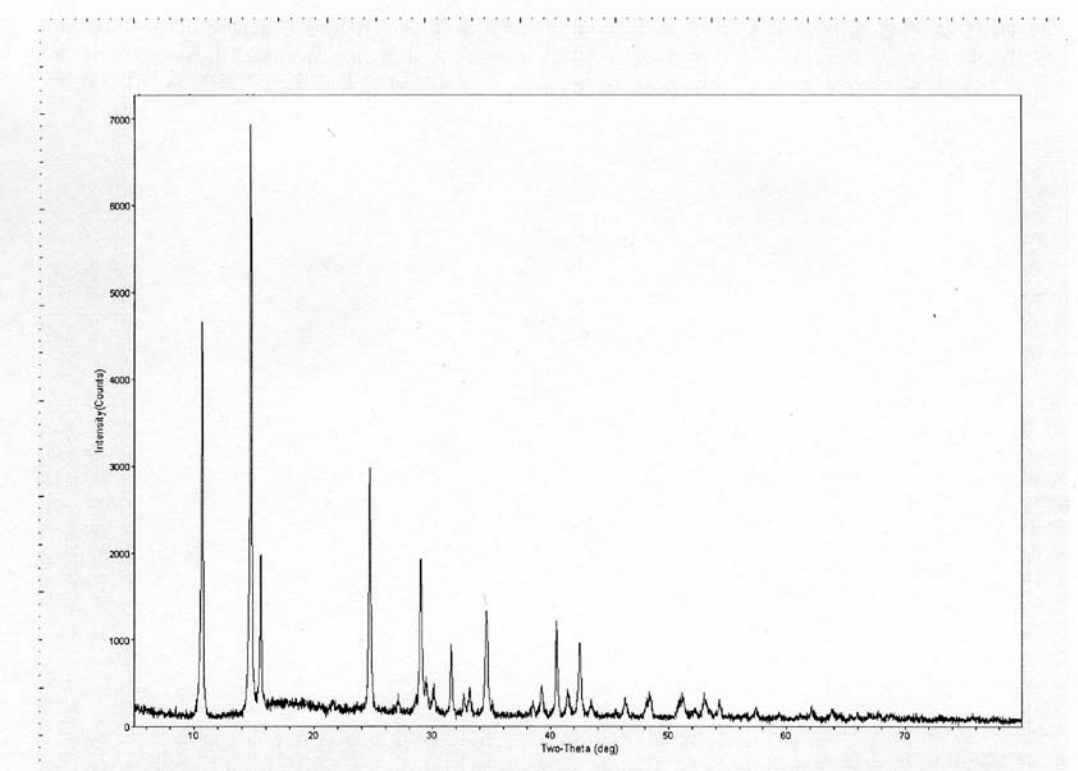

Fig. 4.4. PXRD pattern for $CoCl_2$(4,4'-bipyridine)

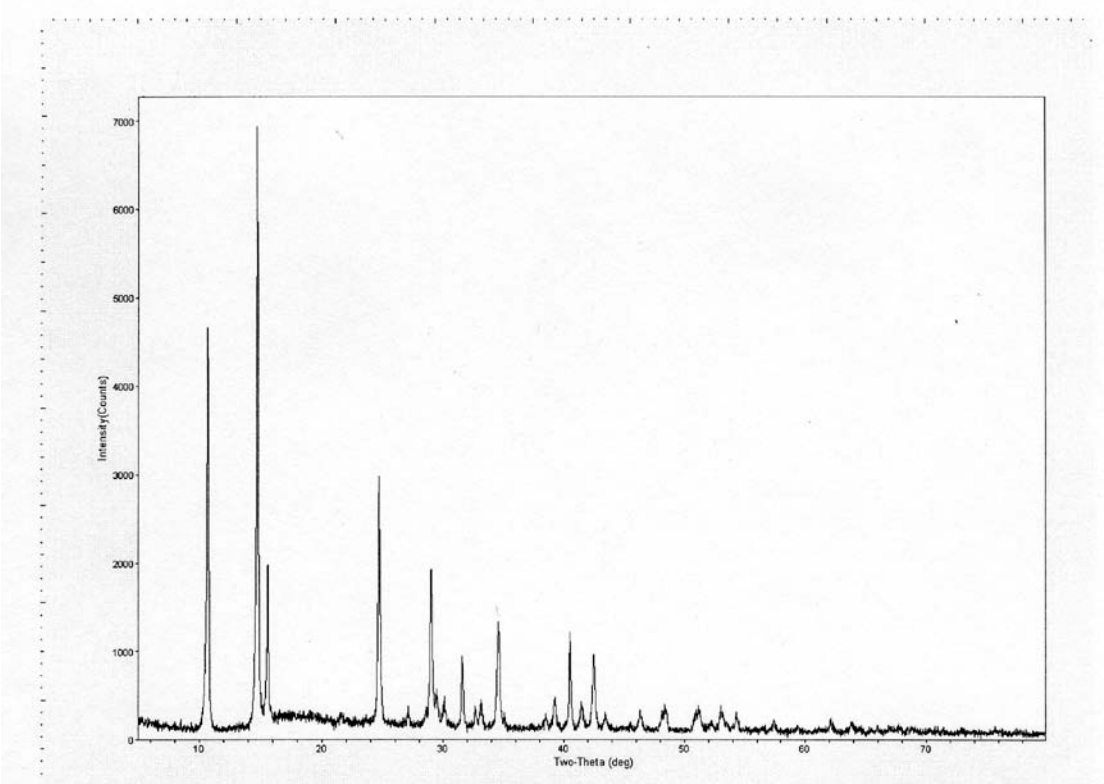

Fig. 4.5. PXRD pattern for $NiCl_2$(4,4'-bipyridine)

4.1.2. Structure: M(ox)(4,4’-bipyridine)

These compounds crystallize in the orthorhombic system, space group *Immm* (No. 71) (Fig 4.6). All the metal atoms are divalent, and they have an octahedral coordination with four O atoms from oxalate ions and two N atoms from bipyridine molecules (Fig 4.6).

The two-dimensional sheets stack on the top of each other in staggered fashion where, the adjacent layers are shifted by ½ *a*+½ *c*, to complete the structure in the third dimension (Fig 4.7).

Values that we have obtained for our compounds from x-ray diffraction for unit cells are:

Compound name	*a*(A)	*b*(A)	*c*(A)
Fe(ox)(4,4’-bipyridine)	5.472(1)	10.940(2)	11.465(2)
Co(ox)(4,4’-bipyridine)	5.375(2)	10.955(1)	11.365(1)
Ni(ox)(4,4’-bipyridine)	5.309(2)	10.953(1)	11.250(2)

Table 4.2. Newly measured parameters M(ox)(4,4’-4, 4’-bipyridine)

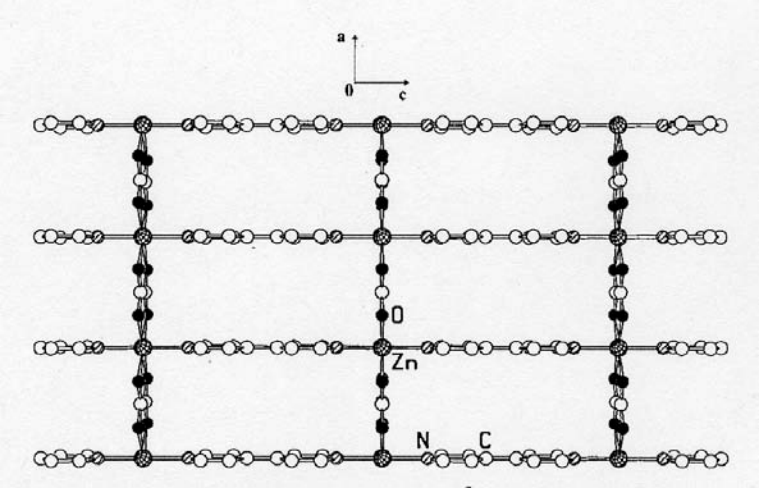

Fig. 4.6. Layer structure of M(ox)(4,4'-bipyridine) family of compounds
[Source of image: Lu, J.Y.; Lawandy, M. A.; Li, J.; Yuen T.; Lin, C.L.; A New Type of Two-Dimensional Metal Coordination Systems: Hydrothermal Synthesis and Properties of the First Oxalate-4, 4'-bipyridine Mixed-Ligand Framework $^{2}_{\infty}$[M(ox)(4, 4'-bipyridine)] (M=Fe(II), Co(II), Ni(II), Zn(II); ox=$C_2O_4^{2-}$; 4, 4'-bipyridine=4,4'-bipyridine), *Inorg. Chem.* **1999**, *38*, Fig. 2]

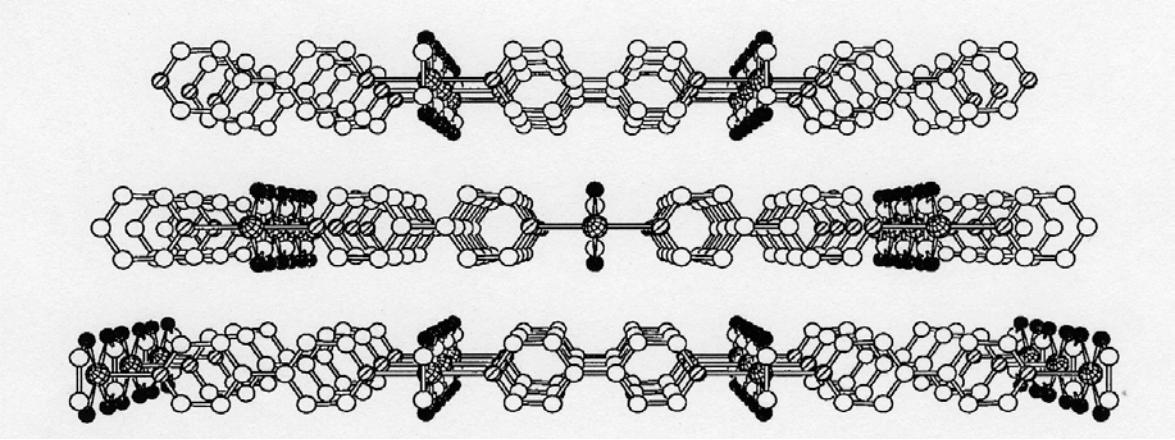

Fig. 4.7. Perspective view of the structure of M(ox)(4,4'-bipyridine) where layers are stacked in staggered fashion along the *b*-axis.
[Source of image: Lu, J.Y.; Lawandy, M. A.; Li, J.; Yuen T.; Lin, C.L.; A New Type of Two-Dimensional Metal Coordination Systems: Hydrothermal Synthesis and Properties of the First Oxalate-4, 4'-bipyridine Mixed-Ligand Framework $^{2}_{\infty}$[M(ox)(4, 4'-bipyridine)] (M=Fe(II), Co(II), Ni(II), Zn(II); ox=$C_2O_4^{2-}$; 4, 4'-bipyridine=4,4'-bipyridine), *Inorg. Chem.* **1999**, *38*, Fig. 3]

Comparing the values that were obtained with the previously reported values of the lattice parameters and the crystal structure can lead to the conclusion that these two sets of compounds have consistent structure. The M-M distances within the two-dimensional net are *a* (5.3-5.5 Å) and *c* (11.3-11.5 Å), respectively

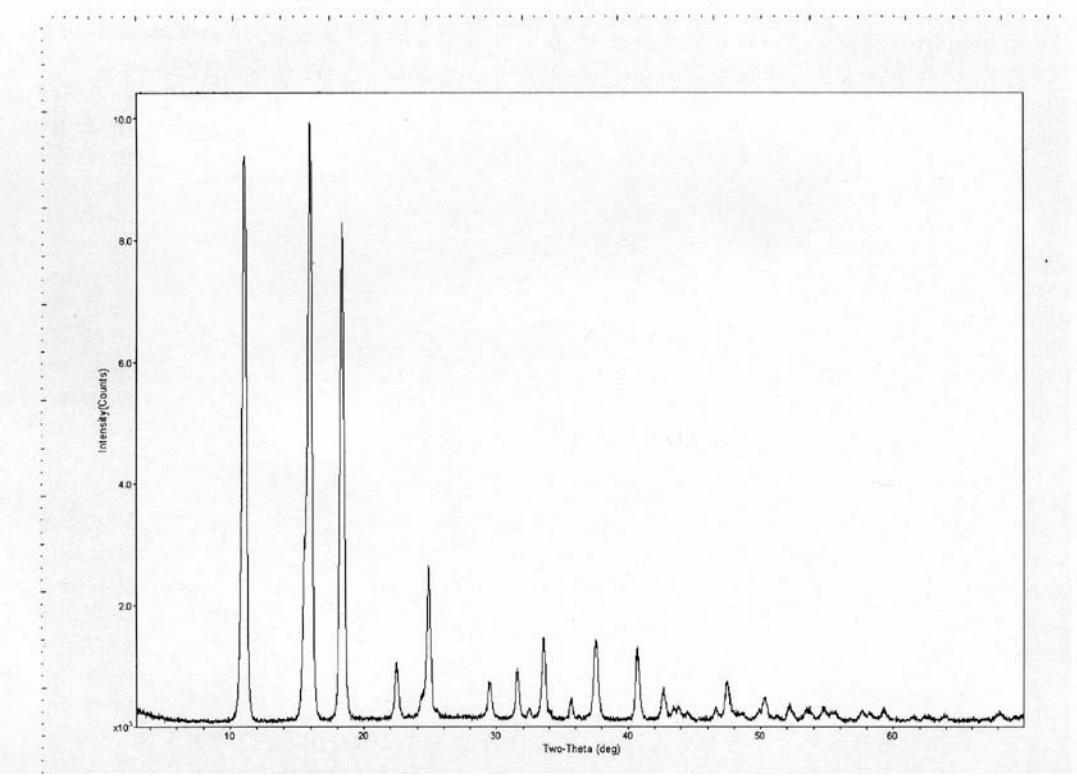

Fig. 4.8. PXRD pattern for Fe(ox)(4,'4-bipyridine)

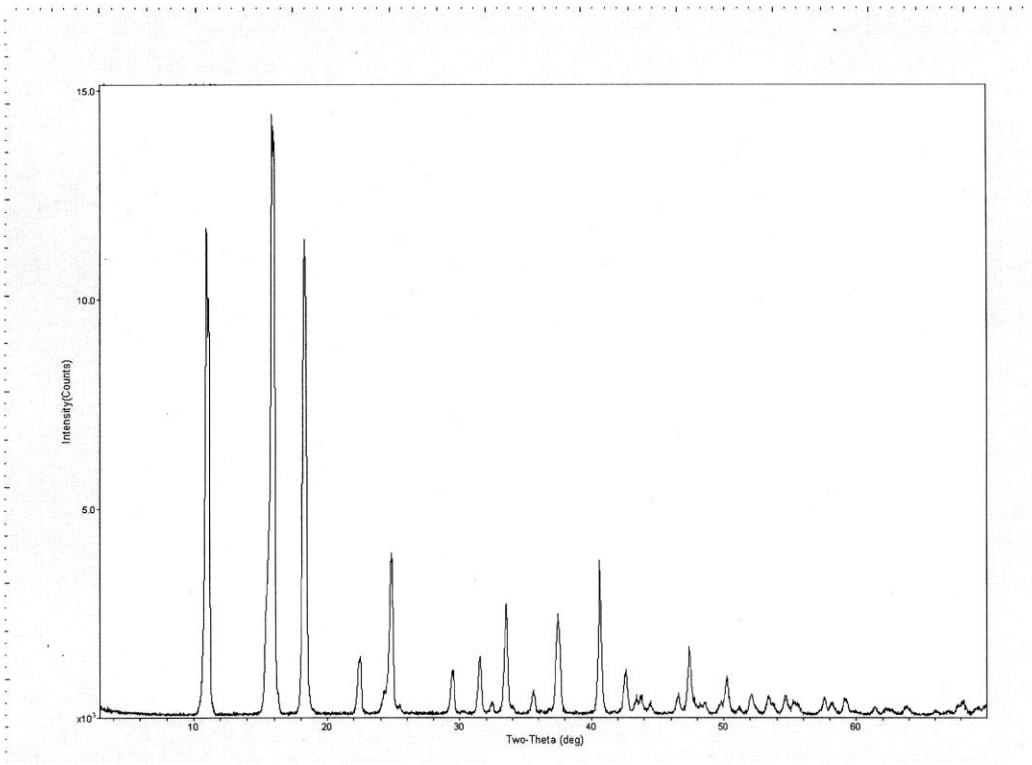

Fig. 4.9. PXRD pattern for Co(ox)(4,'4-bipyridine)

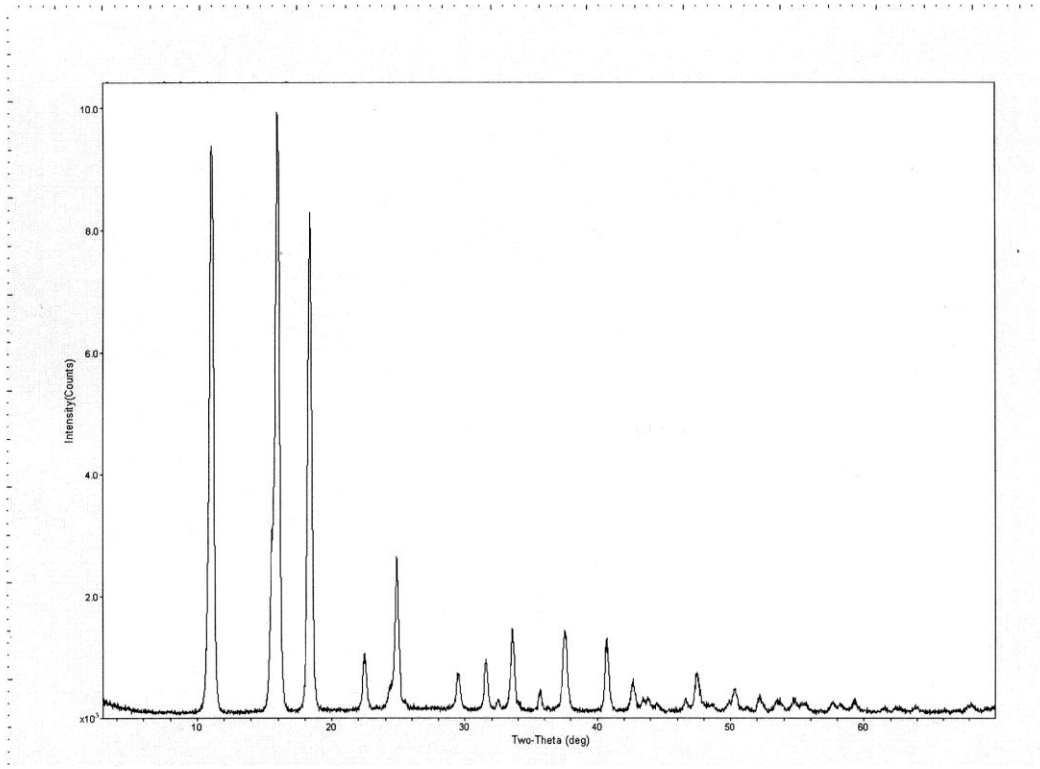

Fig. 4.10. PXRD pattern for Ni(ox)(4,'4-bipyridine)

4.1.3. Structure: $M(N_3)_2$(4,4'-bipyridine)

In previously published research only $Fe(N_3)_2$(4,4'-bipyridine) compound of $M(N_3)_2$(4,4'-bipyridine) family was successfully produced [ref. 28]. This compound crystallizes in an orthorhombic crystal system with the space group *Cmmm* (No. 65).

The crystal structure consists of two-dimensional $Fe(N_3)_2$(4,4'-bipyridine) layers parallel to the crystallographic *ac* plane (Fig 4.11).

Its three-dimensional structure is completed by stacking these layers on the top of each other with shift of ½ *a*+½ *c* between the adjacent layers (Fig 4.12).

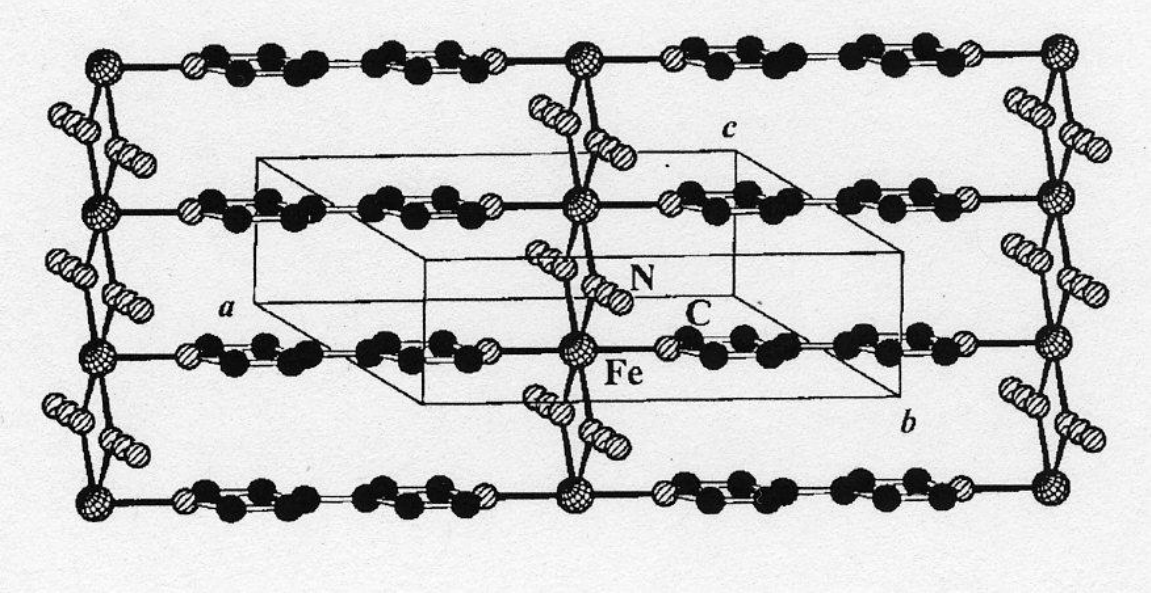

Fig. 4.11. Crystal structure of $M(N_3)_2$(4,4'-bipyridine) family of compounds
[Source of image: Fu, A.; Huang, X.; Li, J.; Yuen T.; Lin, C.L.; Controlled Synthesis and Magnetic properties of 2D and 3D Iron Azide Netvorks $^{2}_{\infty}[Fe(N_3)_2$(4,4'-4, 4'-bipyridine)] and $^{3}_{\infty}[Fe(N_3)_2$(4,4'-4, 4'-bipyridine)], *Chem. Eur.J.* **2002**, *8*, No.10, Fig. 2]

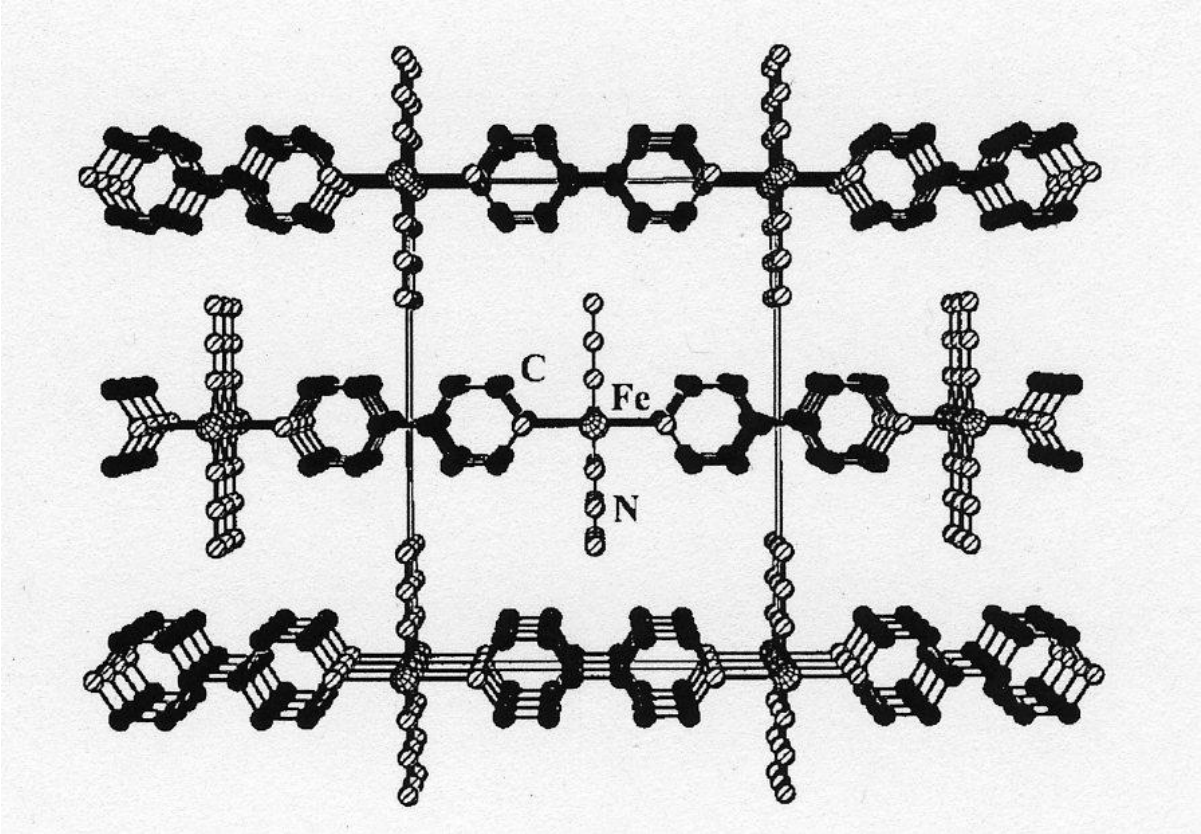

Fig. 4.12. Perspective view of the structure of $M(N_3)_2$(4,4'-bipyridine) where layers are stacked in staggered fashion along the *b*-axis.
[Source of image: Fu, A.; Huang, X.; Li, J.; Yuen T.; Lin, C.L.; Controlled Synthesis and Magnetic properties of 2D and 3D Iron Azide Netvorks $^{2}_{\infty}[Fe(N_3)_2$(4,4'-4, 4'-bipyridine)] and $^{3}_{\infty}[Fe(N_3)_2$(4,4'-4, 4'-bipyridine)], *Chem. Eur.J.* **2002**, *8*, No.10, Fig. 3]

The Fe atoms are octahedrally coordinated with four μ-(1, 1) azide ligands in equatorial plane and two 4, 4'-bipyridine molecules at axial sites. The octahedral geometry around each Fe atom is slightly distorted through axial contraction and equatorial distortion. For each 4, 4'-bipyridine ligand, two pyridyl rings are coplanar and lie in crystallographic *ab* plane.

In this study, additional compounds of the same family were produced with Co, Cu, and Ni as metallic ions. Powder X-ray diffraction was performed in order to determine the crystal structure of the newly produced materials.

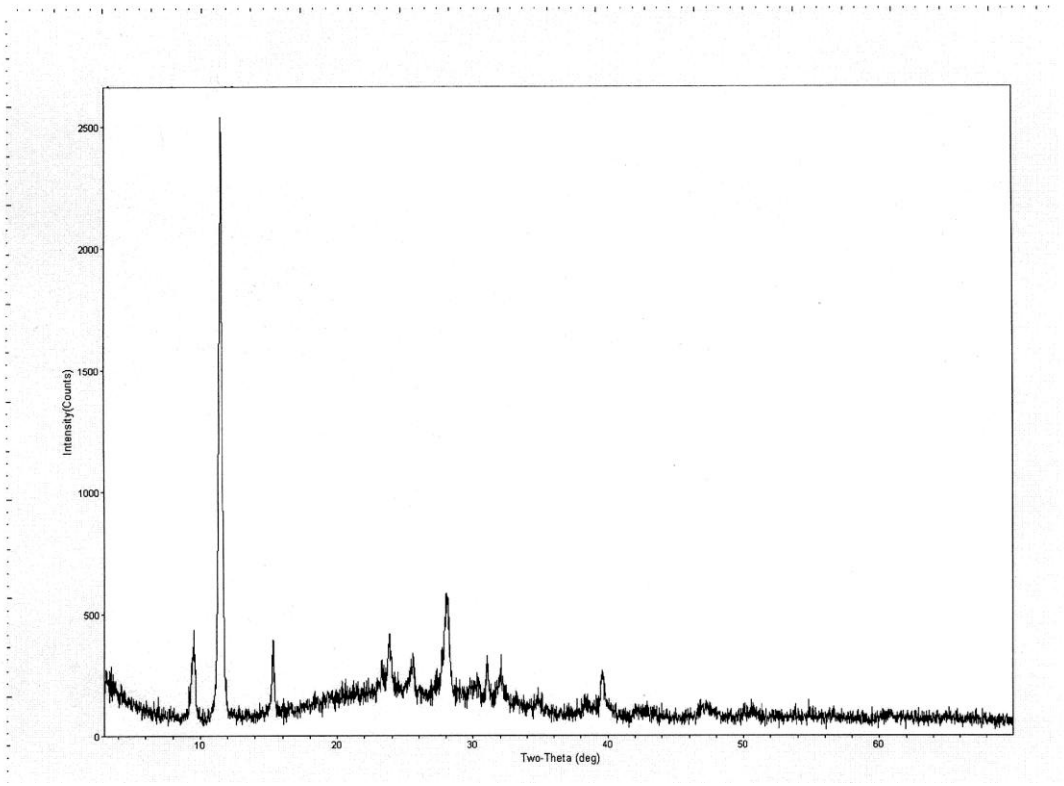

Fig. 4.13. PXRD pattern for $Fe(N_3)_2$(4,4'-bipyridine)

For each of these newly produced compounds the octahedral geometries around metal ions was established. The fact that the peaks on the PXRD data are relatively wide suggests existence of distortions in the structure. These distortions are the greatest in the case of $Co(N_3)_2$(4,4'-bipyridine). The explanation of these distortions can be explained with the existence the Jahn-Teller effect, of the static type, where there is spontaneous distortion along a particular axis of the octahedron. The values that were obtained for $M(N_3)_2$(4,4'-bipyridine) family of compounds for unit cells are:

Compound name	*a*(A)	*b*(A)	*c*(A)
$Fe(N_3)_2$(4,4'-bipyridine)	11.443(2)	15.178(3)	3.459(5)
$Co(N_3)_2$(4,4'-bipyridine)	11.453(1)	15.160(2)	3.420(2)
$Ni(N_3)_2$(4,4'-bipyridine)	11.478(2)	15.145(1)	3.405(1)
$Cu(N_3)_2$(4,4'-bipyridine)	11.460(2)	15.173(3)	3.408(3)

Table 4.3. Newly measured parameters $M(N_3)_2$(4,4'-4, 4'-bipyridine)

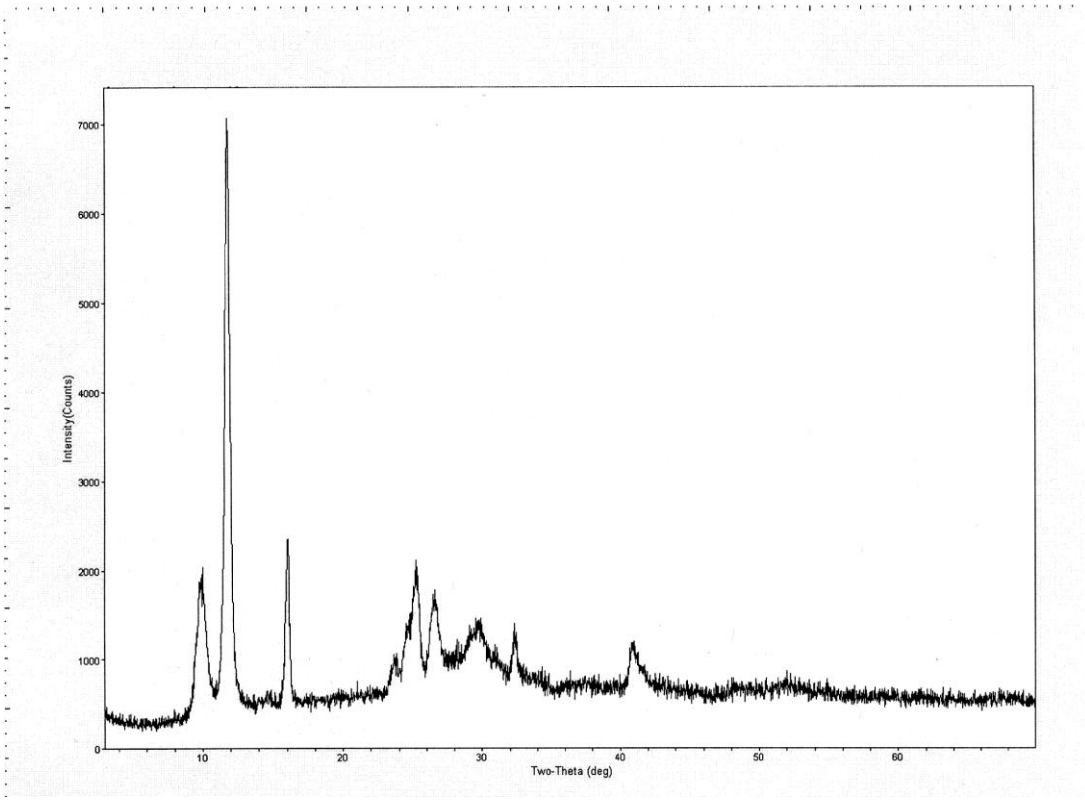

Fig. 4.14. PXRD pattern for $Co(N_3)_2$(4,4'-bipyridine)

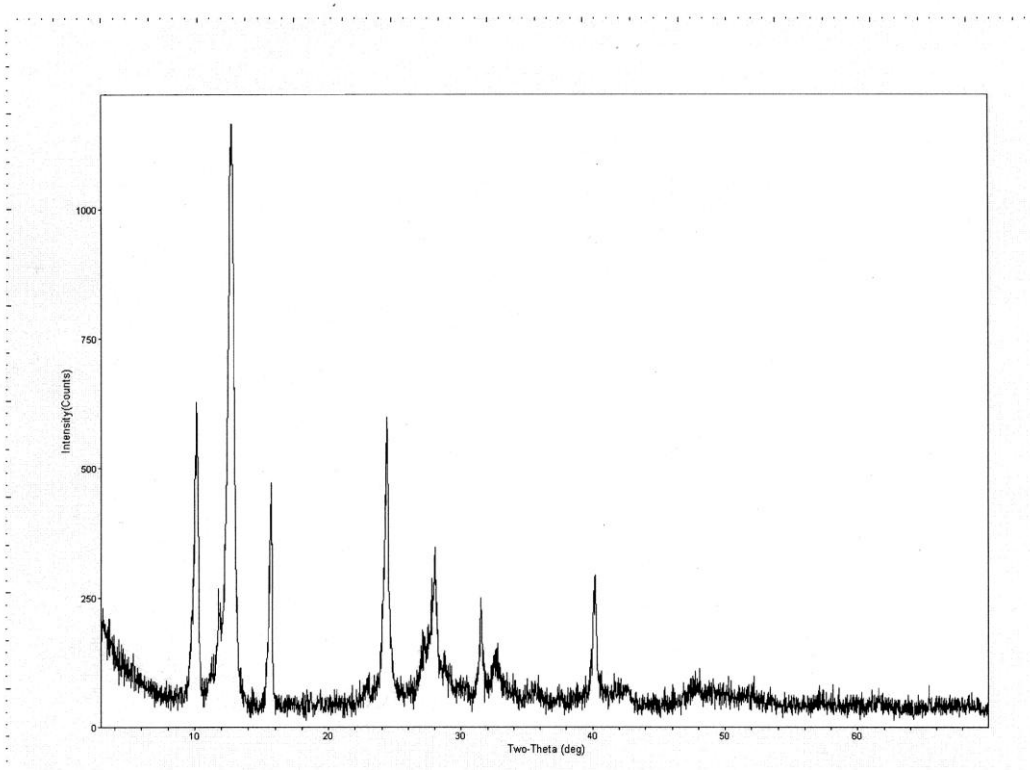

Fig. 4.15. PXRD pattern for $Ni(N_3)_2$(4,4'-bipyridine)

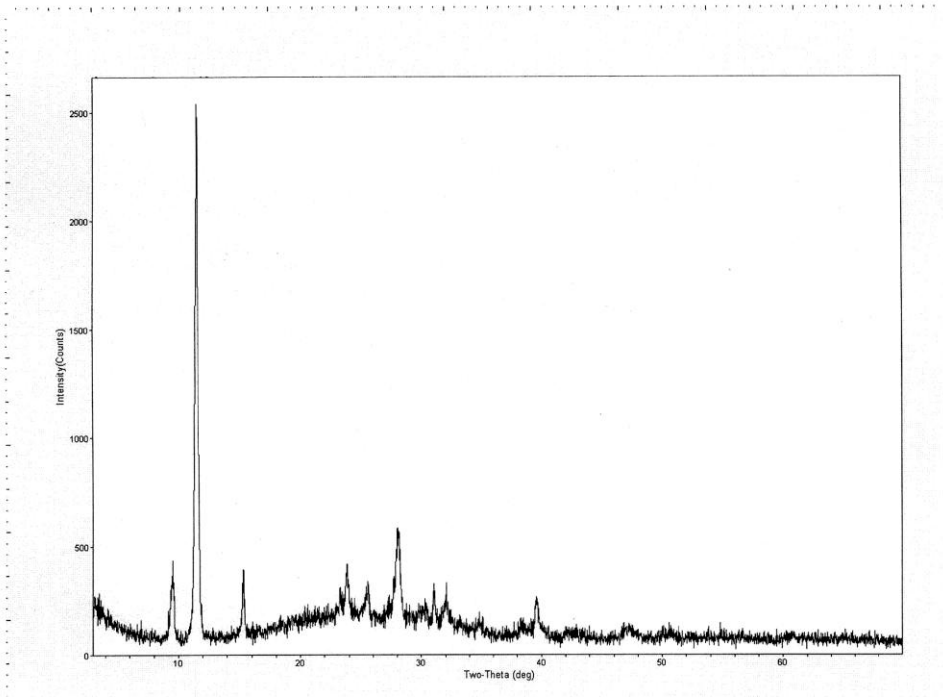

Fig. 4.16. PXRD pattern for $Cu(N_3)_2$(4,4'-bipyridine)

4.2. MAGNETIC MEASUREMENTS

Magnetic Susceptibility $\chi(T) = \frac{M(T)}{H}$, and Isothermal Magnetization $M(H)$ were performed in order to establish the type of magnetic interactions among the magnetic ions within each compound. The *χ(T)* and *M(H)* were measured for every compound under several external magnetic fields and temperatures respectively. In the case of *χ(T)* after that initial fitting was performed in the high temperature range above T= 80 K according to the modified Curie-Weiss law:

$$\chi(T) = \chi_0 + \frac{C}{(T-\theta)} \quad (4.1)$$

The calculation of effective magnetic moment μ_{eff} for transitional metallic ion in every compound was then undertaken by:

$$\mu_{eff} = 2.83\sqrt{C}\,\mu_B \quad (4.2)$$

All compounds studied in this dissertation show that transitional metallic ions are in the high spin state.

4.2.1. Magnetic measurements MCl_2(4,4'-bipyridine)

The initial *χ(T)* behavior for MCl_2(4,4'-bipyridine)in the presence of all applied fields, except in the case of the highest, is of typical antiferromagnetic material, without any noticeable difference in the zero field cooled (ZFC) and field cooled (FC) regimes, as

indicated by the cusplike shape of the data at low temperatures (Fig 4.17). As the field values in which *χ(T)* are measured increase the position of the maximum in the cusp moves to the lower temperatures for all members of this family of metal-organic coordinated networks. All members of MCl_2(4,4'-bipyridine) family have ferromagnetic interaction between metallic ions inside chains as result of high temperature fit.

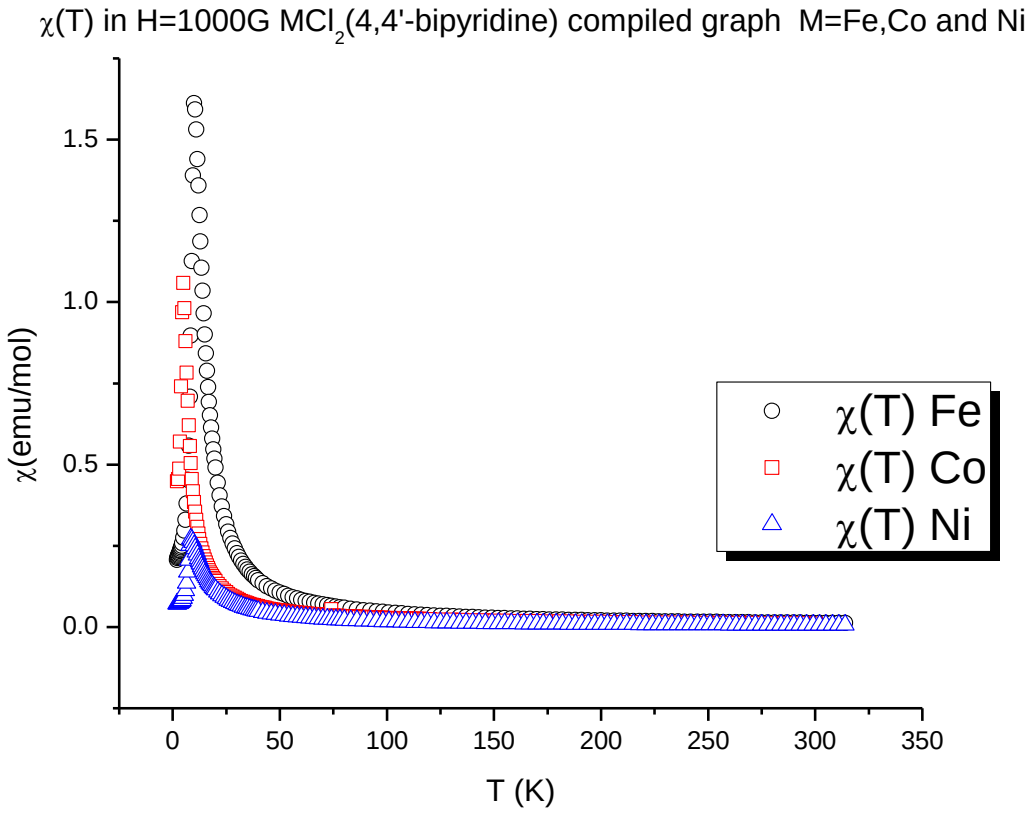

Fig. 4.17. χ(T) MCl_2(4,4'-bipyridine) complied graph

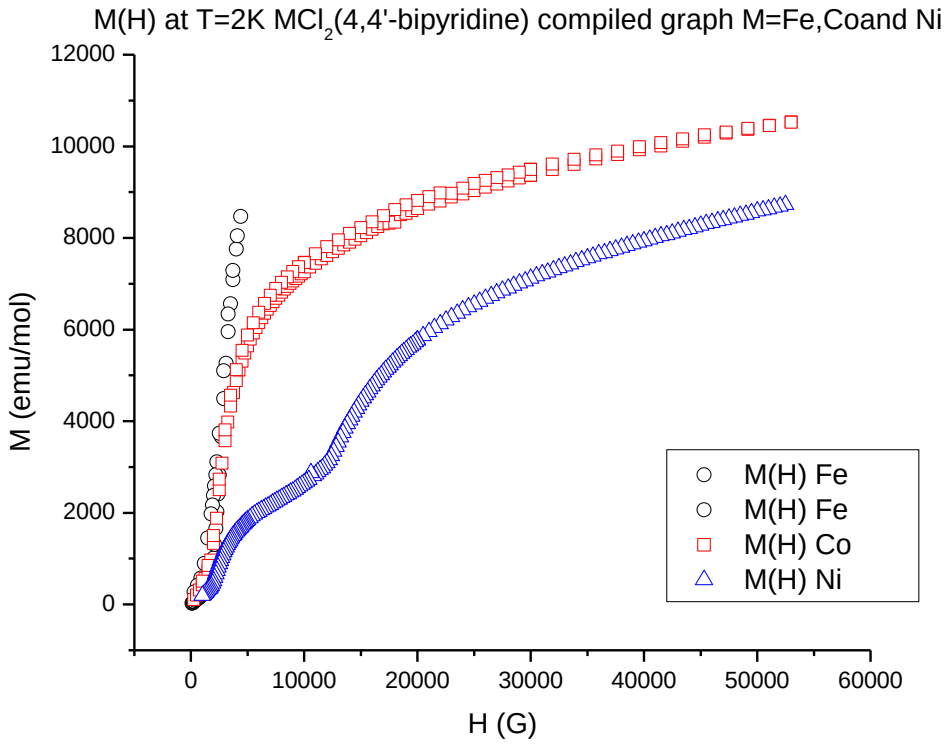

Fig. 4.18. M(H) at T=2K of MCl_2(4,4'-bipyridine) compiled

$FeCl_2$(4,4'-bipyridine): In the low field region, the *M(H)* functional dependence is linear, which is consistent with antiferromagnetic behavior of $\chi(T)$ measured in lower fields (Fig. 4.18). With increasing *H*, the *M(H)* line starts to increase its slope above a critical field H_c and then *M(H)* becomes saturated. In the field *H*=50 kG, *M*= 2.70 μ_B which indicates of high saturation of *M(H)*. The characteristics of $\chi(T)$ in *H*=20 kG suggest typical ferromagnetic behavior, which resembles more complicated magnetic interactions in the compound. Metamagnetic transition is detected having origin in canting.

The $\chi(T)$ and *M(H)* data of the $FeCl_2$(4,4'-bipyridine) compound exhibit a typical metamagnetic behavior, since the ground state magnetic structure changes with the change of applied field. (Fig. 4.20) Below the critical field H_c, the magnetic structure of the material is antiferromagnetic. When the applied field *H* is stronger than H_c, the

ordered magnetic state of the compound is ferromagnetic. The critical field H_c, in the case of $FeCl_2$(4,4'-bipyridine) is H_c =2500 G. The results of the high temperature fit are shown in the Table 4.4.

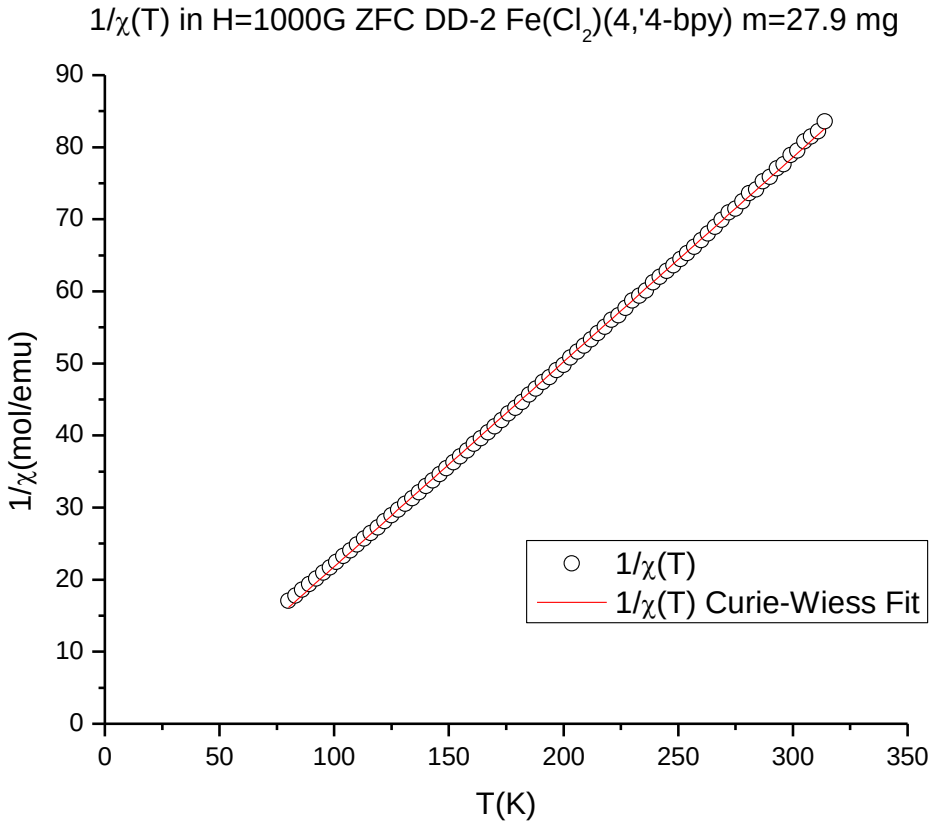

Fig. 4.19. 1/χ(T) ZFC Curie-Weiss fit of $FeCl_2$(4,4'-bipyridine)

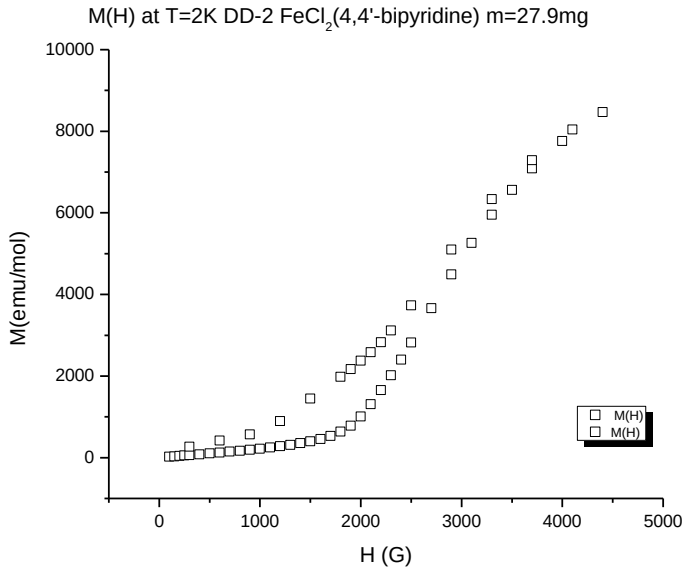

Fig.4.20. Metamagnetic behavior $Fe(Cl_2)$(4,4'-4, 4'-bipyridine)

$CoCl_2$(4,4'-bipyridine): The field dependent magnetization *M(H)* measured at temperature *T*=2 K shows very small hysteresis, very similar to previous measurements. As in the case of $FeCl_2$(4,4'-bipyridine), the Co based network is in the antiferromagnetic ground state when low magnetic fields *H* are applied. When *H* reaches value higher than H_c =2500 G, the magnetic state becomes ferromagnetic. With increasing magnetic field the magnetic moment slowly reaches saturation with m=1.44 μ_B/atom in the case of *H*=50 kG as (Fig 4.18).

The form of *M(H)* points to the metamagnetic behavior of $CoCl_2$(4,4'-bipyridine) in the ground state similar to the case of $FeCl_2$(4,4'-bipyridine). The results of the high temperature fit are shown in the Table 4.4.

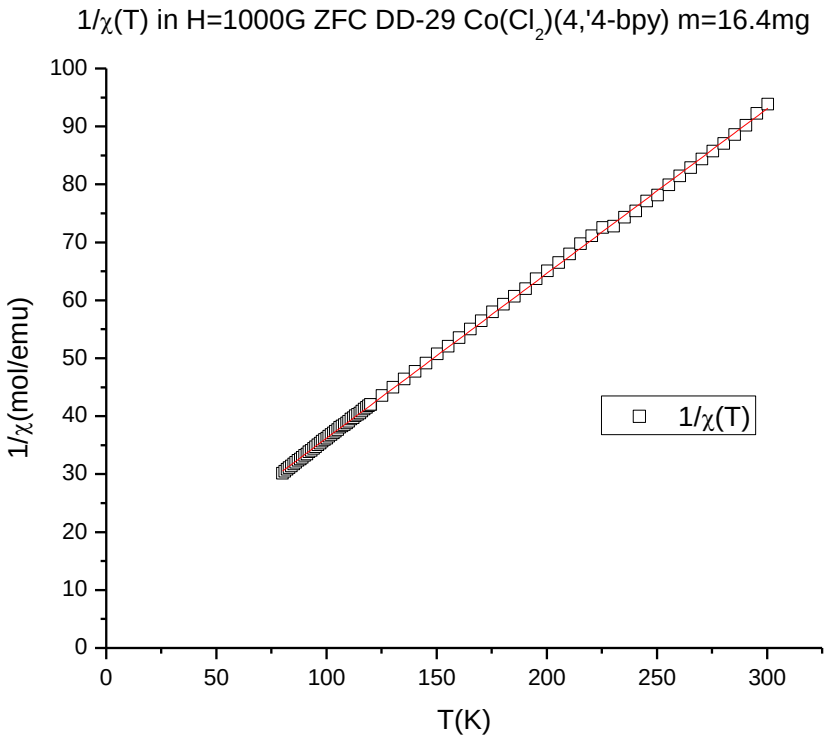

Fig. 4.21. 1/χ(T) ZFC Curie-Weiss fit of $CoCl_2$(4,4'-bipyridine)

$NiCl_2$(4,4'-bipyridine): The field dependent magnetization *M(H)* was measured at temperatures *T*=1.9 K and *T*=2 K. There is no significant difference between the results. Hysteresis is very well pronounced in both cases, slightly bigger in the case of *M(H)* measured at *T*=1.9 K, which is consistent with the model where for ferromagnetic material the magnetic moment of the substance increases with decreasing temperature . We see that the slope of *M(H)* in the case of the Ni based compound changes two times as the external magnetic field increases.(Fig.4.23) Explanation can be found in the canting in two different plains that was detected in previous measurements performed on the single crystal. [ref. 55]

In the low fields, this compound acts as antiferromagnet. After the coercive field H_c =2500 G is reached, $NiCl_2$(4,'4-bipyridine) behaves like a paramagnet, and then *M(H)* reaches saturation value. When we applied the field *H*=50 kG, the saturation magnetization was *M*=1.83 μ_B. This is once again a good example of metamagnetic behavior, which the whole family of the MCl_2(4,'4-bipyridine) compounds exhibits. The results of the high temperature fit are shown in the Table 4.4.

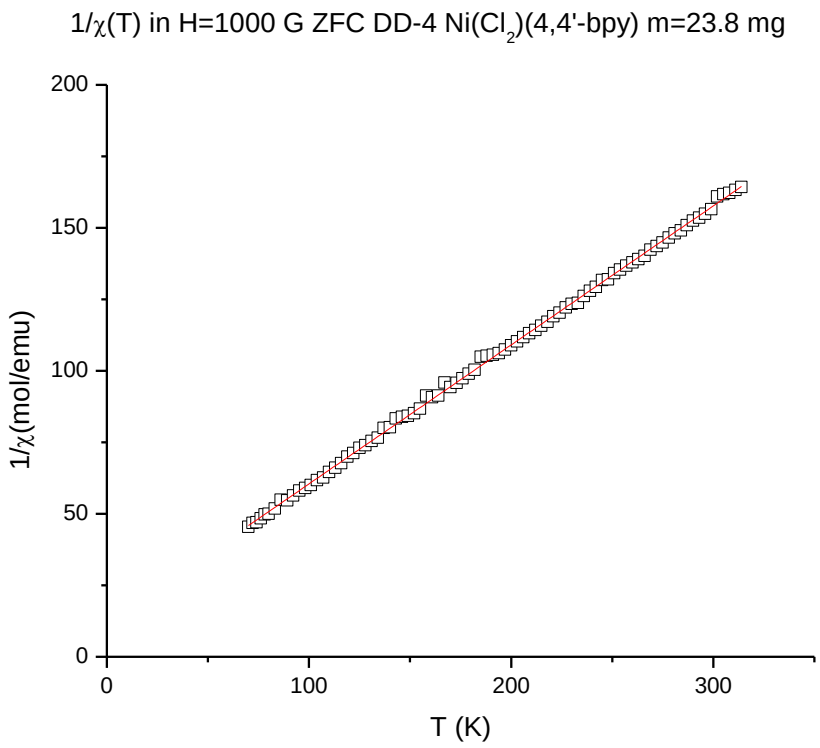

Fig. 4.22. 1/χ(T) ZFC Curie-Weiss fit of $NiCl_2$(4,4'-bipyridine)

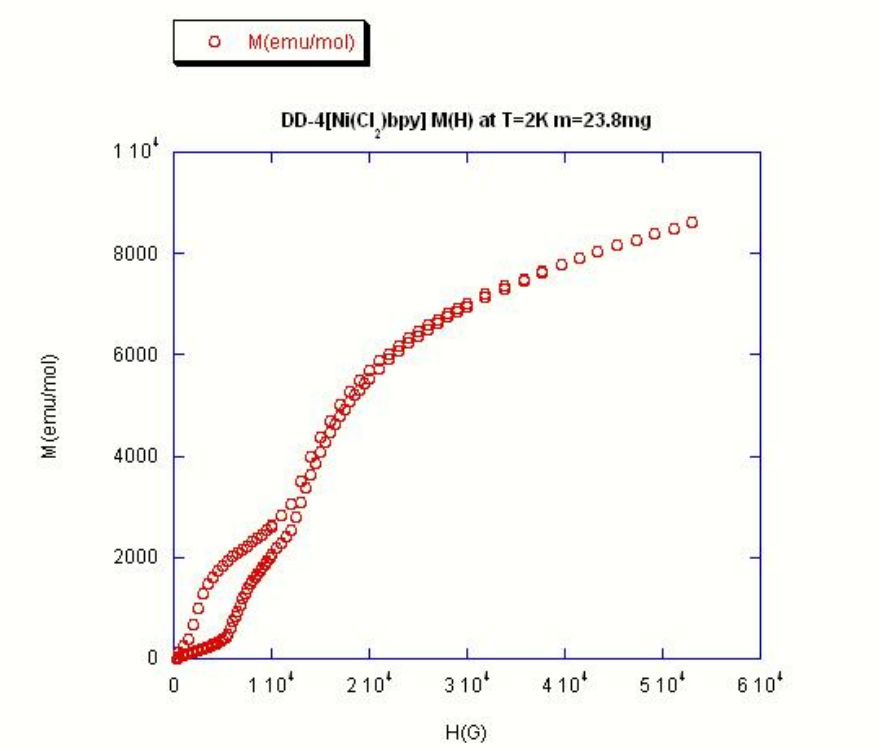

Fig. 4.23. Metamagnetic behavior of $Ni(Cl_2)$(4,4'-4, 4'-bipyridine)

As discussed in the earlier section in the chapter, the magnetic divalent centers M(II) in MCl_2(4,4'-bipyridine) compounds are situated in an octahedral environment, with four Cl and two 4,4'-bipyridine ligands. The Cl-M-Cl angles are very close to right angles, with a small deviation. The length of the M-Cl bonds is approximately 2.5 Å. This facilitates the one dimension magnetic interaction through the M-Cl_2-M pathway that is consistent with previously published data [ref. 55]. In the case of the MCl_2(4,4'-bipyridine) family of compounds, it was observed that ferromagnetic interactions between metal ions within the chains and antiferromagnetic interactions between adjacent chains.

4.2.2. Magnetic measurements M(ox)(4,4'-bipyridine)

M(ox)(4,4'-bipyridine): Behavior of $\chi(T)$ does not show significant differences from previously published work [ref. 61]. In the case of the measurements performed on these compounds, any observable difference in how the compound interact with the applied filed *H* in ZFC and FC measurement modes cannot be detected. M(ox)(4,'4-bipyridine) behave as a typical antiferromagnet with a very prominent maximum (Fig 4.24). Antiferromagnetic interaction between magnetic ions within chains is detected in high temperature fit for all the members of the family.

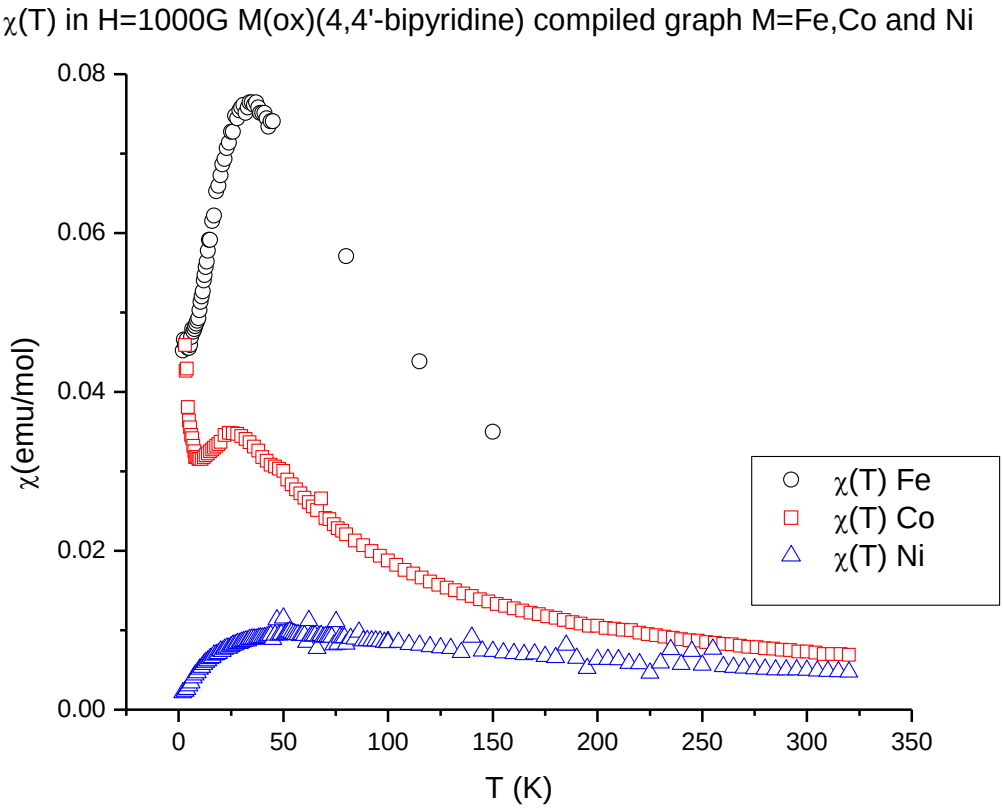

Fig. 4.24. χ(T) M(ox)(4,4'-bipyridine) combined

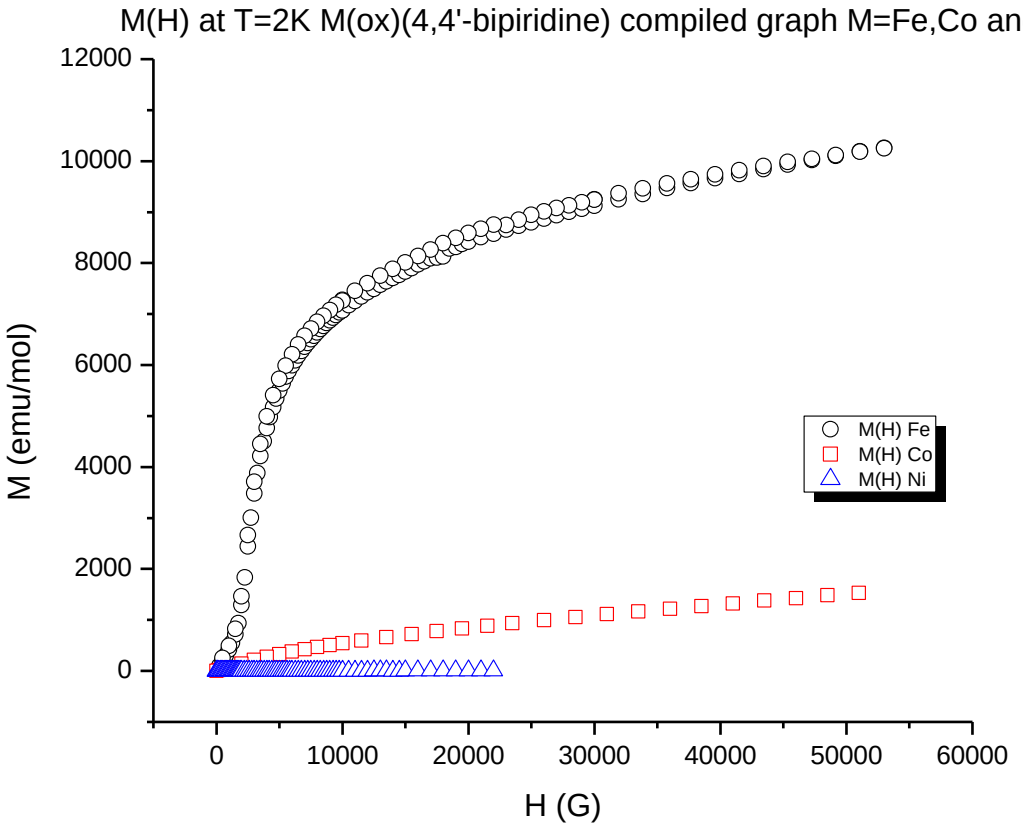

Fig. 4.25. M(H) at T=2K M(ox)(4,4'-bipyridine) combined graph

Fe(ox)(4,4'-bipyridine): The $\chi(T)$ corresponding maximum temperature is T=30 K, which is comparable with earlier measurements previously done [ref. 61].The magnetization as a function of the applied field measurement $M(H)$ was measured at temperature T=2 K. Metamagnetic behavior was detected and the source of it can be found in canting. The $M(H)$ measurements at T=2 K do not show hysteresis (Fig 4.25).

Canted antiferromagnetic substances are primarily antiferromagnetic but exhibit a weak ferromagnetic behavior due to canting of spins. The weak ferromagnetism of canted antiferromagnet is due to an antiferromagnetic alignment of spins of the two sublattices that are equivalent in kind and number of magnetic ions but not exactly antiparellel. The sublattices may exist spontaneously canted, with no external magnetic

field, only if the total symmetry is the same in the canted and uncanted states. The results of the high temperature fit are shown in the Table 4.4.

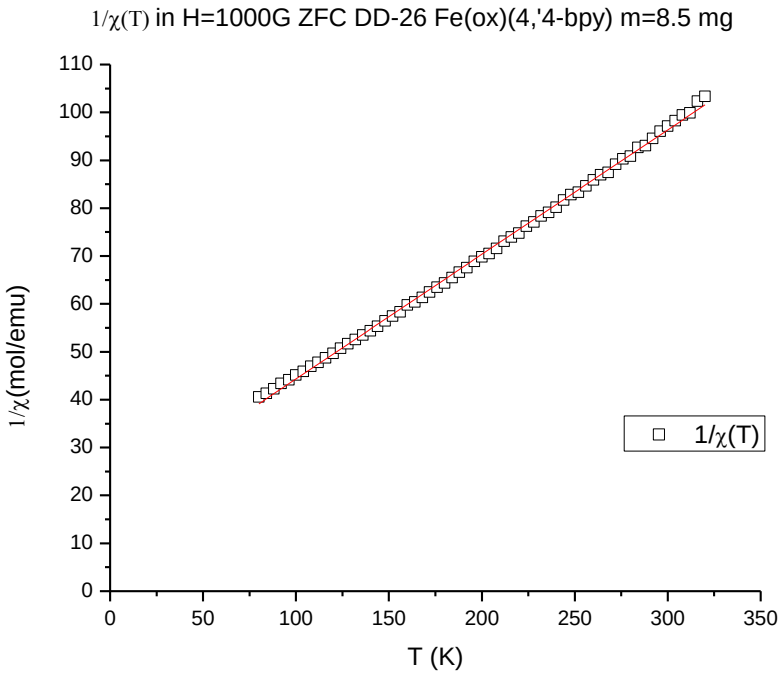

Fig. 4.26. 1/χ(T) ZFC Curie-Weiss fit of Fe(ox)(4,4'-bipyridine)

Ni(ox)(4,4'-bipyridine): The magnetization as a function of the applied field measurement *M(H)* was measured at temperature *T*=2 K. As in the previous measurements [ref. 55] of M(ox)(4,4'-bipyridine), hysteresis was not observed in this compound (Fig 4.25). Metamagnetic behavior is detected with the same source like in Fe(ox)(4,4'-bipyridine)The results of the high temperature fit are shown in the Table 4.4.

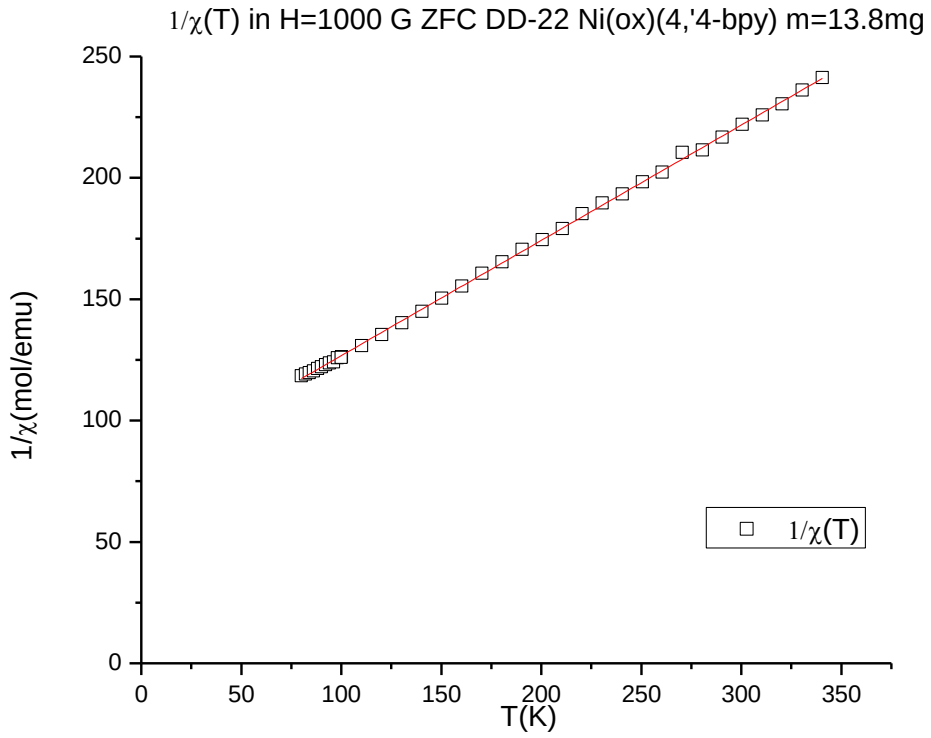

Fig. 4.27. 1/χ(T) ZFC Curie-Weiss fit of Ni(ox)(4,4'-bipyridine)

Co(ox)(4,4'-bipyridine): As the magnetic field increases, the temperature where the maximum occurs value of the local maximum decreases in the value, but spreads along the greater range. However, the position of the maximum on the temperature scale does not change with change of the external magnetic field.

As in the cases of the Fe(ox)(4,4'-bipyridine) and Ni(ox)(4,4'-bipyridine) compounds in the same family, fitting of the Co(ox)(4,4'-bipyridine) ground state suggests canted antiferromagnetic behavior that is in compatible with preliminary fits performed on this compound for magnetic susceptibility. The results of the high temperature fit are shown in the Table 4.4.

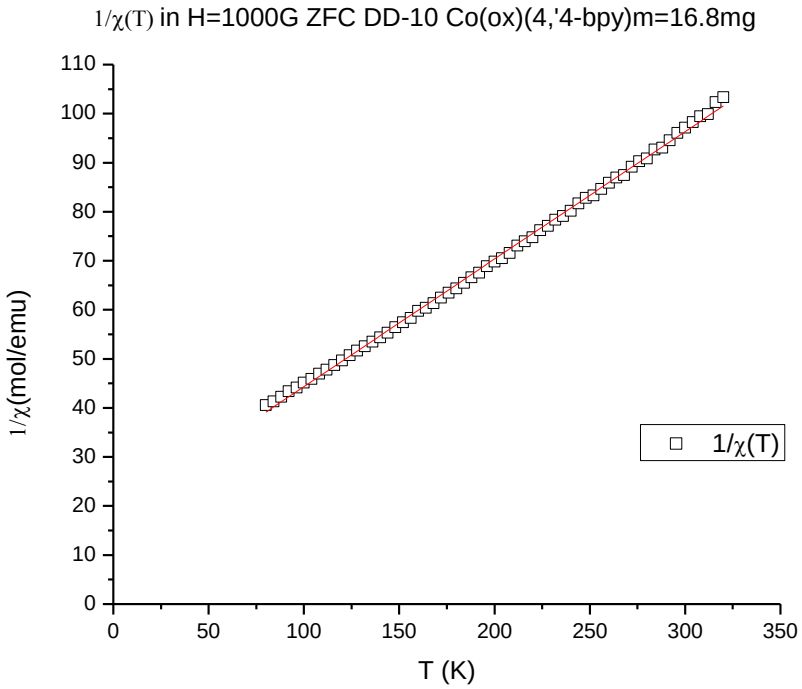

Fig. 4.28. 1/χ(T) ZFC Curie-Weiss fit of Co(ox)(4,4'-bipyridine)

These unusual magnetic properties of M(ox)(4,4'-bipyridine) family probably originate from strong M-M exchange, which is facilitated through oxalate bridges. The magnetic M ions at the octahedral sites form chains with intrachain separation of 5.309-5.472 *Å*. Although the M-M separation is quite large, the bonding between the oxalates and the M ion makes the transmission of magnetic interaction between the M-M magnetic couplings very effective. The M-M interchain separation suggests a possible M-M coupling along this direction, which complicates the magnetic structure of these compounds. Measurements and results of initial fittings are in perfect agreement with the previously published initial investigations performed on M(ox)(4,4'- bipyridine) [ref. 61]. Therefore, the intrachain interaction between metallic ion centers is antiferromagnetic, while the interaction between chains is ferromagnetic.

4.2.3. Magnetic measurements $M(N_3)_2$(4,4'-bipyridine)

$M(N_3)_2$(4,4'-bipyridine): The magnetic behavior of the $M(N_3)_2$(4,4'-bipyridine) compound exhibits characteristics of the typical antiferromagnet, with a very well defined cusp. There is no significant difference between ZFC and FC measurements of χ(T). The only exception is $Cu(N_3)_2$(4,4'-bipyridine) which does not show magnetic ordering in the observed temperature range, and exhibits significant difference between ZFC and FC measurements of $\chi(T)$. Like in the previous cases of M(ox)(4,4'-bipyridine) and MCl_2(4,4'-bipyridine) high temperature data for $M(N_3)_2$(4,4'-bipyridine) was fit to the modified Curie-Weiss law. The results of that fit show magnetic ions interact ferromagnetically inside chains, except in the case of $M(N_3)_2$(4,4'-bipyridine), in which weak antiferromagnetic interaction is found.

$Fe(N_3)_2$(4,4'-bipyridine): The magnetization as a function of the applied field *M(H)* was measured at temperature *T*=3.9 K (Fig. 4.31). The observed hysteresis is consistent with previously published data for this compound [ref. 28]. The observed hysteresis is not symmetric because of a possible problem in instrumentation. The results of the high temperature fit are shown in the Table 4.4.

$Ni(N_3)_2$(4,4'-bipyridine): Magnetization as a function of the applied field measurement *M(H)* was made at temperature T=2 K (Fig 4.34). *M(H)* does not show hysteresis. The results of the high temperature fit are shown in the Table 4.4.

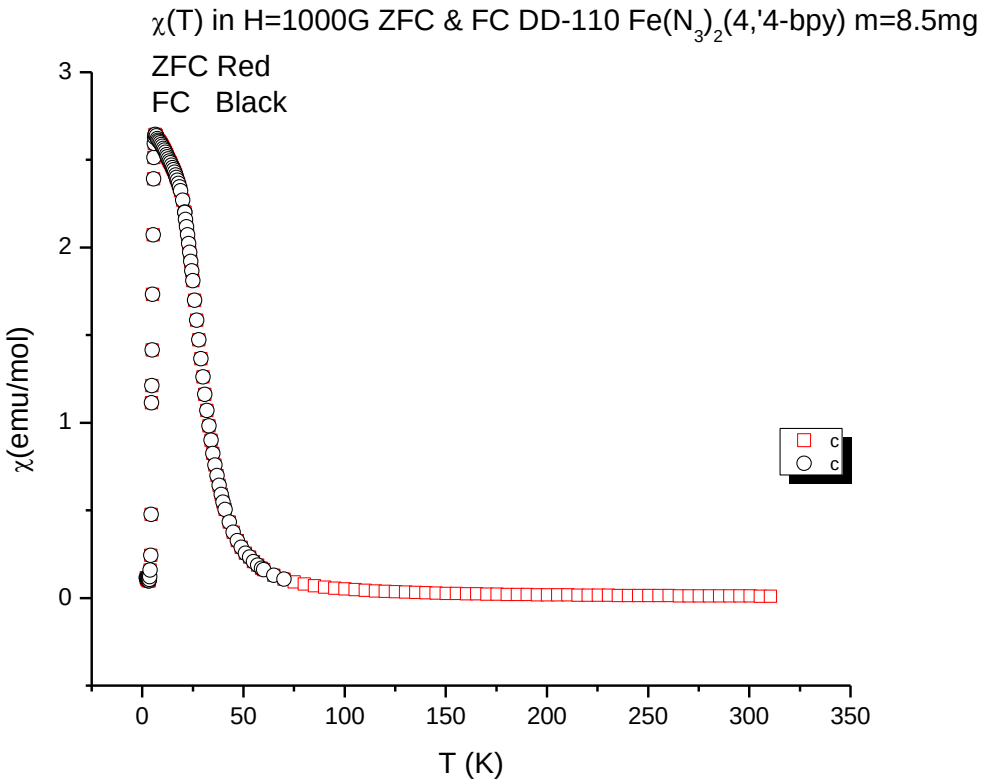

Fig. 4.29. χ(T) ZFC & FC behavior of $Fe(N_3)_2$(4,4'-bipyridine)

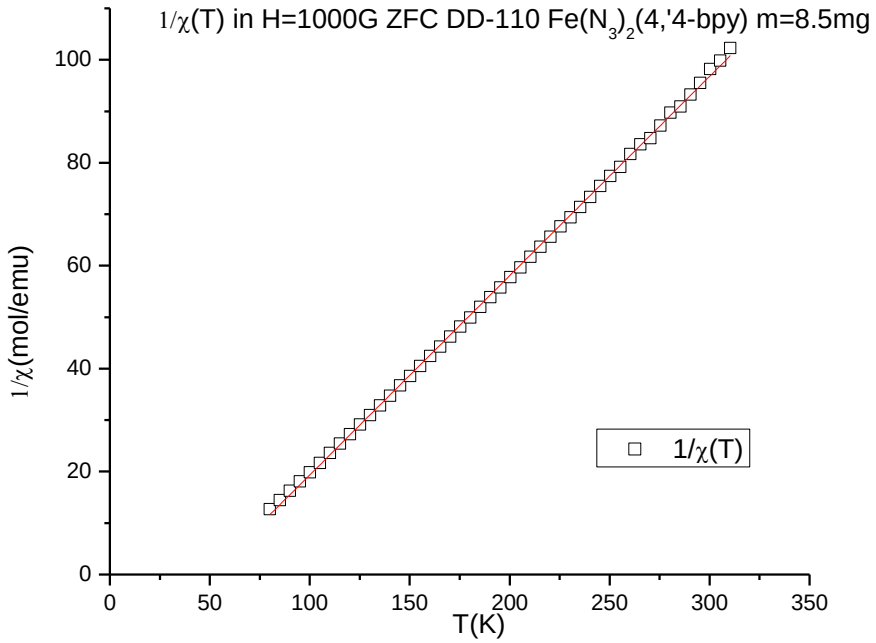

Fig. 4.30. 1/χ(T) ZFC Curie-Weiss fit of $Fe(N_3)_2$(4,4'-bipyridine)

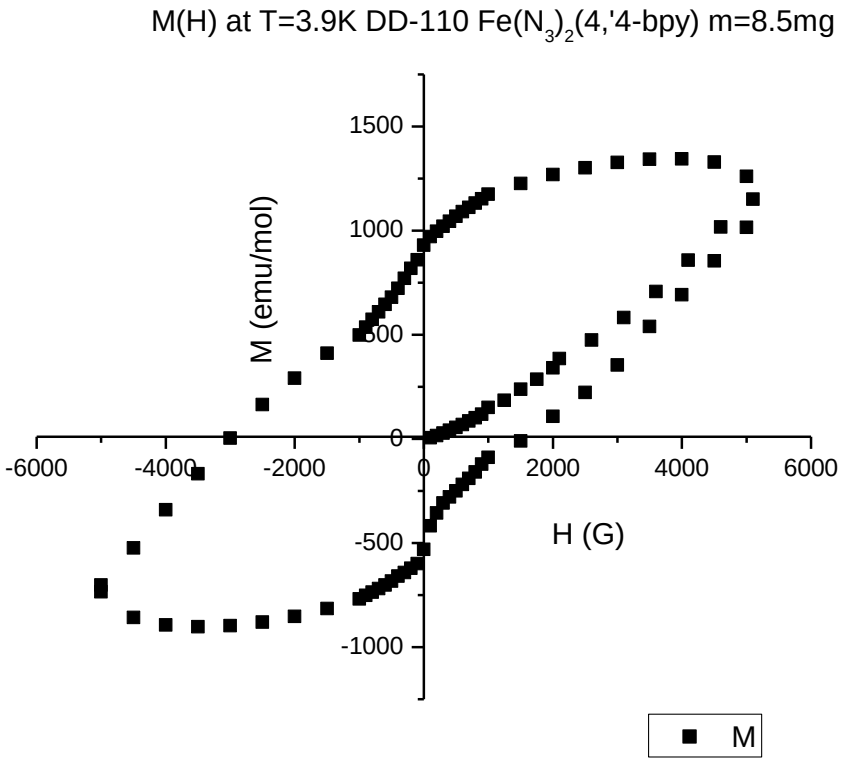

Fig. 4.31. M(H) at T=2K for $Fe(N_3)_2$(4,4'-bipyridine)

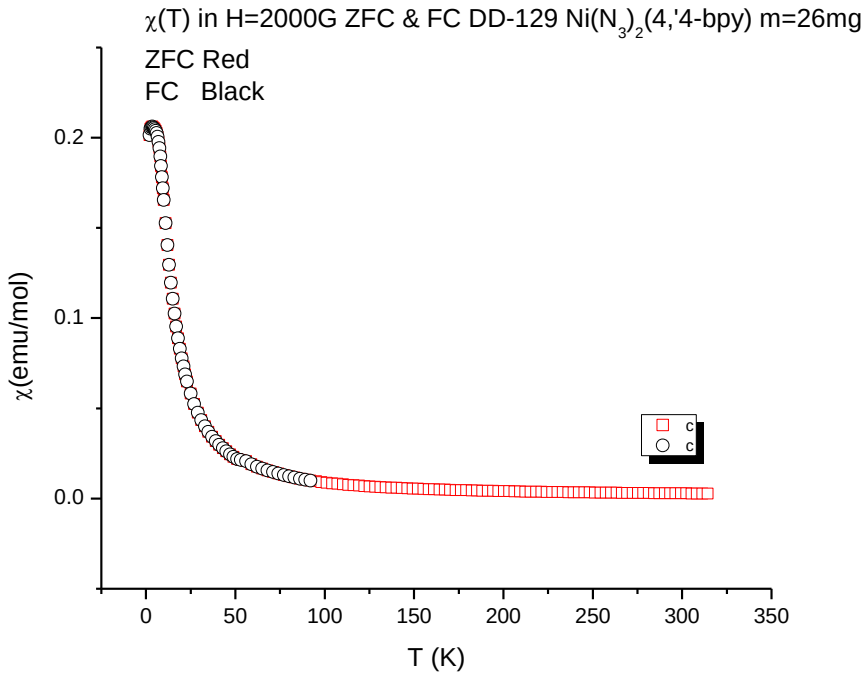

Fig. 4.32. ZFC & FC behavior of χ(T) $Ni(N_3)_2$(4,4'-bipyridine)

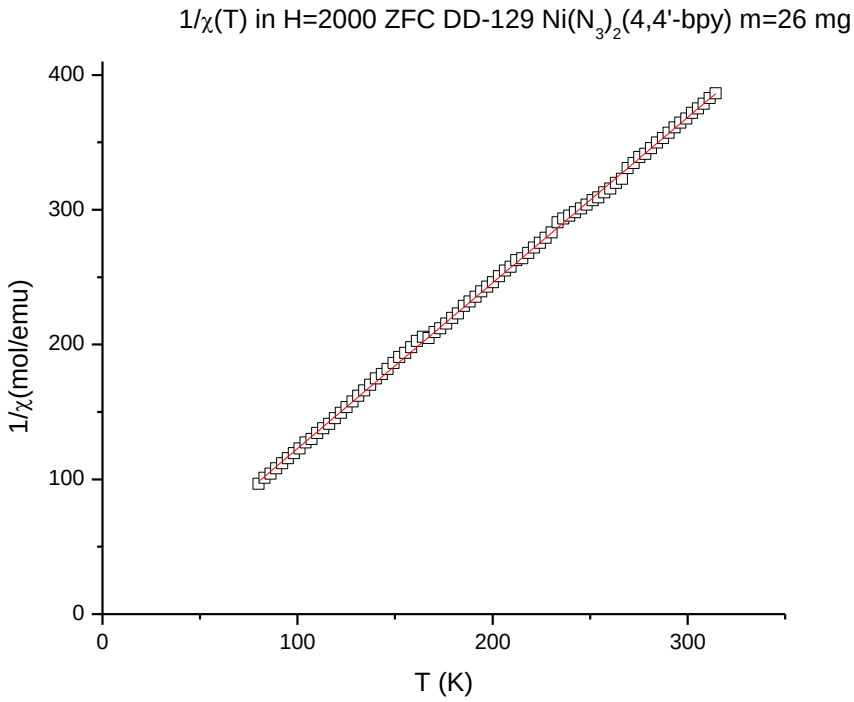

Fig. 4.33. 1/χ(T) ZFC Curie-Weiss fit of $Ni(N_3)_2$(4,4'-bipyridine)

$Co(N_3)_2$(4,4'-bipyridine): Co based azide compound exhibits hysteresis (Fig 4.37). Data show that the amount of the hysteresis diminishes as the temperature of the sample is increased. The magnetic coercive field in the case of *M(H)* measured at temperature T=1.9 K is H_c=2200 G. As the temperature increases, the coercive field decreases, and in the case of T=2.5 K the coercive field has a value of H_c=500 G. The results of the high temperature fit are shown in the Table 4.4.

$Cu(N_3)_2$(4,4'-bipyridine)*:* At the first magnetic behavior of this Cu based compound looks paramagnetic, with noticeable difference in the ZFC and FC measurements at low temperatures (Fig. 4.38).

However, initial fitting suggests that $Cu(N_3)_2$(4,4'-bipyridine) shows antiferromagnetic behavior, within the chains with θ= -5.45 K. Other compound's characteristics obtained from high temperature Curie-Weiss law are presented in the Table 4.4.

The magnetization as a function of the applied field *M(H)* was measured at temperature T=2 K. This compound does not exhibit hysteresis (Fig 4.40). The fit to the Brillouin function in the ground state indicates paramagnetic behavior, which is not surprising, since Cu has a predisposition for such behavior [ref. 16, 46].

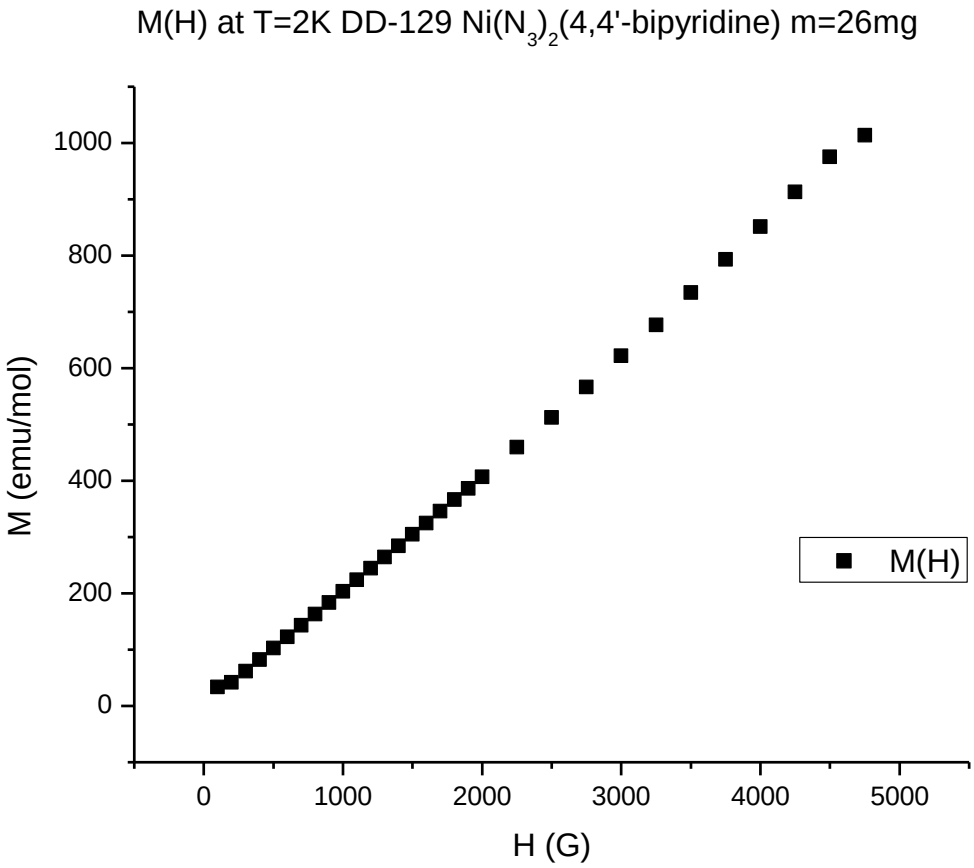

Fig. 4.34. M(H) at T=2K for $Ni(N_3)_2$(4,4'-bipyridine)

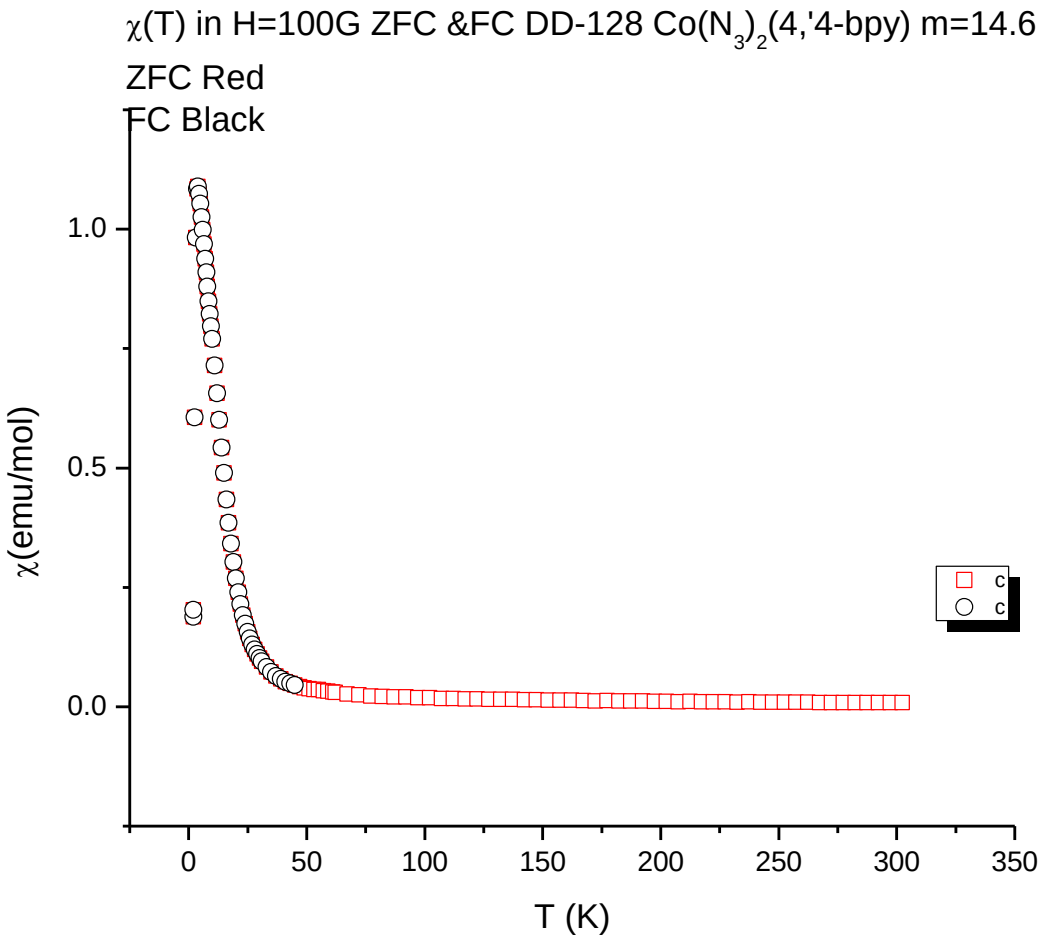

Fig. 4.35. ZFC & FC behavior of χ(T) in $Co(N_3)_2$(4,4'-bipyridine)

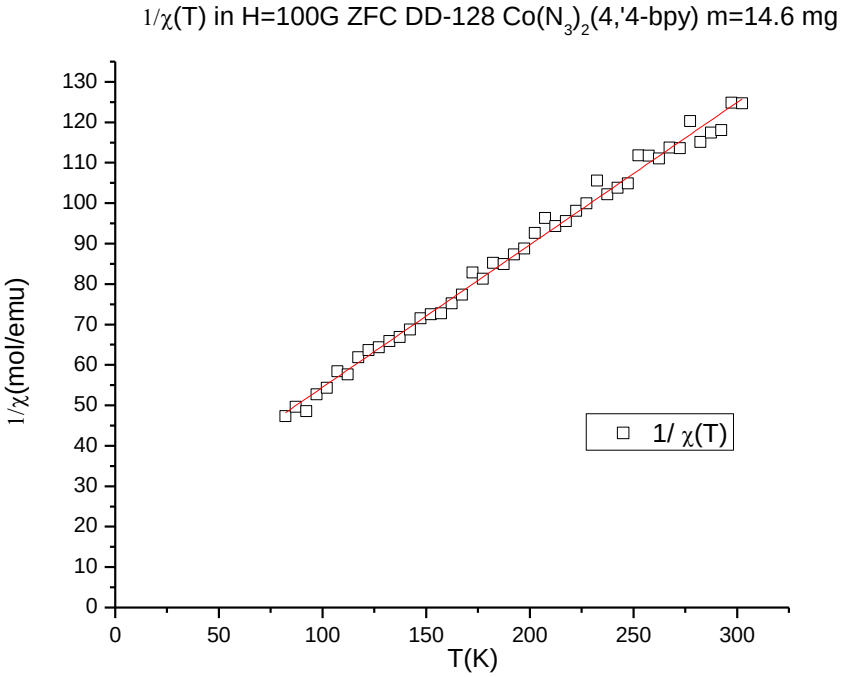

Fig. 4.36. 1/χ(T) ZFC Curie-Weiss fit of $Co(N_3)_2$(4,4'-bipyridine)

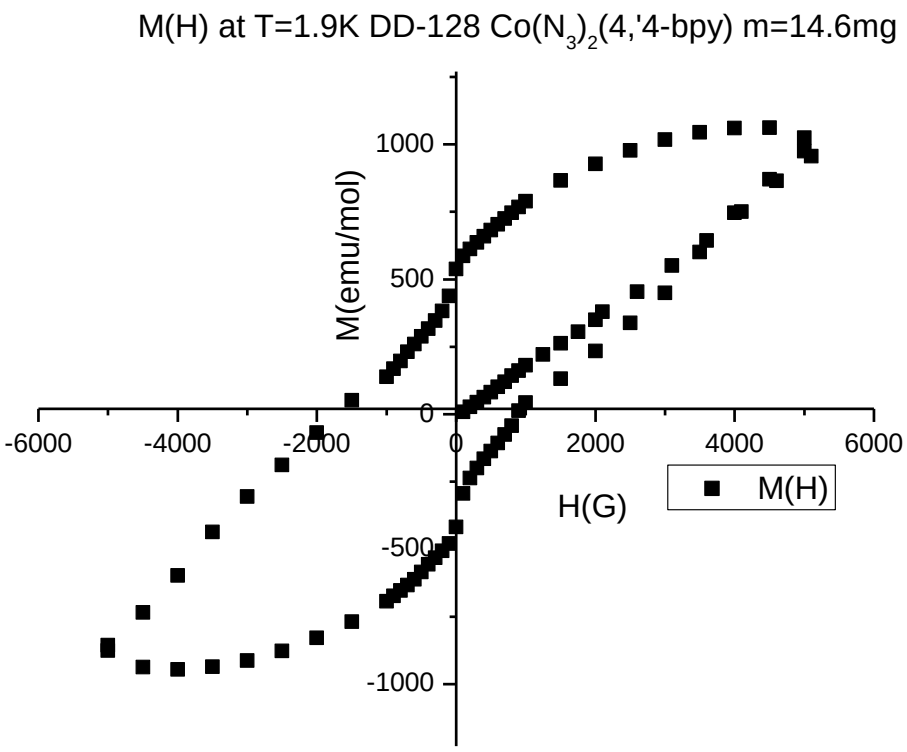

Fig. 4.37. M(H) at T=1.9 K $Co(N_3)_2$(4,4’-bipyridine)

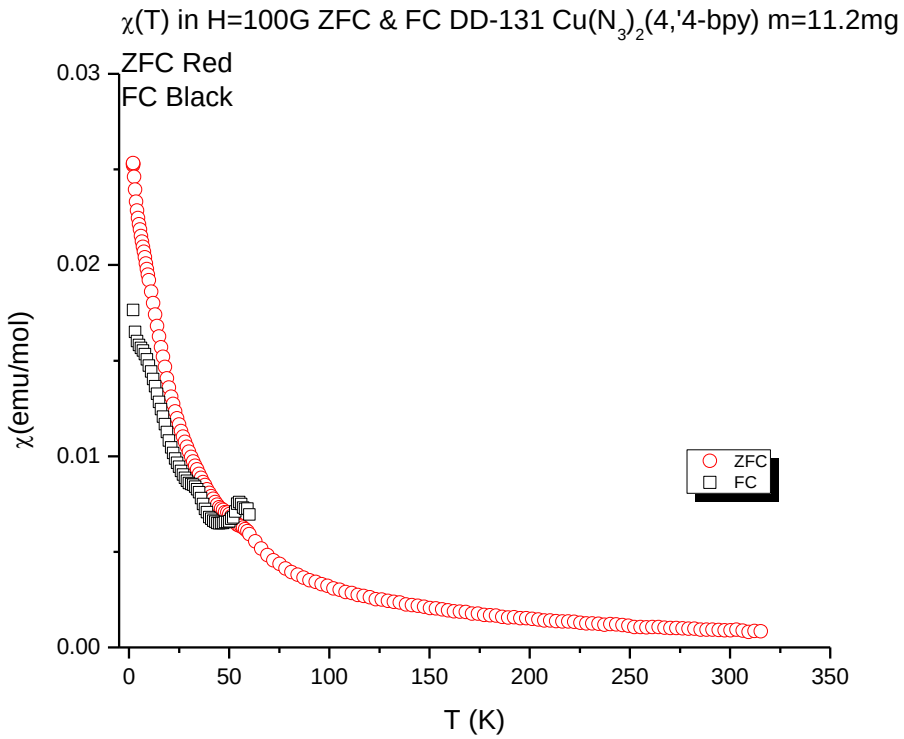

Fig. 4.38. ZFC & FC behavior of χ(T) in $Cu(N_3)_2$(4,4'-bipyridine)

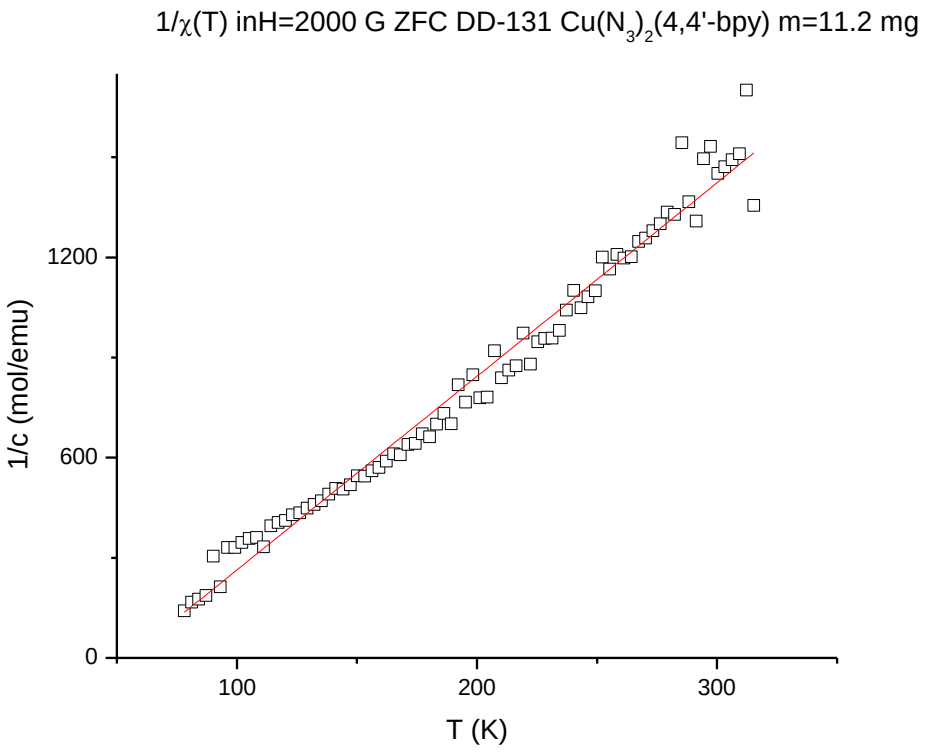

Fig. 4.39. 1/χ(T) ZFC Curie-Weiss fit of $Cu(N_3)_2$(4,4'-bipyridine)

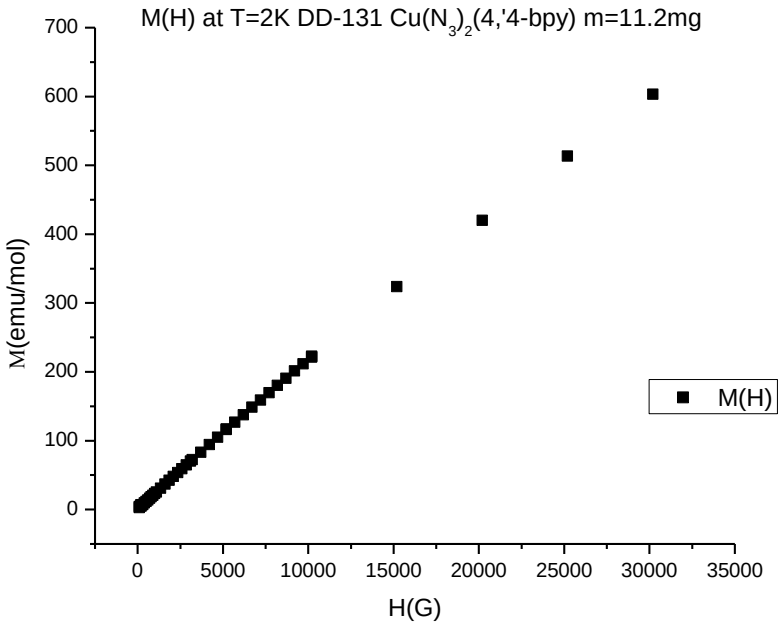

Fig. 4.40. M(H) at T=2K $Cu(N_3)_2$(4,4'-bipyridine)

Compound	$\chi_{0\ (emu/mol)}$	$\mu_{eff(}\mu_B)$	θ(K)
$FeCl_2$(4,4'-bipyridine)	2.7×10^{-5}	5.31	17
$NiCl_2$(4,4'-bipyridine)	2.3×10^{-5}	3.25	12
$CoCl_2$(4,4'-bipyridine)	5.6×10^{-5}	4.12	15
Fe(ox)(4,4'-bipyridine)	1.8×10^{-4}	4.58	-39
Ni(ox)(4,4'-bipyridine)	6.4×10^{-5}	4.18	-37.69
Co(ox)(4,4'-bipyridine)	5.4×10^{-5}	5.55	-4.76
$Fe(N_3)_2$(4,4'-bipyridine)	2.3×10^{-5}	4.55	7.49
$Ni(N_3)_2$(4,4'-bipyridine)	4.2×10^{-5}	2.73	11.06
$Co(N_3)_2$(4,4'-bipyridine)	3.7×10^{-5}	4.77	6.78
$Cu(N_3)_2$(4,4'-bipyridine)	2.2×10^{-5}	1.47	-5.45

Table 4.4. Initial Fitting Parameters

4.3. SPECIFIC HEAT MEASURMENTS

Specific heat measurements were only performed for $M(N_3)_2$(4,4'-bipyridine) since specific heats' behavior of chlorides and azides coordinated networks was addressed in previously published papers [ref. 55, 61]. In the case of $Ni(N_3)_2$(4,4'-bipyridine) and $Co(N_3)_2$(4,4'-bipyridine), the *C(T)* measurements were made in the absence of external magnetic field, while in the case of $Cu(N_3)_2$(4,4'-bipyridine) we made measurements in both zero field and in an external field *H*=7600 G. In the case of $Fe(N_3)_2$(4,4'-bipyridine), all the specific heat data information presented in this dissertation is based on previously published data [ref. 28]. In the case of $Ni(N_3)_2$(4,4'-bipyridine), recording data instrument's error prevented us from discussing specific heat data for this compound. The main characteristic of the specific heat behavior for the members of this family of coordinated networks is that they do not show visible λ-shape phase transition.

$Co(N_3)_2$(4,4’-bipyridine): The C(T) measurement was done made with H=0. (Fig.4.41)

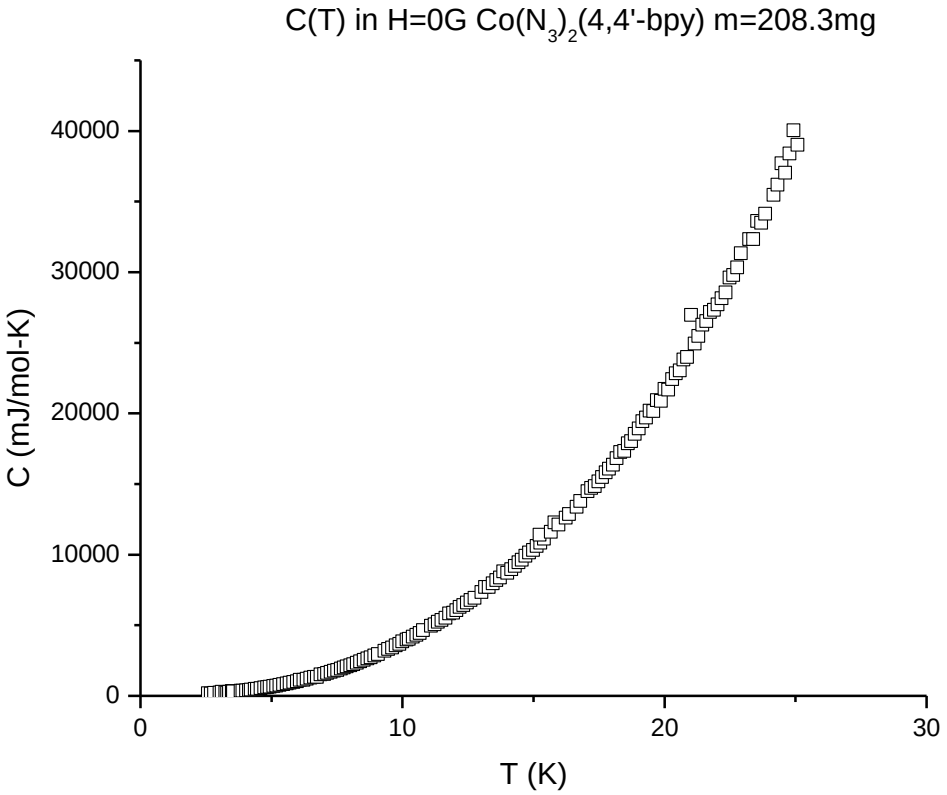

Fig. 4.41. C(T) in H=0G $Co(N_3)_2$(4,4’-bipyridine)

The initial fit to the measured data up to the T=10K was made using:

$C(T) = \gamma T + \beta T^3$ (4.3)

The linear term γT describes the contribution to the specific heat of the electrons and the cubic term βT^3 describes contribution of the specific heat of phonons. (Fig.4.42) The value of is coefficient γ is 160.60 mJ/mol.

The value of γ is unusually high and may indicator of a significant contribution from the magnetic component of the considered metal-organic coordinated network to the specific heat. Additional information which supports this view can be deduced from the graph *C/T* vs. T^2 (Fig.4.43), which deviates from the straight line which would be seen in the case of pure electronic and phonon contributions to the *C(T)*.

$Cu(N_3)_2$(4,4'-bipyridine): The C(T) measurements for this compound were made for in H=0 G and H=7600 G. (Figs. 4.44, 4.47) In the absence of an external magnetic field, this metal-organic, coordinated network does not show the characteristic λ shape, behaving like Co based compound under same conditions.

As in the case of $Co(N_3)_2$(4,4'-bipyridine) the data were fit to the same heat capacity function as for the T=10 K data. (Fig.4.47) The calculated value of γ is γ=220.45 mJ/mol.

Once again, the value of parameter γ is unusually large. Our explanation is the same as in the case of Co based compound, where we attributed it to the magnetic contribution to the specific heat.

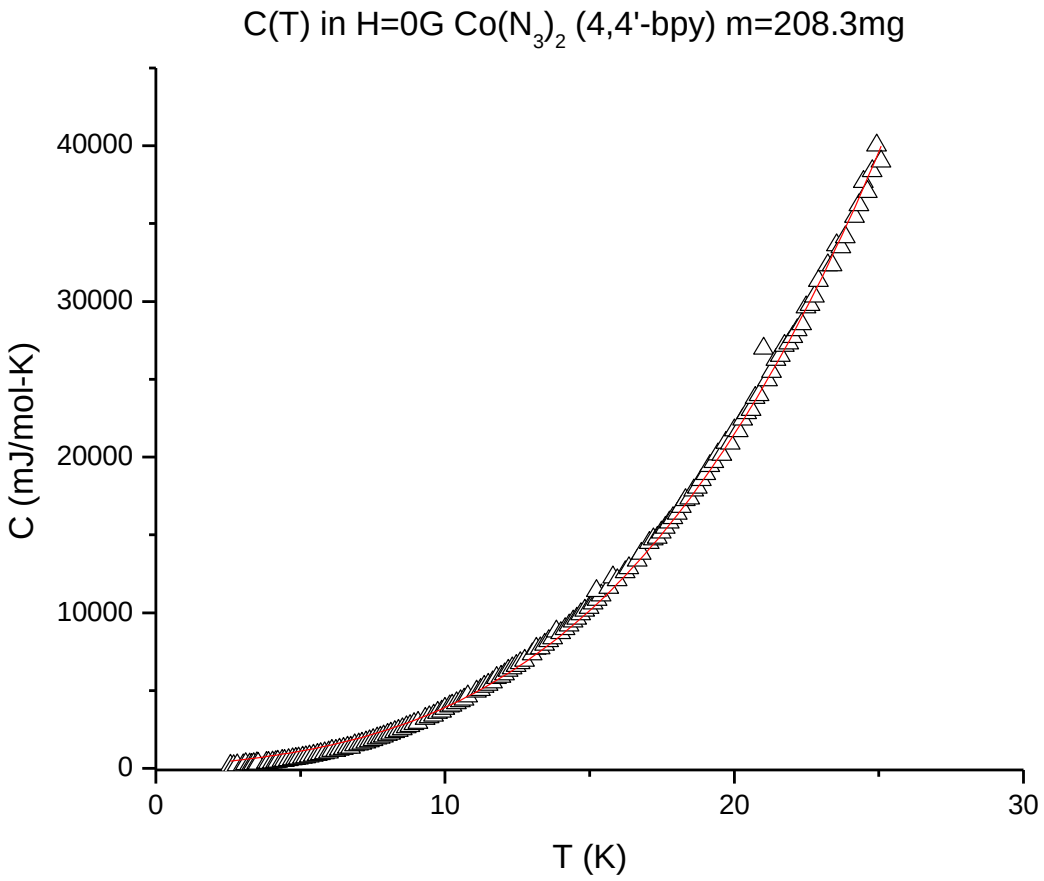

Fig. 4.42. C(T) fit in H=0G $Co(N_3)_2$(4,4'-bipyridine)

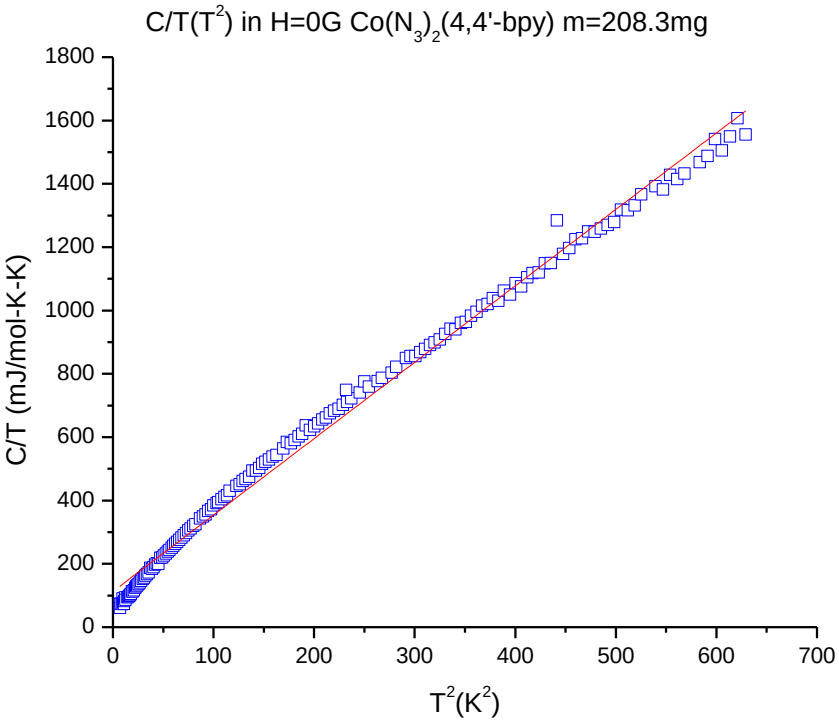

Fig. 4.43. C/T versus T^2 $Co(N_3)_2$(4,4'-bipyridine) for H=0 G

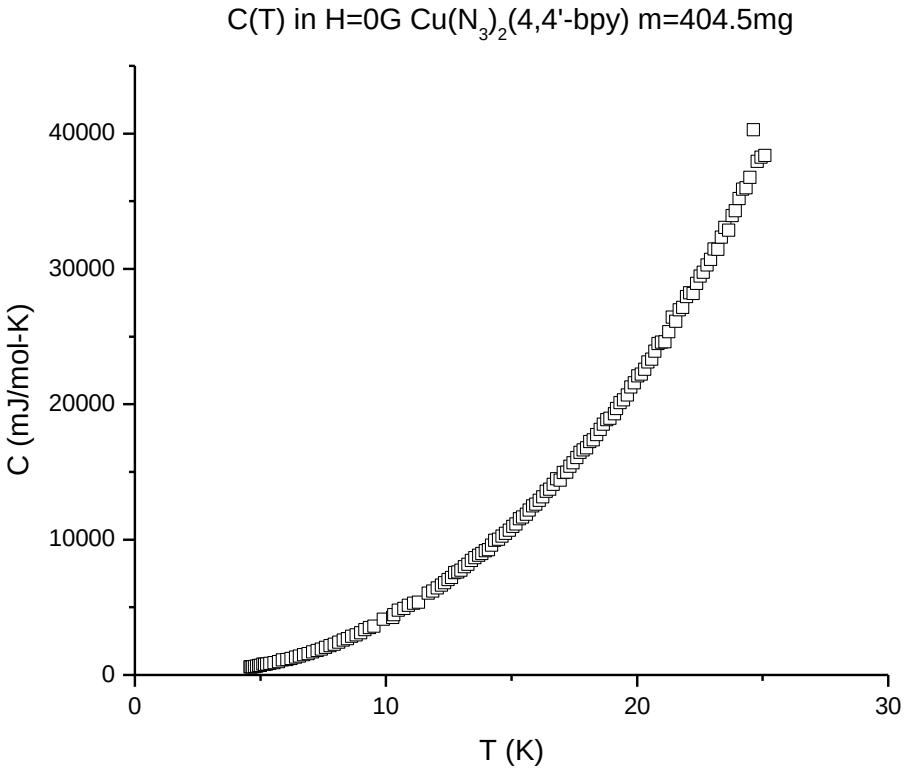

Fig. 4.44. C(T) in $Cu(N_3)_2$(4,4’-bipyridine) for H=0 G

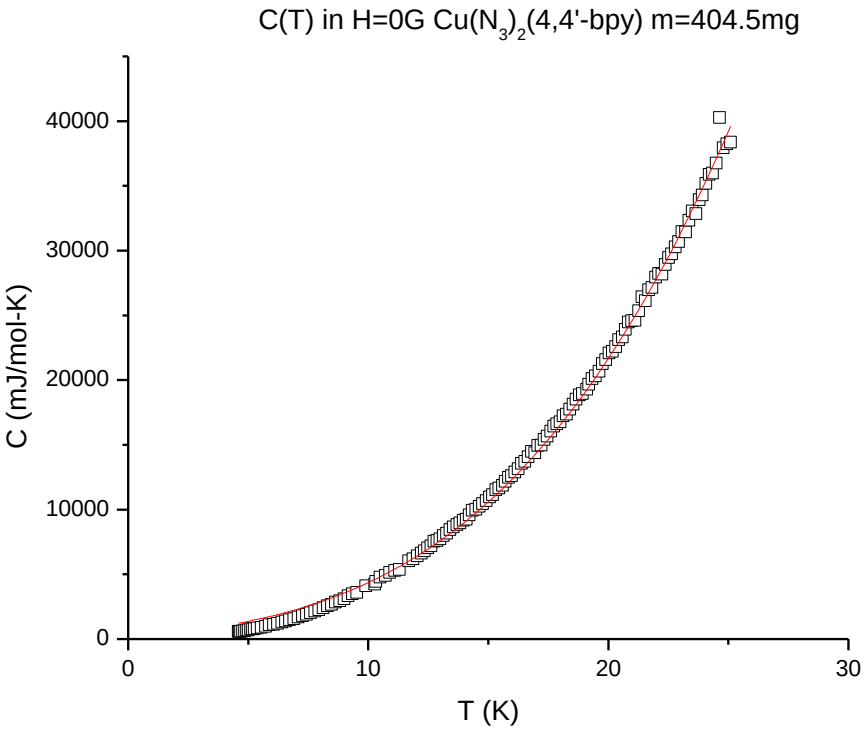

Fig. 4.45. C(T) in $Cu(N_3)_2$(4,4’-bipyridine) fit for H=0 G

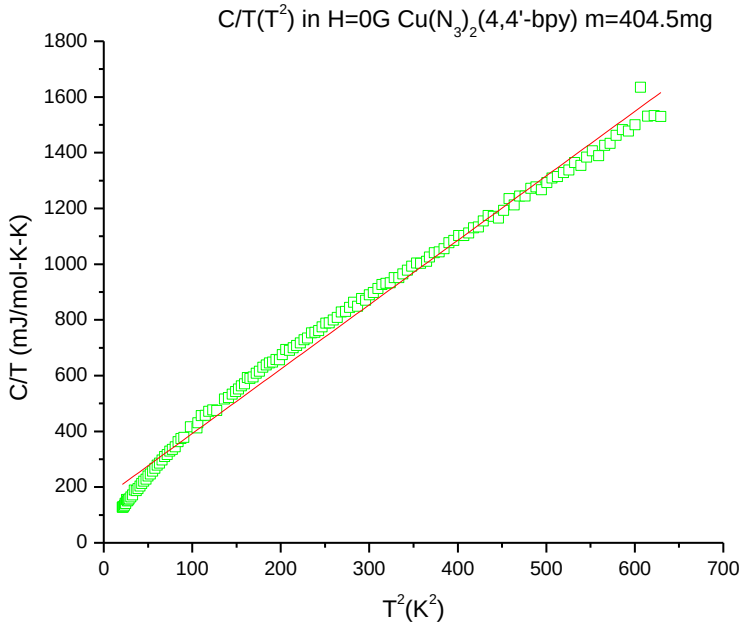

Fig. 4.46. C/T versus T^2 in $Cu(N_3)_2$(4,4'-bipyridine) for H=0 G

The graph of C/T vs. T^2 deviates from a straight line, pointing toward a contribution of the magnetic part to specific heat. (Fig 4.46)

We have also performed specific heat measurement for the Cu based compound in the external magnetic field of H=7600G. The characteristic λ shape behavior is pronounced, although material conduct less resembles one described by the equation $C(T)=\gamma T+\beta T^3$.

The fitting to the specific heat as the function electronic and phonon contribution (Fig. 4.48) resulted in our greatest value of the constant γ:

$$\gamma=490.86 \text{ mJ/mol.}$$

Our opinion is that magnetic contribution to the specific heat is enhanced by the application of external magnetic field.

The graph C/T vs. T^2 deviates significantly from a straight line, supporting the claim that we are detecting a significant magnetic contribution to the specific heat. (Fig. 4.49)

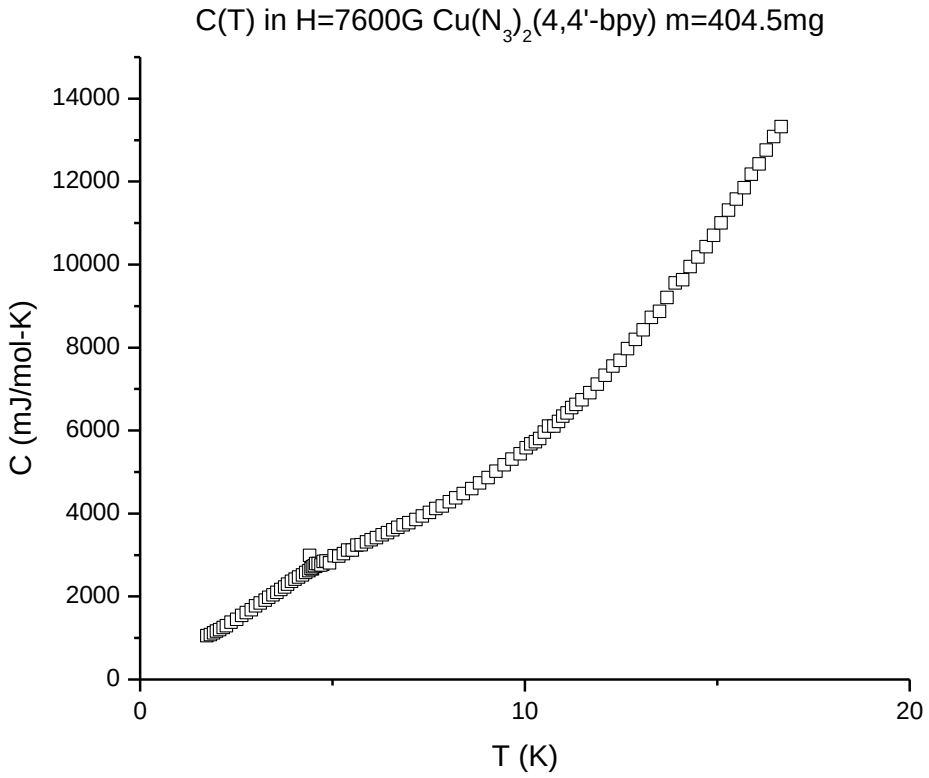

Fig. 4.47. C(T) in $Cu(N_3)_2$(4,4’-bipyridine) for H=7600G

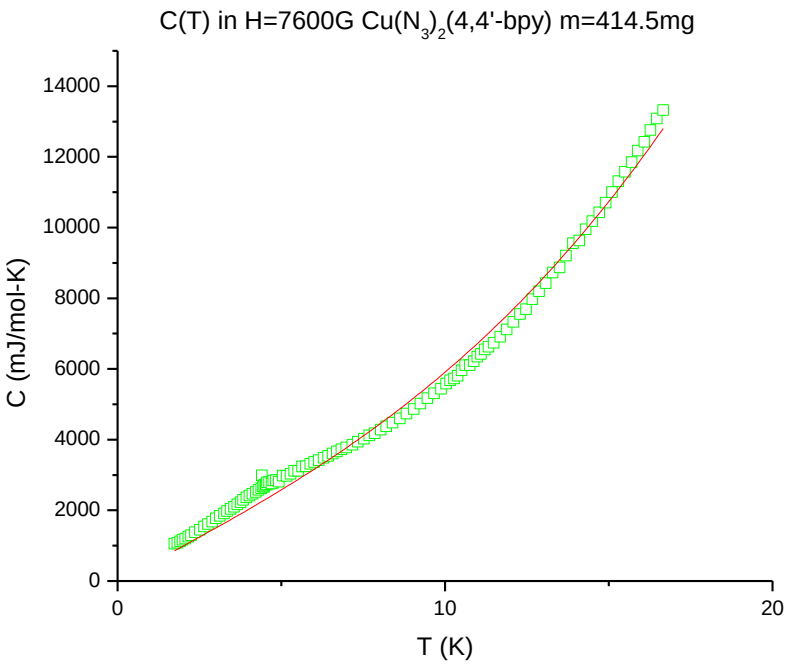

Fig. 4.48. C(T) fit in H=7600G $Cu(N_3)_2$(4,4'-bipyridine)

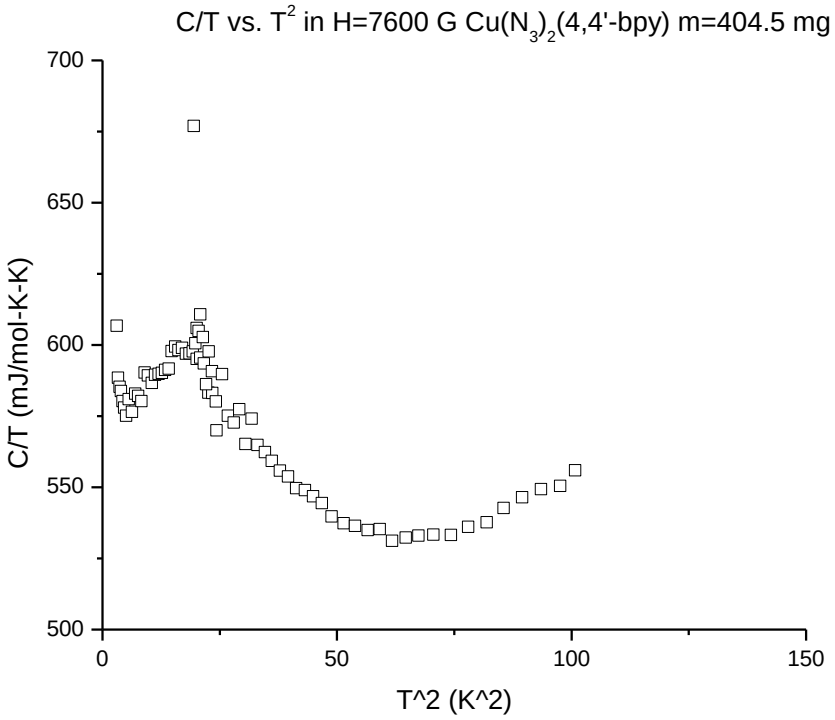

Fig. 4.49. C/T versus T^2 in $Cu(N_3)_2$(4,4'-bipyridine) for H=7600G

Our discussion assumes that there is no contribution of the free electrons in the metal-organic azide compounds since these metal-organic compounds are insulators.

Compound name	H(G)	γ(mJ/mol)
$Co(N_3)_2$(4,4'-bipyridine)	0	164.60
$Cu(N_3)_2$(4,4'-bipyridine)	0	220.45
$Cu(N_3)_2$(4,4'-bipyridine)	7600	490.86

Table 4.5. M(II)$(N_3)_2$(4,4'-bipyridine) fitting parameters

4.4. INTERPRETATION OF THE EXPERIMENTAL RESULTS IN TERMS OF THEORETICAL MODELS

4.4.1 MCl_2(4,4'-bipyridine)

Fe(Cl_2)(4,'4-bipyridine):. The χ(T) data was fit using the Fisher classical spin model of linear chains, above transition temperature. Using this model and spin *S*=2, fitting parameter that characterizes strength of the interaction:

$\frac{|J|}{k_B}$=5.67 K

$CoCl_2$(4,'4-bipyridine): The *χ(T)* data were fit to *χ(T)* for the Fisher classical spin model of linear chains. For this model and spin *S*=3/2:

$\frac{|J|}{k_B}$=2.07 K

$NiCl_2$(4,'4-bipyridine): The χ(T) data were fit to the *χ(T)* for the Fisher classical spin model of linear chains. For this model and spin *S*=1 strength of the interchain interaction can be characterized by:

$\frac{|J|}{k_B}$=1.67 K

A detailed discussion of the results of the fit and their place in understanding the structures of the compounds is given in the concluding paragraphs of this chapter.

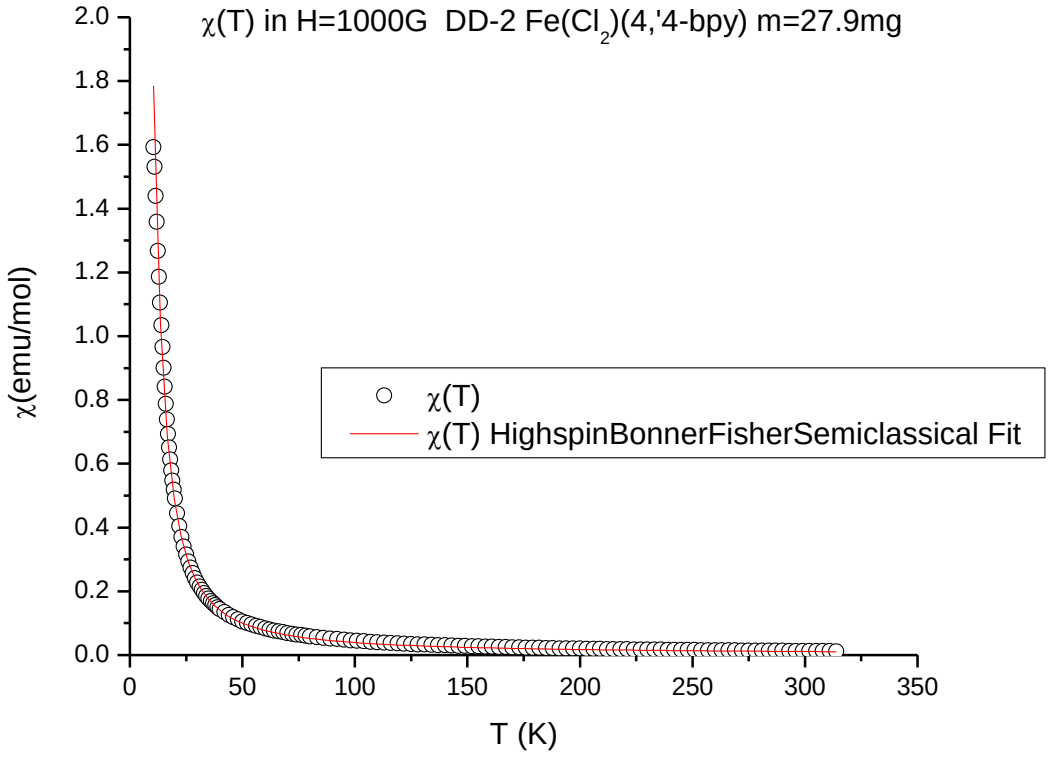

Fig. 4.50. χ(T) fit to the Fisher high spin classical fit for $FeCl_2$(4,4'-bipyridine) S=2

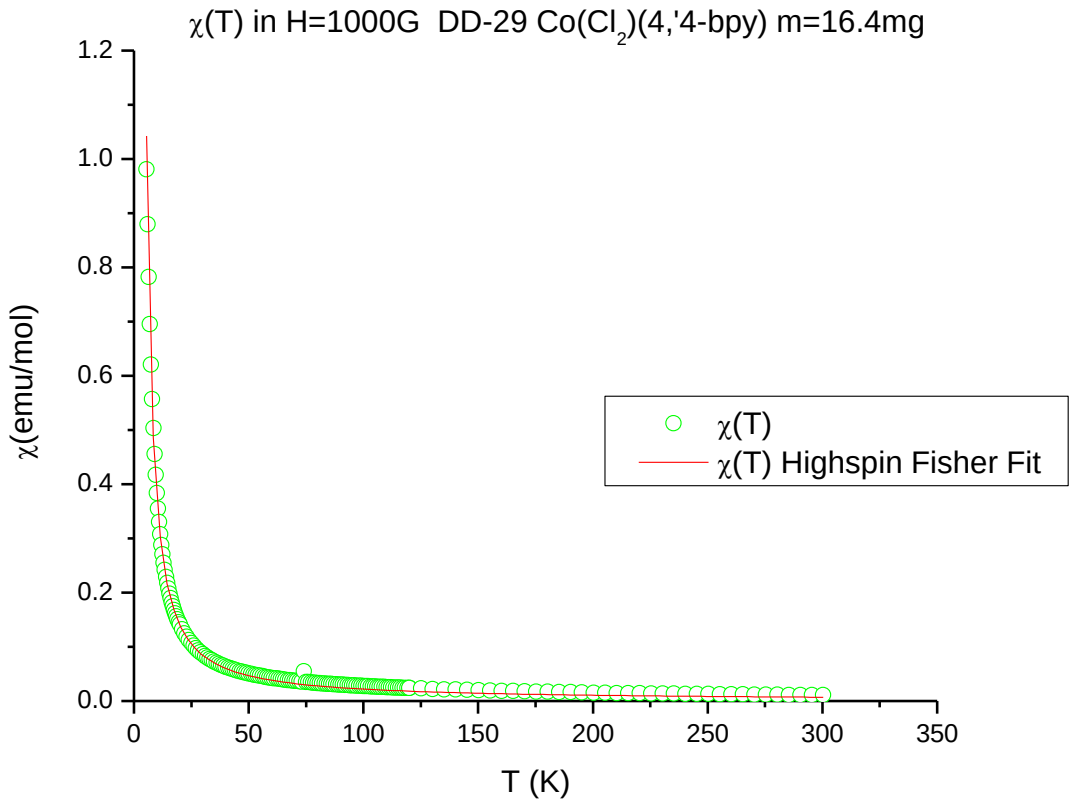

Fig. 4.51. χ(T) fit to the Fisher high spin semi-classical result for $CoCl_2$(4,4'-bipyridine) S=3/2

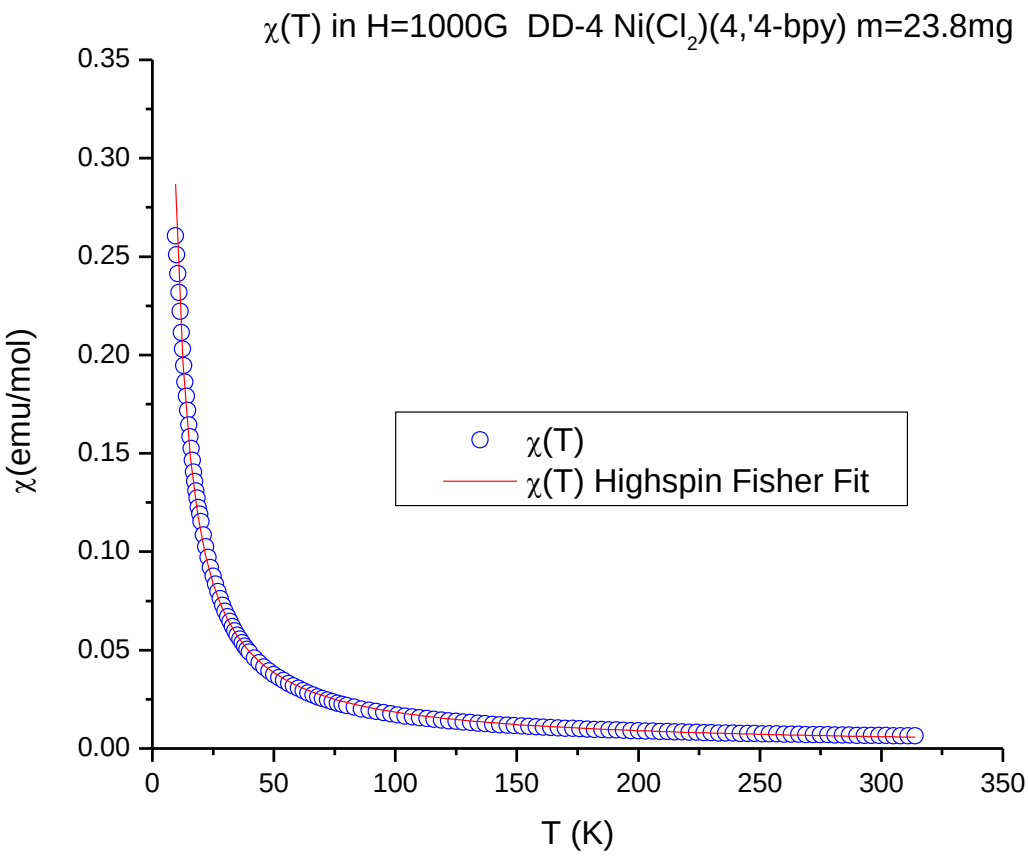

Fig. 4.52. χ(T) fit to the Fisher high spin semi-classical result for $NiCl_2$(4,4'-bipyridine) S=1

4.4.2. M(ox)(4,4'-bipyridine)

The oxalate ligand facilitates antiferromagnetic interaction in metal-organic compounds [ref. 61]. Therefore, we used the Bonner-Fisher model for anisotropic linear chains. The ratios of parallel and perpendicular susceptibilities for each compound were derived from the fit to the theoretical result for this theoretical model.

Fe(ox)(4,'4-bipyridine): The $\chi(T)$ data in the applied magnetic field H=1000 G were fit to the $\chi(T)$ predicted by the Bonner-Fisher model for linear chains with anisotropic interaction. Fitting parameter $\frac{|J|}{k_B}$ has the value:

$$\frac{|J|}{k_B} = -108.22 \text{ K}$$

The ratio of χ_{II} and $\chi_{\perp}$ for Fe(ox)(4,'4-bipyridine) is 0.61:0.39.

Co(ox)(4,'4-bipyridine): The $\chi(T)$ data in the applied magnetic field H=1000 G were fit to the $\chi(T)$ obtained using the Bonner-Fisher prediction for linear chains with anisotropic interaction. On this fit we superimposed the contribution paramagnetic phase in this compound:

$$\chi(T) = 0.08 \times \frac{C}{T} + 0.92 \times (0.45\chi_{II} + 0.55_{\perp}) \quad (4.4)$$

From the fit we concluded that the ratio of the paramagnetic to antiferromagnetic phases is 0.08:0.92. For the fitting parameter $\frac{|J|}{k_B}$ for Co(ox)(4,'4-bipyridine) we obtained:

$$\frac{|J|}{k_B} = -54.32 \text{ K}$$

The ratio of χ_{II} and $\chi_{\perp}$ in the case of Co(ox)(4,'4-bipyridine) is 0.45:0.55.

Ni(ox)(4,'4-bipyridine): The $\chi(T)$ measurement in the applied magnetic field H=1000 G were fit to the theoretical $\chi(T)$ for the Bonner-Fisher model for linear chains with anisotropic interactions. The fitting parameter $\frac{|J|}{k_B}$ that describes the strength of the interaction between magnetic ions in Ni based azide compound for this model has value:

$\frac{|J|}{k_B} = -69.75$ K

The ratio of χ_{II} and $\chi_{\perp}$ in the case of Ni(ox)(4,'4-bipyridine) is 0.80:0.20.

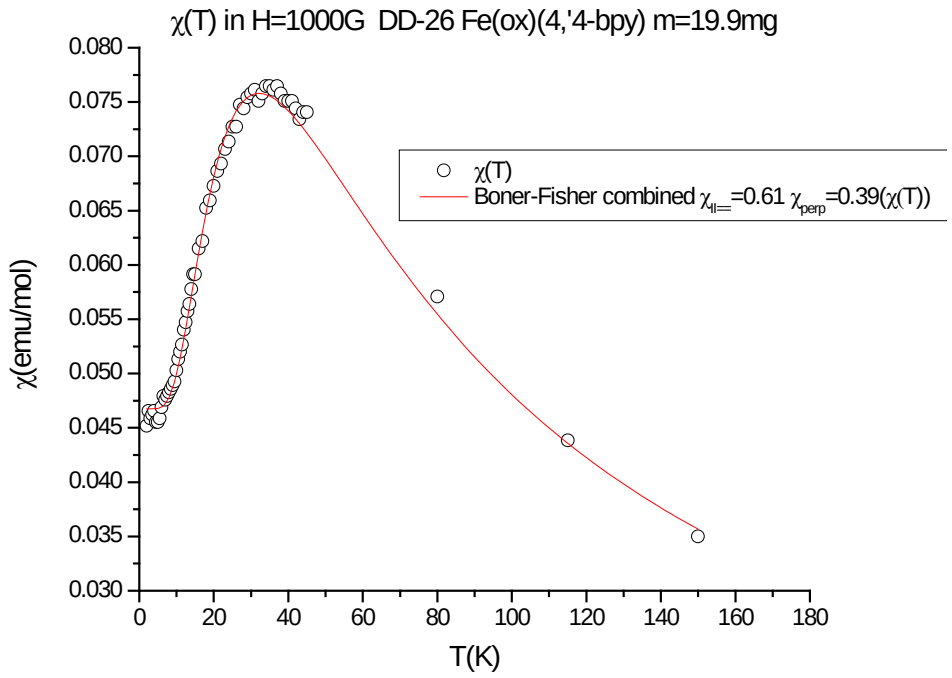

Fig. 4.53. χ(T) fit to the Bonner-Fisher result for Fe(ox)(4,4'-bipyridine) for S=2

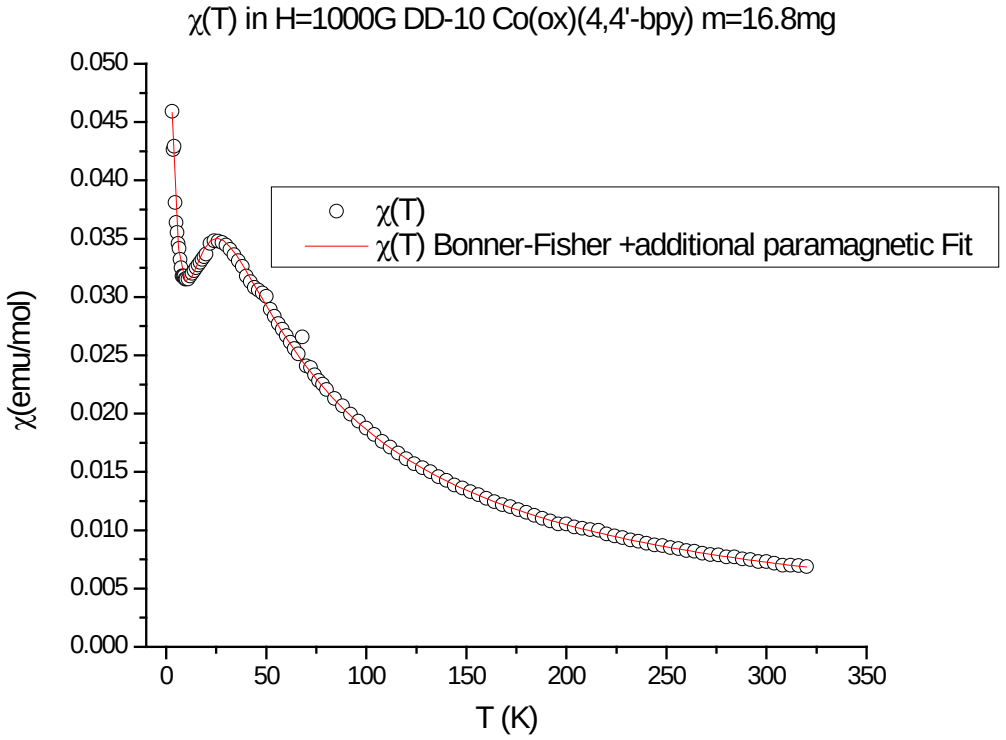

Fig. 4.54. χ(T) fit to the Bonner-Fisher result for Co(ox)(4,4'-bipyridine) for S=3/2

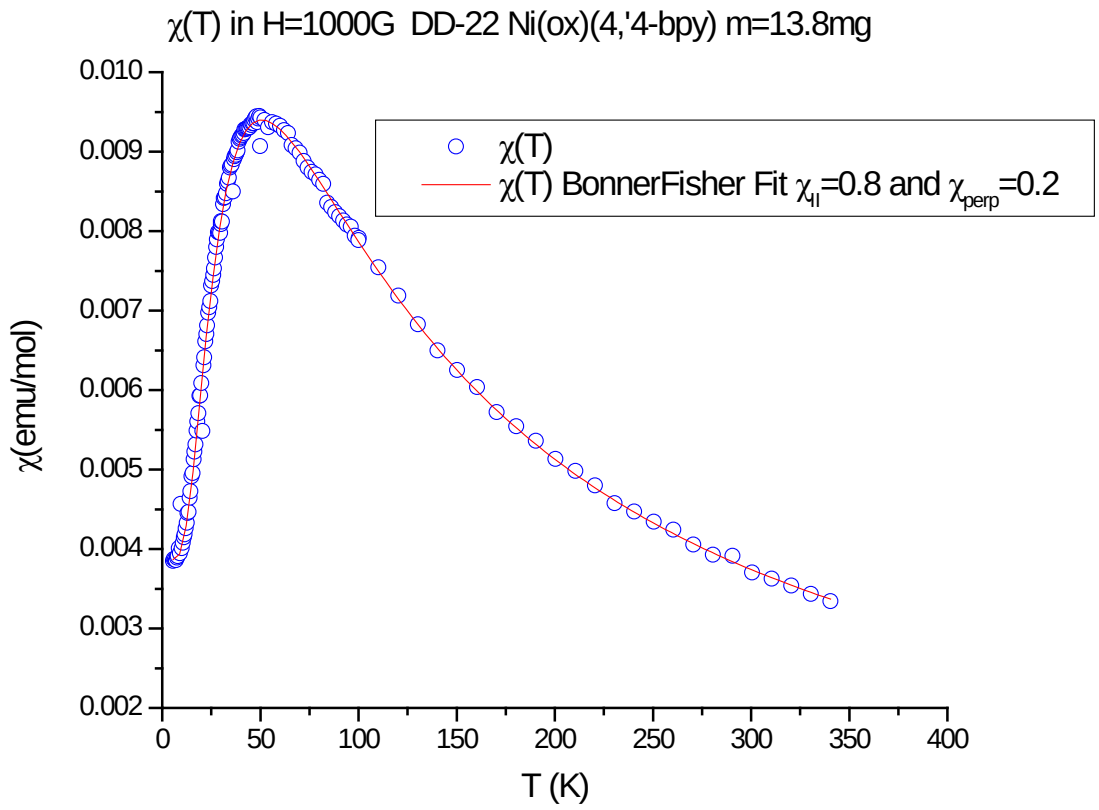

Fig. 4.55. χ(T) fit to the Bonner-Fisher fit for Ni(ox)(4,4'-bipyridine) for S=1

4.4.3. $M(N_3)_2$(4,4'-bipyridine)

$M(N_3)_2$(4,4'-bipyridine) is the family of the compounds which according to the initial fit in the high temperature range exhibits ferromagnetic behavior and is in that aspect similar to the family MCl_2(4,4'-bipyridine). Therefore, the same fitting according to the Fisher semi-classical spin is applied as in the case of Ni, Co, and Fe. In the case of Cu two approaches were tried. First, the quantum statistical form of susceptibility $\chi(T)$ with the spin S=1/2 was used. Second, in order to compare of behavior of this compound with other metal organic compounds of the same family, the Fisher semi-classical spin fit with the value S=1/2 was used.

$Fe(N_3)_2$(4,'4-bipyridine): The $\chi(T)$ data in the applied magnetic field H=1000 G was fit to the theoretical $\chi(T)$ obtained for the Fisher theoretical model with the classical spins as in the previously discussed cases. The only difference is that fit was applied at a slightly higher temperature, approximately T= 10 K. The fitting parameter $\frac{|J|}{k_B}$ that characterizes interchain interaction between magnetic ions in this compound has the value:

$\frac{|J|}{k_B}$=31.13 K

$Co(N_3)_2$(4,'4-bipyridine): The $\chi(T)$ data in the applied magnetic field H=1000 G was fit to the theoretical $\chi(T)$ for the Fisher model with classical spins Fitting parameter $\frac{|J|}{k_B}$ has the value:

$\frac{|J|}{k_B}$=5.23 K

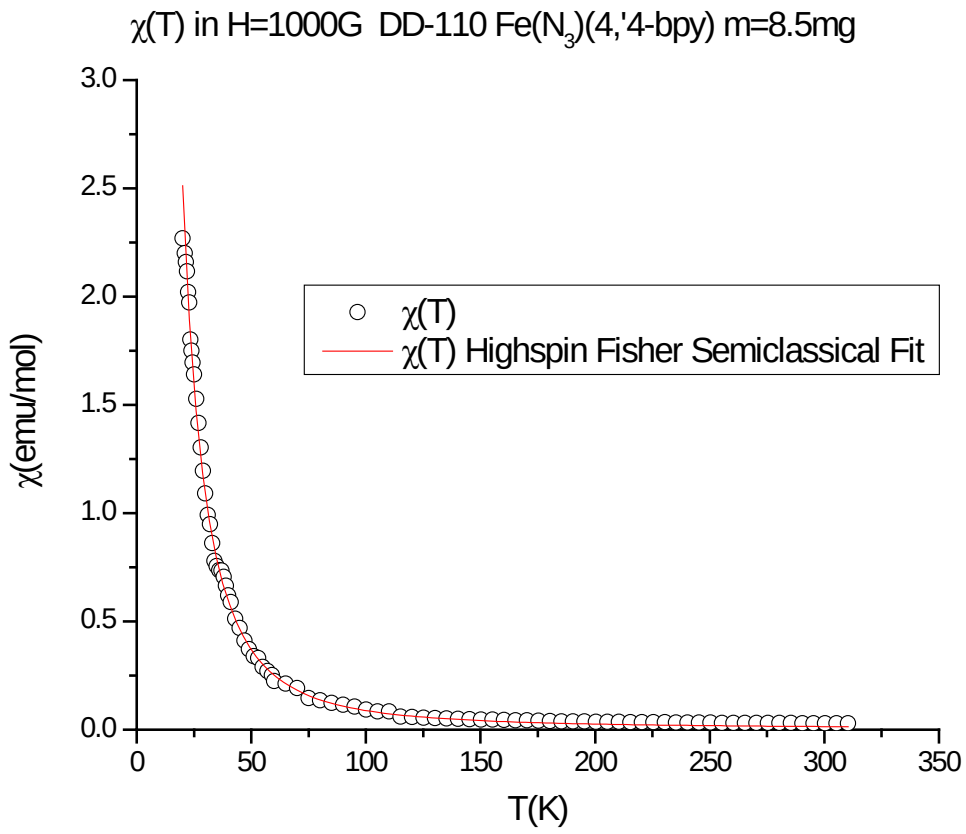

Fig. 4.56. χ(T) fit to the Fisher high spin classical result for $Fe(N_3)_2$(4,4'-bipyridine) S=2

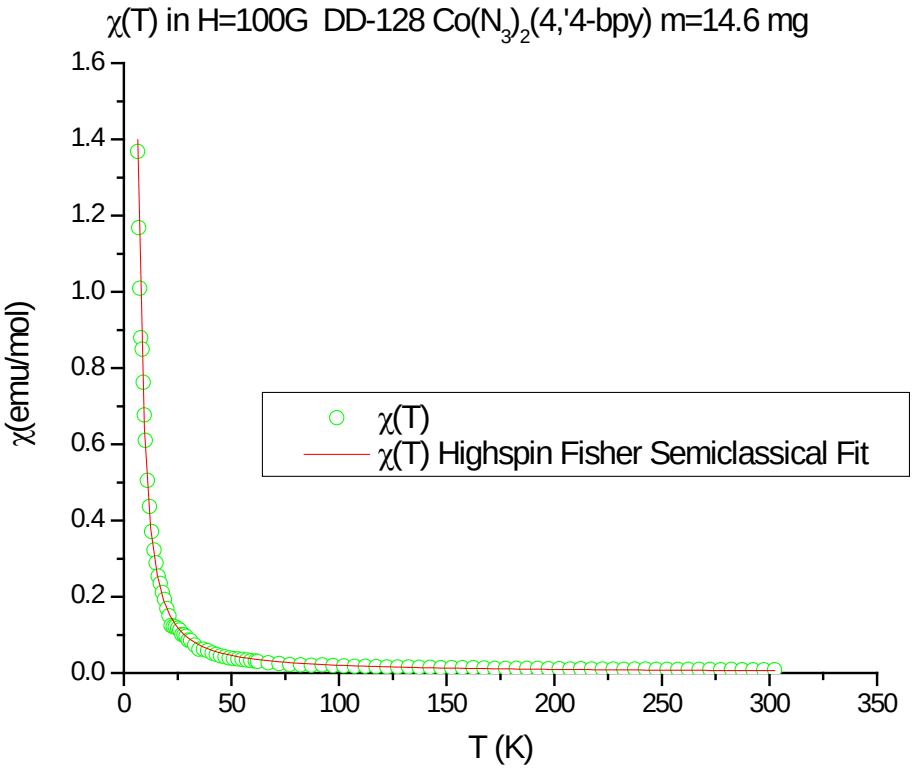

Fig. 4.57. χ(T) fit to the Fisher high spin semi-classical result for $Co(N_3)_2$(4,4'-bipyridine) S=3/2

$Ni(N_3)_2$(4,'4-bipyridine): The $\chi(T)$ data in the applied magnetic field H=500 G were fit to the theoretical $\chi(T)$ for the Fisher classical spin linear chain. The fit parameter $\frac{|J|}{k_B}$ has the f value:

$\frac{|J|}{k_B}$=2.49 K

$Cu(N_3)_2$(4,'4-bipyridine): Fitting was performed in two ways: 1) quantum statistical form of susceptibility $\chi(T)$ with spin S=1/2; and 2) Fisher semi-classical spin fit with S=1/2. In addition, we subtracted the diamagnetic susceptibility of the weighing paper and ligands, since the measured susceptibility $\chi(T)$ is very small and can be affected by these values [ref. 16, 17, 31, 46]. The fitting was calculated in H=2000 G and yielded:

$\frac{|J|}{k_B}$=−12.18 K

In the case of the high spin Fisher semiclassical fit with S=1/2 the statistical agreement between theoretical and experimental data is 0.995.

$\frac{|J|}{k_B}$=−4.66 K

In the case of the Bonner-Fisher quantum mechanical fit for the Heisenberg ferromagnet with S=1/2, the statistical agreement between theoretical and experimental data is 0.984. The measurements and fitting procedures were repeated two times with consistent results. That both these two different theoretical approaches describe the data so well is surprising, and at this moment, we do not have an adequate theoretical explanation.

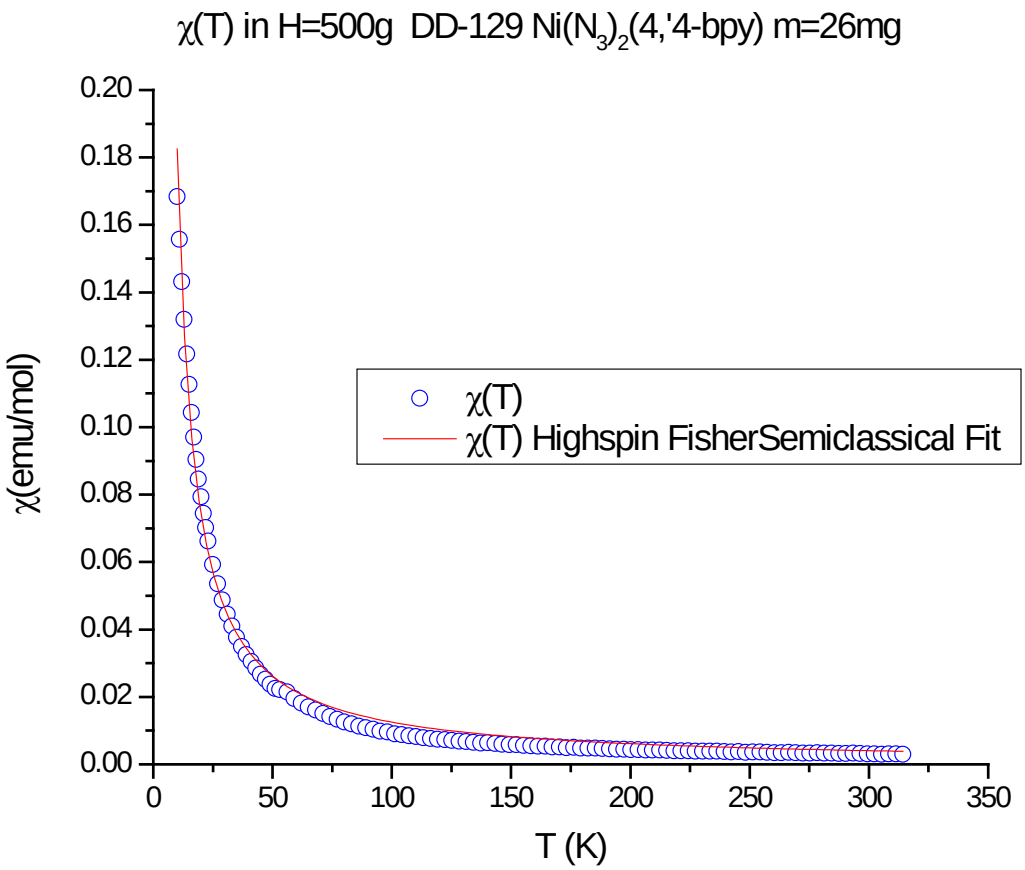

Fig. 4.58. χ(T) fit to the Fisher high spin semi-classical result for $Ni(N_3)_2$(4,4'-bipyridine) with S=1

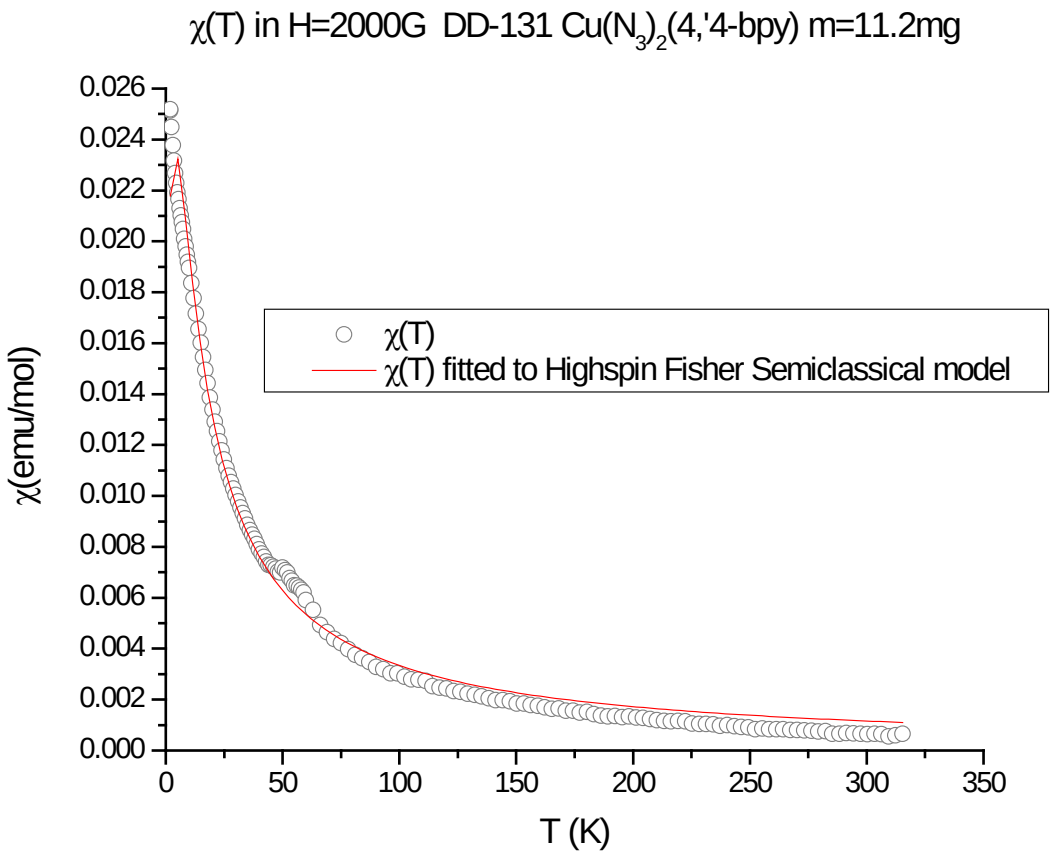

Fig. 4.59. χ(T) fit to the Fisher high spin semi-classical result for $Cu(N_3)_2$(4,4'-bipyridine) S=1/2

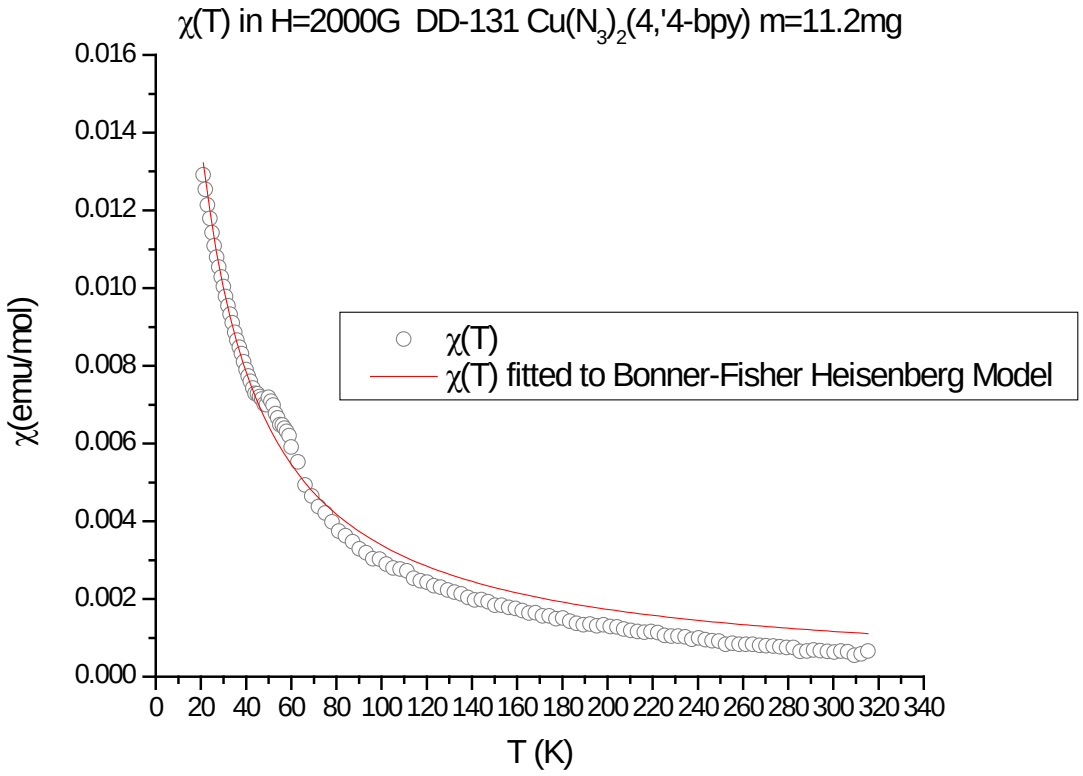

Fig. 4.60. χ(T) fit to the Bonner-Fisher Heisenberg results for $Cu(N_3)_2$(4,4'-bipyridine) S=1/2

Compound	Model	$\frac{J}{k_B}$ (K)	Remarks
$FeCl_2$(4,4'-bipyridine)	Fisher Classical Spin Linear Chain	5.67	S=2
$NiCl_2$(4,4'-bipyridine)	Fisher Classical Spin Linear Chain	1.67	S=1
$CoCl_2$(4,4'-bipyridine)	Fisher Classical Spin Linear Chain	2.07	S=1.5
Fe(ox)(4,4'-bipyridine)	Bonner-Fisher Linear Chain	-108.22	S=2 $\chi_{\perp}$=0.39, χ_{II}=0.61
Ni(ox)(4,4'-bipyridine)	Bonner-Fisher Linear Chain	-69.75	S=1 $\chi_{\perp}$=0.20, χ_{II}=0.80
Co(ox)(4,4'-bipyridine)	Bonner-Fisher Linear Chain	-54.32	S=3/2 $\chi_{\perp}$=0.55, χ_{II}=0.45
$Fe(N_3)_2$(4,4'-bipyridine)	Fisher Classical Spin Linear Chain	6.70	S=2
$Ni(N_3)_2$(4,4'-bipyridine)	Fisher Classical Spin Linear Chain	2.49	S=1
$Co(N_3)_2$(4,4'-bipyridine)	Fisher Classical Spin Linear Chain	5.23	S=1.5
$Cu(N_3)_2$(4,4'-bipyridine)	Bonner-Fisher Ferromagnetic Chain	-4.23	S=1/2
$Cu(N_3)_2$(4,4'-bipyridine)	Fisher Classical Spin Linear Chain	-12.18	S=1/2

Table 4.6. Theoretical models main characteristics

4.5. ANALYSIS OF SPECIFIC HEAT DATA

As we already stated earlier, the specific heat was measured for $Cu(N_3)_2$(4,'4-bipyridine), and $Co(N_3)_2$(4,4'-bipyridine). In the analysis we will compare *C(T)* for these two coordinated networks with the previously measured specific heat data for $Fe(N_3)_2$(4,4'-bipyridine). [ref. 28] The characteristic λ shape transition that indicates magnetic ordering in metal-organic coordinated networks was not observed. However, when the specific heat data were fit to the electron and lattice contribution $\gamma T+\beta T^3$, we ended up with large values of the γ coefficient. If number of the free electrons in studied compounds as we assumed is negligible, then the high value of γ comes from the magnetic contribution in each of these materials. In that case, specific heat is given by:

$$c_{M(II)}(T) = c_{latt} + c_{mM(II)} \quad (4.5)$$

where c_{latt} is specific heat contribution of the lattice and $c_{mM(II)}$ is the contribution of magnetic component of the transitional metal in question. Since the materials are isostructural, we assume c_{latt} is the same in all coordination networks, so that differences between specific heats come from magnetic contributions that, in turn, depend on the value of the spin of transitional metal in question. First we compared *C(T)* in the case of copper and cobalt based compounds. (Fig. 4.61)

Comparing the specific heat data for cobalt and copper azide compounds, it can be concluded that Co is in the low spin state in the observed temperature range, since *C(T)* for Co and Cu based compounds have similar values, and Cu always has spin S=1/2. The explanation of such Co behavior comes from the large spin-orbital coupling that splits ground state of Co in this compound. [16, 46] The value of the spin has a strong

influence on the behavior of *C(T)*. That is clearly seen if we plot together specific heat data for Co and Cu with those measured previously in the case of Fe azide. (Fig. 4.62)

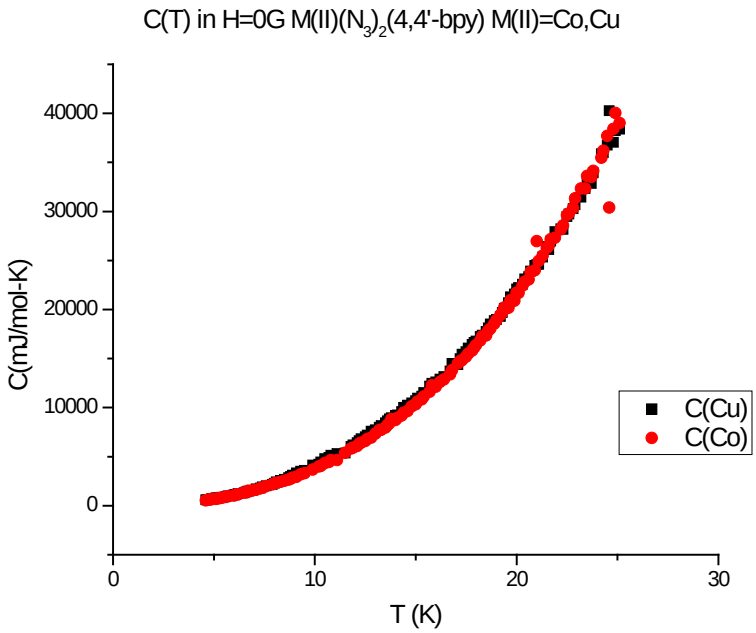

Fig. 4.61. Specific heat comparison for $Cu(N_3)_2$(4,'4-bipyridine) and $Co(N_3)_2$(4,4'-bipyridine)

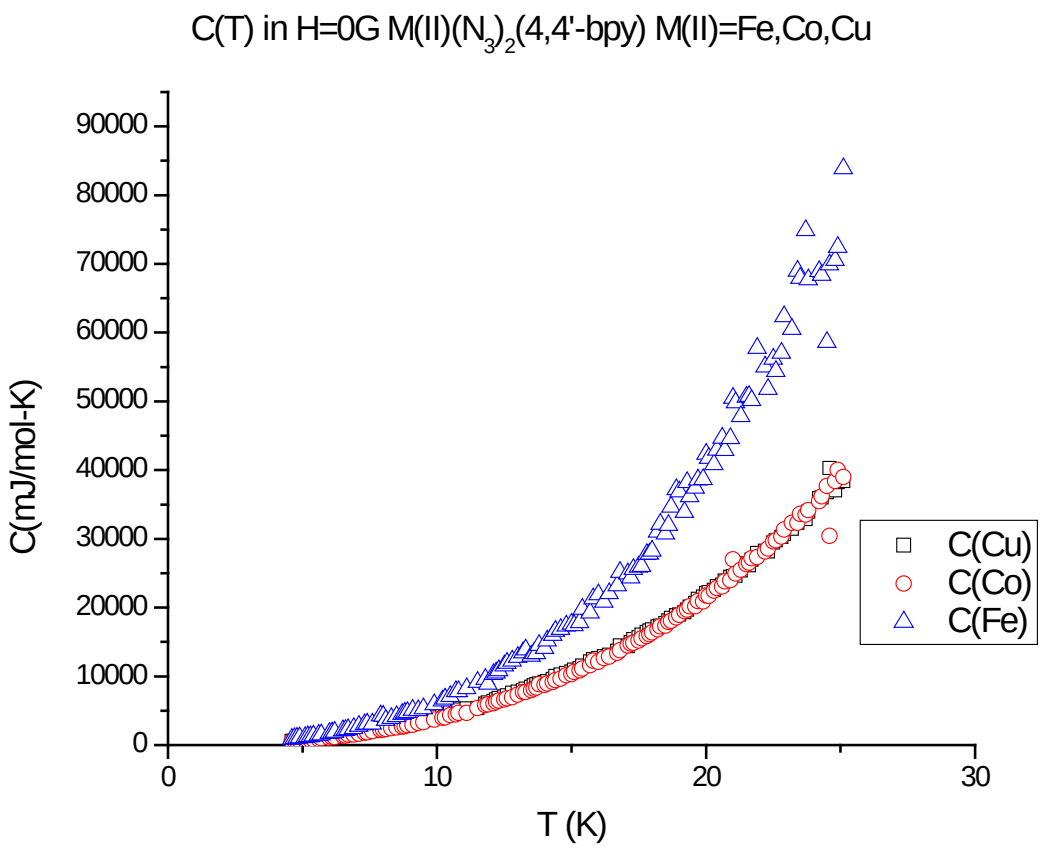

Fig. 4.62. Specific heat comparison for $Cu(N_3)_2$(4,'4-bipyridine), $Co(N_3)_2$(4,4'-bipyridine) and $Fe(N_3)_2$(4,4'-bipyridine)

In explaining the behavior of *C(T)* in the case of azide family of compounds, the Fisher classical spin model was used and Heisenberg model in the case of *S*=1/2. [ref. 26] For these models, the specific heat has the form shown at the figures (Figs. 4.63, 4.64)

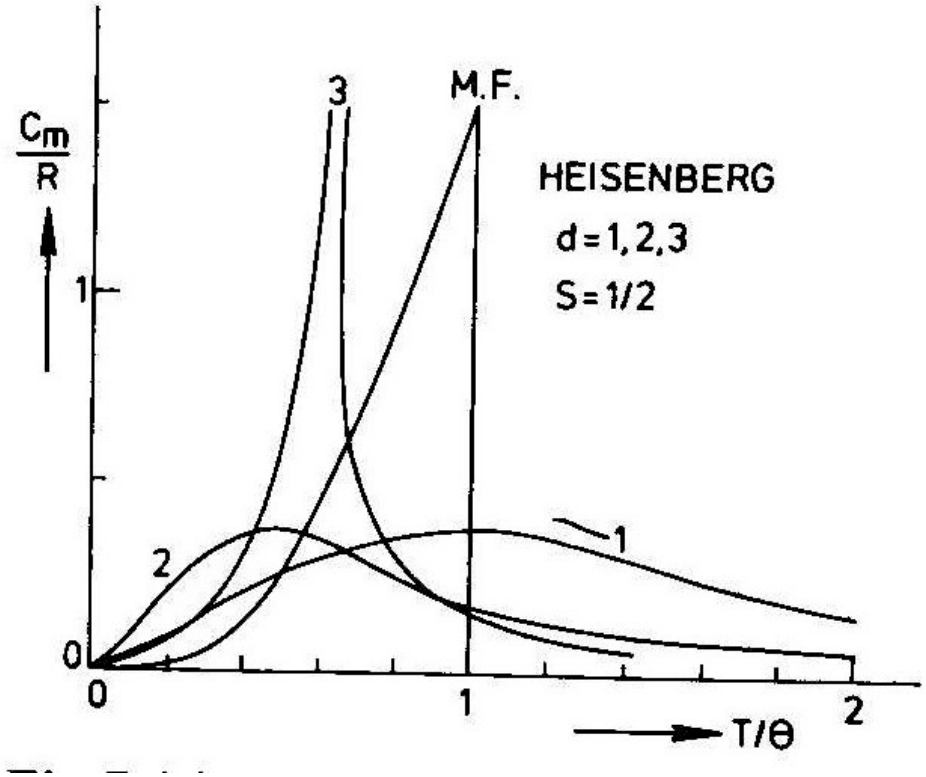

Fig. 4.63. Theoretical C_m of S=1/2 Heisenberg model

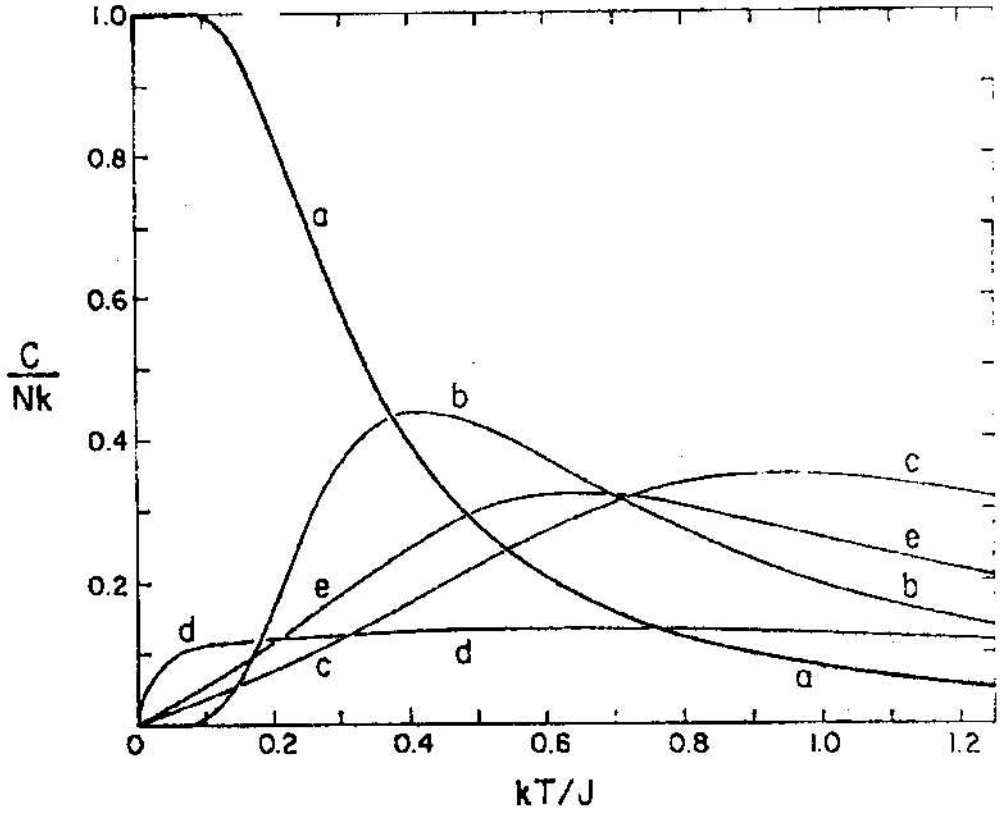

Fig. 4.64. Theoretical C_m of Heisenberg classical spin model

$$C_N(T) = Nk_B(1-\frac{K^2}{\sinh^2 K}) \quad (4.6)$$

$$K = \frac{1}{2}\frac{J}{k_B T} \quad (4.7)$$

Thus we can write the heat capacity for M(II)(N_3)$_2$(4,4'-bipyridine) in the form:

$$c_{M(II)} = c_{latt} + Nk_B(1-\frac{K^2}{\sinh^2 K}) \quad (4.8)$$

Fe(N_3)$_2$(4,'4-bipyridine): Fitting specific heat data the Fisher model, and we obtained:

$$\frac{J}{k_B} = 7.05 \text{ K}$$

Thus value of fitting parameter is close to the value fitting that was obtained by fitting χ(T) for the same theoretical model.

Co(N_3)$_2$(4,4'-bipyridine): The data was fit to the same model, and the of fitting parameter is:

$$\frac{J}{k_B} = 4.40 \text{ K}$$

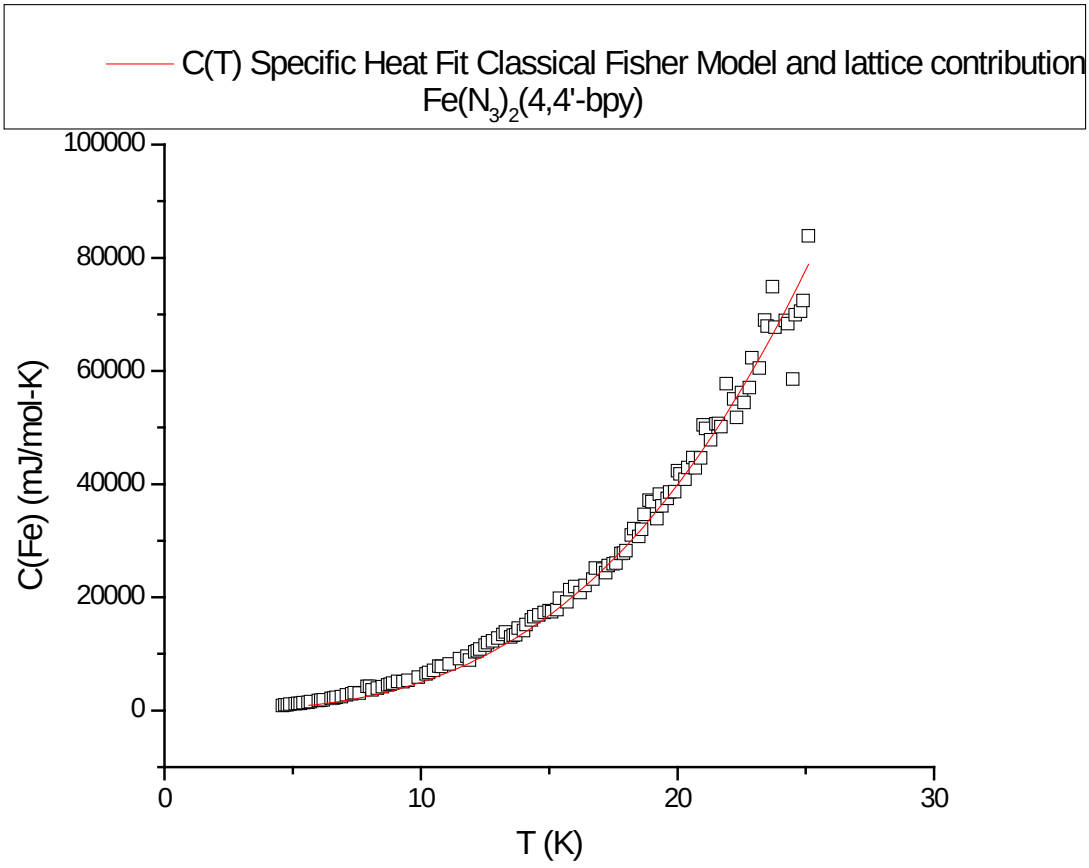

Fig. 4.65. Specific heat fit of classical Fisher model and lattice contribution $Fe(N_3)_2$(4,4'-bipyridine)

The difference observed between this value of the strength interaction parameter $\frac{J}{k_B}$ and the value that was obtained by fitting $\chi(T)$ for the same model and compound probably comes from the fact that *C(T)* fitting was made for the material for the low spin state while $\chi(T)$ was calculated for the high spin state. That is because wide temperature range where both high and low spin states of Co were present.

$Cu(N_3)_2$(4,4'-bipyridine): The data were fit to the Fisher model, and fitting parameter is:

$$\frac{J}{k_B} = 4.47\,\mathrm{K}$$

The value is very close in absolute value to the one that was obtained when $\chi(T)$ was fit to the same theoretical model. The difference between these two fitting parameters probably indicates the limits of applicability of the theoretical model in the case of $Cu(N_3)_2$(4, 4'-bipyridine).

Next, the lattice contribution was subtracted from the specific heat data in the case of $Fe(N_3)_2$(4,4'-bipyridine) and $Co(N_3)_2$(4,4'-bipyridine), and then magnetic contribution ratios of these two coordination networks were compared. (Fig. 4.68)

Another phase in our study of the specific heat of these materials was the attempt to determine the coefficient β in the lattice contribution βT^3 the from the lattice part. Since the metallic ions, arranged in the same geometries with the same ligands, it is natural to assume β would be characteristic of the whole family. There are two problems with this approach. The first one comes from the fact that non-magnetic zinc analog in this family was not synthesized, although numerous attempts were made. The second

problem arose from the fact that two of the studied materials $Co(N_3)_2$(4,4'-bipyridine) and $Cu(N_3)_2$(4,4'-bipyridine) apparently have the same spin $S = 1/2$, while almost identical *C(T)* in the observed temperature range, which reduces observation to the study of one of these coordinated networks with $Fe(N_3)_2$(4,4'-bipyridine).

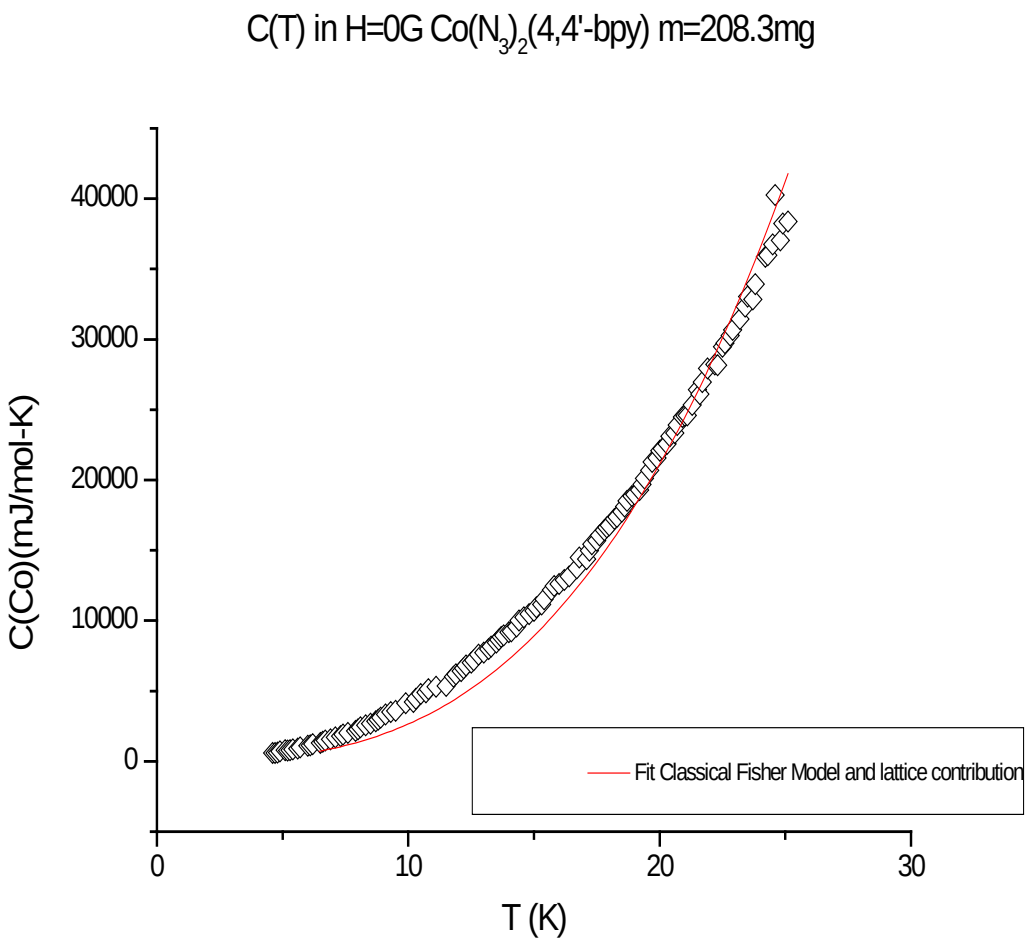

Fig. 4.66. Specific heat fit to classical Fisher model and lattice contribution of $Co(N_3)_2$(4,4'-bipyridine)

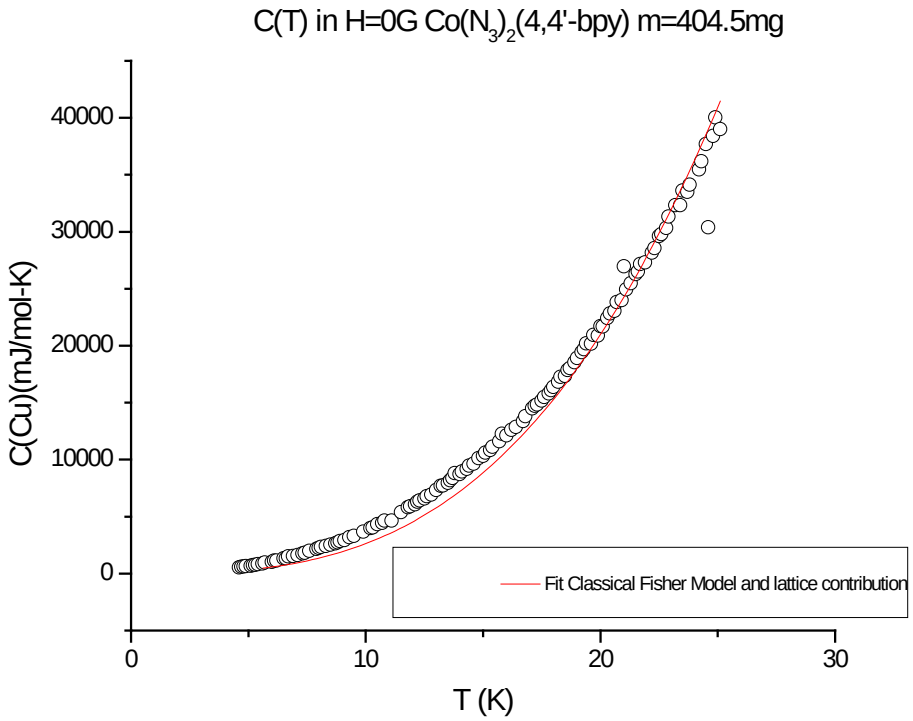

Fig. 4.67. Specific heat fit to classical Fisher model and lattice contribution of $Cu(N_3)_2(4,4'$-bipyridine)

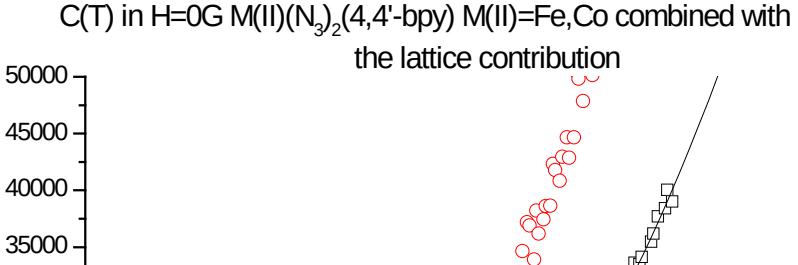

Fig. 4.68. Specific heat of $Fe(N_3)_2$(4,4'-4, 4'-bipyridine) and $Co(N_3)_2$(4,4'bipyridine) with lattice contribution

The network $Co(N_3)_2$(4,'4-bipyridine) was treated as a Heisenberg chain with spin $S = 1/2$. The value of β was determined from the initial fit, and then it was compared to results in the literature. [ref. 16] The value β=2.54 satisfies this requirement very well. (Fig.4.68)

When compared with specific heat data for $Fe(N_3)_2$(4,'4-bipyridine), this value of β did not give produce satisfactory results for the theoretical model considered in this work as linear chain with classical spin. Possibly new measurements on $Ni(N_3)_2$(4,'4-bipyridine) could help clarify this inconsistency.

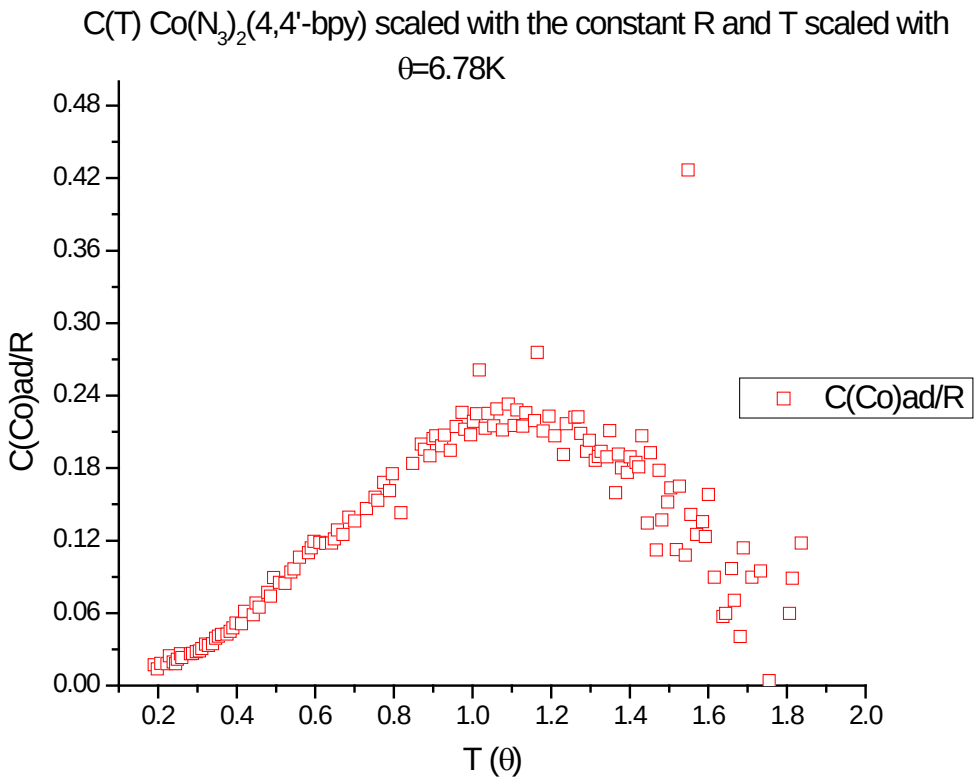

Fig. 4.69. Magnetic specific heat of the $Co(N_3)_2$(4,'4-bipyridine) Heisenberg chain

4.6. SUMMARY OF THE CHAPTER

The work on 1D metal-organic compounds in this dissertation had a twofold goal. We wanted to examine how three different kinds of ligands – chloride Cl_2, oxalate (ox), and azide (N_3) – interact with another ligand 4,'4-bipyridine and transitional metal ions Fe, Ni, Co, and Cu, although copper has a tendency to form different structures. We were interested to understand what kind of physical structure they have, and how they transmit exchange interactions between metallic ions. We also wanted to study how these transitional metal ions interact with the same ligand, and determine which the factors are the most influential in producing such an interaction.

4.6.1. MCl_2(4,4'-bipyridine)

As our discussion of structure has shown, the magnetic divalent centers M(II) in MCl_2(4,4'-bipyridine) compounds are situated in an octahedral environment with four Cl and two 4,4'-bipyridine ligands. The Cl-M-Cl angles are very close to a right angle but deviate from it. The length of the M-Cl bonds is approximately 2.5 Å. This facilitates the 1D magnetic interaction through the M-Cl_2-M pathway, which is consistent with previously published data [ref. 55]. The experimental results and fitting to the Fisher Classical spin model suggests that shorter Cl-M-Cl distances facilitate ferromagnetic interactions, which are more sensitive to the total spin value than to the distance between metal ions. The strongest interaction is in the case of Fe(II) which has the greatest spin, although the distance between the metal centers is the largest. As the spin value is

decreases, the strength of the ferromagnetic interaction also decreases, in spite the fact that the distance between ions becomes shorter. From our measurements we conclude that in the case of MCl_2(4,4'-bipyridine), the total spin value is the decisive parameter as far as the strength of interaction is concerned. The 4,4'-bipyridine ligands, which facilitate negative exchange between interacting metal centers, are the most probable reason for the antiferromagnetic behavior below the ordering temperature.

4.6.2. M(ox)(4,4'-bipyridine)

The M(ox)(4,4'-bipyridine) family of compounds are antiferromagnetic, which is expected, knowing how the oxalate ligand mediates magnetic interactions between metallic ions [ref. 46, 61]. The strength of the antiferromagnetic exchange decreases with the decreasing spin, being strongest for the Fe(II) ions with spin S=2, where the value of the spin is more important than the distance between magnetic ions. The observed fact that the antiferromagnetic interactions between Ni(II) metallic ions in the chains are stronger than in the case of Co(II) chains results from the paramagnetic phase in Co(ox)(4,4'-bipyridine) sample. Although small in total percentage, not more than 8% of the sample, according to the fit performed, the paramagnetic phase diminishes the strength of antiferromagnetic interaction in Co(ox)(4,4'-bipyridine). Fitting results for all compounds of M(ox)(4,4'-bipyridine) family have shown that there is strong anisotropy in all of them, being highest in Ni(ox)(4,'4-bipyridine) and lowest in Co(ox)(4,4'-bipyridine). Single crystal neutron diffraction and measurements of magnetic susceptibility in that regimen are needed for a deeper understanding of these anisotropies.

4.6.3 $M(N_3)_2$(4,4'-bipyridine)

The magnetic behavior of the $M(N_3)_2$(4,4'-bipyridine) family of coordinated metal-organic compounds is very interesting because family members exhibit both ferromagnetic and antiferromagnetic behavior. The ferromagnetic characteristics decrease with decreasing spin, and in the case of $Cu(N_3)_2$(4,'4-bipyridine), there is no evidence of ordering in the experimental data. Heat capacity measurements that were performed for $Ni(N_3)_2$(4,4'-bipyridine) and $Co(N_3)_2$(4,4'-bipyridine) do not show any phase transitions in the temperature interval from T=1.2K to T=30K. Moreover, the chain distance between metallic centers decreases from Fe to Cu compound, and again ferromagnetic characteristics of the materials decrease. This finding is in accordance with the one in MCl_2(4,4'-bipyridine), where the shorter distance between the metallic centers meant more pronounced ferromagnetic interaction. In the case of chlorides and oxalates, there is a consistent transfer of the exchange interactions through the ligands. The chlorides only facilitate ferromagnetic exchange, which depends more on spin than the distance between ions, while oxalates favor antiferromagnetic interaction. In azides, the spin of the ions and the distance between these centers have very important roles. Additional studies in different geometries and with ligands different from 4,4'-bipyridine would be useful in determining the superexchange characteristics of the azide ligand group.

When we perform cross-referencing, and compare how each transitional metallic ion interacts with the ligands we obtain the following results:

Fe(II) in coordinate network with oxalate has the strongest of interaction between two ions, which is antiferromagnetic in nature. In the case of ferromagnetic bonding in the observed compounds, the interaction is more pronounced in the azide chain, which is shorter in length. The oxalate ligand is significantly longer than the other two, and it is well known facilitator of antiferromagnetic interactions. To conclude how its dimensions influence interaction strength in the case of ferromagnetic interaction it is prudent to compare how other two ligands influence magnetic interaction between metallic ions included in coordinated network. In the case of ferromagnetic interaction in MCl_2(4,4'-bipyridine) and $M(N_3)_2$(4,4'-bipyridine), the strength of the interaction is more pronounced in azide chain, which is shorter in length. The distance between metal and organic ligand is 4.9% longer in the case of Fe(II) ion and ligand Cl_2 than in the case of Fe(II) and ligand $(N_3)_2$, which results in the 15% decrease of ferromagnetic interaction.

Co(II) and Ni(II) behave similarly to Fe(II) in the corresponding metal organic compounds. In the case of Co(II) we find that the difference between interaction strengths in azides and chlorides is of the greater magnitude than the difference in lengths would suggest, which is the case of Fe(II) and Ni(II) in chlorides and azides, respectively. At present, we do not have a satisfactory explanation for this behavior.

Cu(II) in our investigation exists only occurs in the azide coordinate network, and hence it is excluded from this discussion.

CHAPTER 5

CONCLUDING REMARKS

The work on one-dimensional metal-organic compounds in this dissertation had a twofold goal. First, we examined the magnetic and spatial characteristics of several families of one-dimensional metal-organic compounds. We studied how three different kinds of ligands – chloride Cl_2, oxalate (ox), and azide (N_3) – interact with another ligand, 4,'4-bipyridine, and transitional metal ions Fe, Ni, Co, and Cu, in cases when Cu ion forms isostructural compounds that are comparable to those formed with Fe, Ni, and Co metal ions. Then, we investigated the behavior of the ligands as pathways of exchange interactions between metallic ions in the compounds. Previously performed investigations on these ligands and transitional metals did not focus on the one-dimensional magnetic compounds, although in the case of the oxalate ligand extensive work has been done. We applied different synthesis procedures and produced Ni, Co, and Cu azide compounds for the first time, thus leaving the hydrothermal route procedure. Second, we used these three families of metal-organic coordinated networks as the testing ground for existing theoretical models in one- and higher dimensional magnetism. Finally, the prospectus of this and potential future work on the subject of one-dimensional metal-organic compounds is proposed.

5.1 Magnetic and spatial characteristics of 1D metal-organic compounds

5.1.1. MCl_2(4,4'-bipyridine) compounds

The magnetic divalent centers M(II) in MCl_2(4,4'-bipyridine) compounds are situated in octahedral environment with four Cl and two 4,4'-bipyridine ligands. The Cl-M-Cl angles are very close to right angles but deviate slightly. The length of the M-Cl bonds is approximately 2.5 A. This facilitates the one-dimensional magnetic interaction through M-Cl_2-M pathway, which is consistent with previously published data (ref. 4). The experimental results and fitting to the appropriate model with an accuracy of 0.995 suggests that shorter Cl-M-Cl distances favor ferromagnetic interactions, which are more sensitive to the total spin value than to the distance between the metal ions. The 4,4'-bipyridine ligands, which favor negative exchange between interacting metal centers, are the most probable reason for antiferromagnetic behavior below the ordering temperature.

5.1.2. M(ox)(4,4'-bipyridine) compounds

The M(ox)(4,4'-bipyridine) compounds behave as antiferromagnets in all temperature ranges, which is expected from the way the oxalate ligand mediates magnetic interaction between metallic ions (ref. 1, 3). The strength of antiferromagnetic exchange decreases with decreasing spin value, being strongest for the Fe(II) ions for spin S=2, with the value of the spin more important than the distance between magnetic ions. The observed fact that antiferromagnetic interaction between Ni(II) metallic ions in the chains

is stronger than in the case of Co(II) chains results from the presence of the paramagnetic phase in a Co(ox)(4,4'-bipyridine). Although small in total percentage, not more than 8% of the sample, according to our fit, the paramagnetic phase diminishes the strength of the antiferromagnetic interaction in Co(ox)(4,4'-bipyridine). Fitting results for all compounds of M(ox)(4,4'-bipyridine) family have shown that strong anisotropy exists in all of them, being strongest in Ni(ox)(4,'4-bipyridine) and lowest in Co(ox)(4,4'-bipyridine). Single crystal neutron diffraction and measurements of magnetic susceptibility in that regime would be essential for a deeper understanding of these anisotropies.

5.1.3. $M(N_3)_2$(4,4'-bipyridine) compounds

In each of the compounds of the $M(N_3)_2$(4,4'-bipyridine) coordinated metal-organic network, there are octahedral geometries around metal ions which are slightly distorted through axial contraction and equatorial distortions. The magnetic behavior of $M(N_3)_2$(4,4'-bipyridine) family of coordinated metal-organic compounds is very interesting because family members exhibit both ferromagnetic and antiferromagnetic behavior. The ferromagnetic characteristics decrease with decreasing spin, and in the case of $Cu(N_3)_2$(4,'4-bipyridine) we do not observe any sign of ordering in the experimental data. The heat capacity measurements that were performed for Cu $(N_3)_2$(4,4'-bipyridine) and $Co(N_3)_2$(4,4'-bipyridine) have not shown any phase transitions in the temperature interval from T=1.2K to T=30K. Moreover, the inside chain distance

between metallic centers decreases from Fe to Cu compounds and ferromagnetic characteristics of the materials decrease.

5.2. LIGANDS AS FACILITATORS OF MAGNETIC INTERACTIONS

Cross-referencing suggests that Fe(II) in the coordinate network with oxalate has the interaction between ions is strongest and is antiferromagnetic in nature. In the case of ferromagnetic bonding, the interaction is more pronounced in the azide chain, which is shorter in length. The oxalate ligand is longer significantly than other two and it is a well known facilitator of antiferromagnetic interactions. To learn how its dimensions influence the interaction, it would be prudent to compare it with other ligands that are bearers of the same type of magnetic interaction between metallic ions in coordinated networks.

Co(II) and Ni(II) behave similarly to Fe(II) in their corresponding metal organic compounds. In the case of Co(II) we observe that the difference between interaction strengths in azides and chlorides is of the greater magnitude than the difference in lengths would suggest, and which is the case of Fe(II) and Ni(II) in chlorides and azides, respectively. At this point we do not have satisfactory explanation for this behavior.

5.3. APPLIED THEORETICAL MAGNETISM MODELS

With great accuracy the Fisher Classical Spin Linear Chain Model describes the magnetic behavior of the MCl_2(4,4'-bipyridine) and $M(N_3)_2$(4,4'-bipyridine) families of compounds. Similarly, the Bonner-Fisher Linear Chain Model reproduces the magnetic characteristics of M(ox)(4,4'-bipyridine). It is worth emphasizing that the Fisher Classical Spin Linear Chain Model fits the data better than the Bonner-Fisher Ferromagnetic Chain Model with quantum mechanical spin S=1/2 for Cu(II)$(N_3)_2$(4,4'-bipyridine), despite the fact that Cu(II) always has spin S=1/2.

5.4. SPECIFIC HEAT MEASUREMENTS

Specific heat measurements were performed for Cu(II)$(N_3)_2$(4,4'-bipyridine) and Co(II)$(N_3)_2$(4,4'-bipyridine), and the data were compared with earlier studies of Fe(II)$(N_3)_2$(4,4'-bipyridine). None of these compounds shows the characteristic λ shape of a transition, but large values of γ parameters indicate of possible magnetic contribution. The Fisher Classical Spin Model, which was used in explaining χ(T) gives good fit to the experimental data.

5.5. PROSPECTUS FOR FUTURE WORK

Single crystal production investigated metal organic coordinated networks have thus far unsuccessful. That is probably the most important step needed to better understand the magnetic behavior of MCl_2(4,4'-bipyridine), M(ox)(4,4'-bipyridine), and $M(N_3)_2$(4,4'-bipyridine) systems and their ligands. To continue our attempts to produce single crystal samples, we will continue to collaborate closely with Prof. Jing Li's chemistry research lab, because the experience of the trained chemist is essential.

An other crucial investigation would be Mossbauer measurements for compounds that contain Fe(II) as a metallic ion. The study of the Mossbauer effect for $FeCl_2$(4,4'-bipyridine), Fe(ox)(4,'4-bipyridine), and $Fe(N_3)_2$(4,'4-bipyridine) would help us better understand the magnetic ground states of the three studied compounds, thus providing us with more information about ligands in compounds as facilitators of the interaction between magnetic ions of transitional metals in question.

Neutron scattering experiment is a useful technique for measuring magnetic ordering and magnetic structure of the compounds. We plan to collaborate with another research group to perform a neutron scattering experiment.

Last but not the least, an improved probe for resistivity and heat capacity requiring a much smaller mass, preferably around 100 mg of the samples, would allow investigation of all the samples including those only produced in small quantities. More detailed studies of the specific heat for all three families of compounds. These new investigations will be performed in the future could be carried out at Temple University.

These further investigations, in conjunction with the existing body of work, are important for a better understanding of MCl_2(4,4'-bipyridine), M(ox)(4,4'-bipyridine), and $M(N_3)_2$(4,4'-bipyridine) systems and their ligands.

REFERENCES CITED

1. Ascroft, N.W.; Mermin, N.D.; *Solid State Physics*, Brooks/Cole, New York, **1976**.
2. Baxter, R.J.; Enting I.G.; 399th solution of Ising problem, *J. Phys. A: Math. Gen.*, **1978**. vol. 11. , No.12., 2463-2473.
3. Belanda, M.; Falk, K.; Griesar, K.; Tomkowicz, Z.; Hasse, W.; Characterization of magnetic ordering in porphyrin-based molecular magnets, [Mn(R)$_4$TPP][TCNE] (R=O$C_{12}H_{25}$,F, CN), *JMMM*, **1999**. No.205, 14-19.
4. Berkowitz, A.E.; Takano, K.; Exchange anisotropy-a review, *JMMM*, **1999**. No.200, 552-570.
5. Blum, K., *Density Matrix Theory and Applications*, Plenum Press, New York, **1989**.
6. Blundell S.J.; Molecular magnets, *Contemporary Physics*, **2007.**vol.45, No.5, 275-290.
7. Blundell, S.; *Magnetism in Condensed Matter*, Oxford University Press, Oxford, **2001**.
8. Bogani, L.; Wernsdorfer, W.; Molecular-spintronics, using single molecule magnets, *Nature Materials*, **2008**. vol.7, 179-186.
9. Bonner, J.C.; Fisher, M.E.: Linear Magnetic Chains with Anisotropic Coupling, *Phys .Rev.* **1964**. vol.135, No.3A, 640-658.
10. Bonner, J.C.; One-dimensional Model Systems: Theoretical Survey, *J. Appl. Phys.*, **1978.** vol.49, No.3, 1299-1304.
11. Bordallo, H.N.; Chapon, L.; Manson, J.L.; Hernandez-Velasco, J.; Ravot, D.; Argyriou, D.N.; S=1/2 Ising behavior in the two-dimensional molecular magnet Fe$(NSC)_2$$(pyrazine)_2$, *Phys. Rev. B* , **2004**. 69, 224405.
12. Brooks, H.; Ferromagnetic anisotropy and itinerant electron model, *Phys. Rev.*, **1940**. vol.58, 909-918.
13. Buschow, K.H.J.; Boer F.R.; *Physics of Magnetism and Magnetic Materials*, Kluwer Academic/Plenum Publishers, New York, **2003**.

14. Callaway, J., *Quantum Theory of the Solid State*, Academic Press, New York, **1973**.
15. Caneschi, A.; Gatteschi, D.; Renard, J.P.; Rey, P.; Sessoli, R.; Magnetic Phase-Transition and Low-Temperature EPR-Spectra of a One-Dimensional Ferrimagnet Formed by Mn(II) and a Nitronyl Nitroxide, *Inorg. Chem*. **1989**. *28*, 1976-1980.
16. Carlin, R.L.; *Magnetochemistry*, Springer-Verlag, New York, **1986**.
17. Carlin, R.L.; van Duyneveldt, A.J.; *Magnetic Properties of Transitional Metal Compounds*, Springer-Verlag, New York, **1977.**
18. Craik, D.; *Magnetism*, John Wiley & Sons, Chichester, **1995**.
19. Daalderop, G.H.O.; Kelly, P.J.; Schuurmans, M.F.H.; First-principles calculation of the magnetocrystalline anisotropy energy of iron, cobalt, and nickel, *Phys .Rev. B* , **1990**. vol. 41, No. 17, 11919-11937.
20. de Jongh, L.J.; Miedema A.R.; Experiments on simple magnetic model systems, *Adv. Phy.*, **1974**. vol. 23, 947-1170.
21. De Munno, G.; Ruiz, R.; Lloret, F.; Sessoil, R.; Julve, M.; Oxalate and 2,'2-bypimiridine as useful Tool in Designing Layered Compounds *Inorg. Chem.* **1995**, *34*, 408-412.
22. Des Cloizeaux, J.; Pearson, J.J.; Spin-Wave Spectrum of the Antiferromagnetic Linear Chain, *Phys. Rev.*, **1962**. vol.128, No.5, 2131-2135.
23. Dirac P.A.M., *Principles of Quantum Mechanics*, Oxford University Press, Oxford, **1947**.
24. Eriksson, O.; Johansson, B.; Albers, R.C.; Boring, A.M.; Brooks, M.S.S.; Orbital magnetism in Fe, Co, and Ni, *Phys .Rev. B* , **1990**. vol.42, No.4, 2707-2710.
25. Fahnle, M.; Correlated molecular field theory of amorphous ferromagnets and the Gibbs free energy, *JMMM*, **2000**. No.210, L1-L4.
26. Fisher, M.E.; Magnetism in 1-Dimensional Systems-Heisenberg Model for the Infinite Spin, *Amer. J. Phys.*, **1964**. vol.32, No.5, 343-347.
27. Fisher, M.L.; Sykes, M.F.; Antiferromagnetic Susceptibility of the Simple Cubic and Body-Centered Cubic Ising Lattices, *Physica* **1962**. No.28, 939-956.

28. Fu, A.; Huang, X.; Li, J.; Yuen T.; Lin, C.L.; Controlled Synthesis and Magnetic properties of 2D and 3D Iron Azide Networks $^{2}_{\infty}[Fe(N_3)_2(4,4'\text{-bpy})]$ and $^{3}_{\infty}[Fe(N_3)_2(4,4'\text{-bpy})]$, *Chem. Eur.J.* **2002**, *8*, No.10, 2239-2247.
29. Fujita, S.; Godoy, S.; *Theory of High Temperature Superconductivity*, Kluwer Academic Publishers, Dordrecht, **2001**.
30. Gatteschi, D.; A coupling powered by nature, *Nature Materials*, **2007**. vol. 6, 471-472.
31. Gerloch, M.; Constable, E.C.; *Transition Metal Chemistry*, John Wiley & Sons-VCH, New York, **1994**.
32. Goodenough, J.B., *Magnetism and the Chemical Bond*, John Wiley & Sons, New York, **1963**.
33. Griffith, J.S., *The Theory of Transition Metal Ions*, Cambridge University Press, Cambridge, **1964**.
34. Griffiths, R. B.; Nonanalytic behavior above the critical point in random Ising ferromagnet, *Phys. Rev. Letts.*, **1969**. vol. 23, No.1, 17-19.
35. Griffiths, R.B.; Correlations in Ising ferromagnets, *J. Math. Phys.*, **1967**. vol.8, No.3, 478-484.
36. Groenendijk, H.A.; van Duyneveldt, A.J.; Spin Canting and Exchange in the Two-Dimensional Antiferromagnets $(C_3H_7NH_3)_2MnCl4$ and $(C_3H_7NH_3)_2MnBr_4$, *Physica B*, **1979**. No.98, 53-59.
37. Hall, G.G., *Applied Group Theory*, Longmans, London, **1967**.
38. Harrison, W.A., *Solid State Theory*, McGraw-Hill Book Company, New York, **1970**.
39. Hurd, C.M.; Varieties of Magnetic Order in Solids, *Cont. Phys.* **1982**. *23*, 469-493.
40. Imry, Y.; On the statistical mechanics of coupled order parameters, *J. Phys. C: Solid State Phys.*, **1975**. vol. 8. , 567-577.
41. Ising, E.; Report on the Theory of Ferromagnetism, *Zeitschrift fur Physik* **1925**, *31*, 253-258.
42. Jiang, W.; Wei, G.; Xin, Z-H.; Effect of crystal field on phase transitions in a spin 3/2 transverse Ising model, *JMMM*, **2000**. No.217, 225-230.

43. Jiles, D.; *Introduction into Magnetism and Magnetic Materials*, Chapman and Hall, London, **1990**.
44. Joshua, S.J.; *Symmetry Principles and Magnetic Symmetry in Solid State Physics*, Adam Hilger, New York, **1991.**
45. Kahn, O.; Chemistry and Physics of Supramolecular Magnetic Materials, *Acc. Chem. Res.* **2000**, *33*, 647-657.
46. Kahn, O.; *Molecular Magnetism*, John Wiley & Sons-VCH, New York, **1993**.
47. Katsura, S., Statistical Mechanics of the Anisotropic Linear Heisenberg Model, *Phys. Rev.*, **1962**. vol. 127, No.5, 1508-1518.
48. Keller, E.; SCHAKAL97, Computer Program for the Graphics Representation of Molecular and Crystallographic Models, University of Freiburg, Freiburg, **1997**.
49. Kenzelmann, M.; Batista C.D.; Chen, Y.; Broholm, C.; Reich, D.H.; Park, S.; Qiu, Y.; S=1/2 in Staggered Field: High-energy bound-spinon state and the effects of the discrete lattice, *Phys. Rev. B*, **2005**. vol.71, 094411.
50. Kitaigorodskii, A.I.; *Molecular Crystal and Molecules*, Academic Press, New York, **1973**.
51. Kittel, C., *Quantum Theory Solids*, John Wiley & Sons, New York, **1963**.
52. Kittel, C., *Solid State Physics*, John Wiley & Sons, New York, **2004**.
53. Lackova, S.; Jaščur, M.; Phase diagrams of spin ½ planar Ising models with four-spin interactions, *JMMM*, **2000**. No.217, 216-224.
54. Lake, B.; Cowley, R.A.; Tennant, D.A.; A dimmer theory of the magnetic excitations in the ordered phase oh the alternating-chain compound $CuWO_4$, *J.Phys. :Condens. Matter*, **1997**. 9, 10951-10975.
55. Lawandy, M. A.; Huang, X.; Wang R.; Li, J.; Lu, J.Y.; Yuen T.; Lin, C.L.; Two-Dimensional Coordination Polymers with One-Dimensional Magnetic Chains: Hydrothermal Synthesis, Crystal Structure, and Magnetic and Thermal Properties of $^{2}{}_{\infty}[MCl_2(4,4'\text{-bipyridine})]$ (M=Fe, Co, Ni, Co/Ni), *Inorg. Chem.* **1999**, *38*, 5410-5414.

56. Lee, T. D.; Yang, C.N.; Statistical theory of equations state and phase transitions. II. Lattice gas and Ising model, *Phys. Rev.*, **1952**. vol. 87, No.3, 410-419.

57. Lévy, L.P.; *Magnetism and Superconductivity*, Springer-Verlag, New York, **2000**.

58. Lieb, E.H., Mattis, D.C. (eds.), *Mathematical Physics in One Dimension*, Academic Press, New York, **1966**.

59. Losee, D.B.; McElearney, J.N.; Shankle, G.E.; Carlin, R.L; Cresswell, P.J.; Robinson, W.T.; An Anisotropic Ising System $[(CH_3)_3NH]CoCl_3*2H_2O$: Its Structure and Canted Antiferromagnetic Behavior, *Phys .Rev. B*, **1973**. vol.8, No.5, 2185-2200.

60. Lu, J.Y.; Cabrera, B.R.; Wang, R.; Li, J.; Cu-X-bpy (X=Cl, Br; bpy=4,4'-bipyridine) Coordination Polymers: The Stoichiometric Control and Structural Relations of $[Cu_2X_2(bpy)]$ and [CuBr(bpy)], *Inorg. Chem.* **1999**, 38, 4608-4611.

61. Lu, J.Y.; Lawandy, M. A.; Li, J.; Yuen T.; Lin, C.L.; A New Type of Two-Dimensional Metal Coordination Systems: Hydrothermal Synthesis and Properties of the First Oxalate-bpy Mixed-Ligand Framework $^2{}_\infty[M(ox)(bpy)]$ (M=Fe(II), Co(II), Ni(II), Zn(II); ox=$C_2O_4^{2-}$; bpy=4,4'-bipyridine), *Inorg. Chem.* **1999**, *38*, 2695-2704.

62. Maeshima, N.; Okunishi, K.; Okamoto, K.; Sakai, T.; Frustration-Induced η Inversion in S=1/2 Bond-Alternating Spin Chain, *PRL*, **2004**. vol. 93, No.12, 127203.

63. Mariot, L., *Group Theory and Solid State Physics*, Prentice-Hall Inc., Englewood Cliffs, **1962**.

64. Martin, J.D.; Hess, R.F.; Boyle, P.D.; Synthesis of [NH]MnCl(OAc) and [NH]MnCl(HO) by Solvothermal Dehydration and Structure/Properties Correlation in One-Dimensional Antiferromagnetic, *Inorg. Chem.* **2004**. vol.43, 3242-3247.

65. Matsubara, K.; Katsura, S.; Magnetic Properties of One-Dimensional Random XY Model, *Prog. Theo. Phys.*, **1973**. vol. 49, No.1, 367-368.

66. Mattis, D.C., *The Theory of Magnetism Made Simple*, World Scientific, Singapore, **2006**.
67. Mattis, D.C., *The Theory of Magnetism*, Harper & Row Publishers, New York, **1965**.
68. Mattis, D.C.; *Theory of Magnetism*, vol. 1 Springer-Verlag, Berlin, **1981**.
69. Matveev, V.; Shrock, R.; On the properties of the Ising model for complex energy/temperature and magnetic field, *J. Phys. A: Math. Theor. ,* **2008**. 41, 135002.
70. Miller, S.A., *Magnetic Interactions in Molecular Materials*, PhD Dissertation, California Institute of Technology, Pasadena, **1998**.
71. Mohn, P.; *Magnetism in the Solid State*, Springer-Verlag, New York, **2003**.
72. Newman D.J., Ng, B.; The superposition model of crystal fields, *Rep. Prog. Phys.*, **1989**. 52, 699-763.
73. Onsager, L.; Crystal statistics. I. A two-dimensional model with an order-disorder transition, *Phys. Rev.*, **1944**. , vol. 65, Nos. 3&4, 117-149.
74. Peierls, R.E., *Quantum Theory of Solids*, Calderon Press, Oxford, **1965**.
75. Pokrovsky, V.L.; Two-dimensional magnetic phase transitions, *JMMM*, **1999**. No.200, 515-535.
76. Qinian, Q.; Skomski, R.; Coey, J.M.D.; Strong ferromagnets: Curie temperature and density of states, *J. Phys.: Condens. Matter*, **1994**. 6, 3245-3252.
77. Rado, G.T., Suhl, H. (eds.), *Magnetism*, vol. I, Academic Press, New York, **1963**.
78. Rado, G.T., Suhl, H. (eds.), *Magnetism*, vol. III, Academic Press, New York, **1963**.
79. Sato, M.; Oshikawa, M.; Coupled S=1/2 Heisenberg antiferromagnetic chains in an effective staggered field, *Phys. Rev. B* , **2004**. 69, 054406.
80. Scalapino, D.J.; Imry, Y.; Pincus, P.; Generalized Ginzburg-Landau theory of pseudo-one-dimensional systems, *Phys. Rev. B* , **1975**. vol.11, No.5, 2042-2048.
81. Senthill, T.; Vishwanath, A.; Balents, L.; Sadchev, S.;Fisher, M.P.A.; Deconfined Quantum Critical Points, *Science*, **2004**. 303, 1490-1494.

82. Sheahen, T.P.; *Introduction to High-Temperature Superconductivity*, Plenum Press, New York, **1994**.
83. Sheldrick, G.M.; SHELX-97, Program for Structure Refinement, University of Göttingen, Göttingen, **1997**.
84. Sirker, J.; Thermodynamics of one-dimensional S=1/2 spin-orbital model, *Phys. Rev. B*, **2004**. 69, 104428
85. Skomski, R., *Simple Models of Magnetism*, Oxford University Press, Oxford, **2008**.
86. Skomski, R.; Kashyap, A.; Zhou, J.; Sellmyer D.J.; Anisotropic exchange, *J. of Appl. Phys.*, **2005**., 97, 10B302.
87. Stone, M.B.; Broholm, C.; Reich, D.H.; Schiffer, P.; Tchernyshyov, O.; Harrison, N.; Field-driven phase transitions in quasi-two-dimensional quantum antiferromagnet, *NJP*, **2007**. 9, 1-30.
88. Sykes, M. F.; Fisher, M. E.; Susceptibility of the Ising model of an antiferromagnet, *Phys. Rev. Letts.*, **1958**. vol. 1, No. 9, 321-322.
89. Sykes, M.F.; Fisher, M.L.; Antiferromagnetic Susceptibility of the Plane Square and Honeycomb Ising Lattices, *Physica* **1962**. No.28, 919-938.
90. Takeda, K.; Wada, M.; An Experimental Study of the Ising Chain Statistics under the Magnetic Field, *JPSP*, **1981**. vol. 50, No.11, 3603-3611.
91. Tanaka, Y.; Uryû, N.; Magnetic Susceptibility of the Two-Dimensional Ising Ferromagnet, *Phys .Rev. B,* **1980**. vol.21, No.5, 1994-2000.
92. Taylor, P.L.; Heinonen, O.; *Quantum Approach to Condensed Matter Physics*, Cambridge University Press, Cambridge, **2002**.
93. Trygg, J.; Eriksson, O.; Johansson, B.; Wills, J.M.; Total Energy Calculation of Magnetocrystalline Anisotropy Energy in the Ferromagnetic 3d Metals, *Phys. Rev. Letts.*, **1995**. vol.75, No.15, 2871-2874.
94. Tucker, J.W.; Cluster variation theory of spin 3/2 Ising models, *JMMM*, **2000**. No.214, 121-129.
95. Turner, S.; Kahn, O.; Rabadel L., Crossover between Three-Dimensional Antiferromagnetic and Ferromagnetic States in Co(II) Cu(II) Ferromagnetic

Chain Compounds. A New Molecular-Based Magnet with Tc=38K and Coercive Field of $5.66x10^3$Oe, *J .Am. Chem. Soc.* **1996**, *118*, 6428-6432.

96. White, R.M., *Quantum Theory of Magnetism*, McGraw-Hill, New York, **1970**.
97. Willis, A.S.; Raymond, S.; Henry J-Y.; Magnetic ordering in distorted S=1/2 pyrochlore antiferromagnet, *JMMM*, **2004**. No.272-276, 850-851.
98. Wilson, A.H., *The Theory of Metals*, Cambridge University Press, Cambridge, **1953**.
99. Yang, C.N.; Lee, T. D.; Statistical theory of equations state and phase transitions. I. Theory of condensations, *Phys. Rev.*, **1952**. vol. 87, No.3, 404-409.
100. Yang, C.N.; The spontaneous magnetization of two-dimensional Ising model, *Phys. Rev.*, **1952**. vol. 85, No.5, 808-816.
101. Yuen, T.; *^{119}Sn Mossbauer Study of U-based Intermetallic Systems-$U(Sn_{1-x}Pb_x)_3$, $U(In_{1-x}Sn_x)_3$, and UNiSn*, PhD Dissertation, Temple University, Philadelphia **1990**.
102. Zan, J.A., *Anomalous Magnetic Ground States of $CeGe_X$ System*, PhD Dissertation, Temple University, Philadelphia, **2004**.